IN-SITU EXPERIMENTS AND NUMERICAL SIMULATION OF VERTICAL-AXIS HYDROKINETIC TURBINES FOR SMALL-SCALE POWER GENERATION

A Thesis

Submitted in Partial Fulfillment of the Requirement

for the Award of the Degree of

DOCTOR OF PHILOSOPHY

By

PARAG KAMAL TALUKDAR

DEPARTMENT OF MECHANICAL ENGINEERING
INDIAN INSTITUTE OF TECHNOLOGY GUWAHATI
GUWAHATI - 781039

July, 2019

Dedicated to my Parents ...

Mrs. Damayanti Talukdar

&

Mr. Padum Kumar Talukdar

Declaration

I hereby certify that the work which is being presented in this thesis entitled "**In-Situ Experiments and Numerical Simulation of Vertical-axis Hydrokinetic Turbines for Small-Scale Power Generation**" is the outcome of my research work under the supervision of Dr. Vinayak Kulkarni and Prof. Ujjwal K. Saha in the Department of Mechanical Engineering, Indian Institute of Technology Guwahati, Assam, India.

Any part of the work has not earlier been submitted for the award of any other degree of this or any other institute.

(**Parag Kamal Talukdar**)
Registration No. 136103039
Department of Mechanical Engineering
Indian Institute of Technology Guwahati

Department of Mechanical Engineering
Indian Institute of Technology Guwahati
Guwahati-781039
INDIA

Certificate

It is certified that the work contained in the thesis entitled **"In-Situ Experiments and Numerical Simulation of Vertical-axis Hydrokinetic Turbines for Small-Scale Power Generation**" submitted by **Mr. Parag Kamal Talukdar** to the Indian Institute of technology Guwahati for the award of the degree of Doctor of Philosophy has been carried out under my supervision in the Department of Mechanical Engineering, Indian Institute of Technology Guwahati. This work has not been submitted elsewhere for the award of any other degree or diploma.

Dr. Vinayak Kulkarni
Associate Professor
Department of Mechanical Engineering
Indian Institute of Technology Guwahati
Guwahati-781039, India

Prof. Ujjwal K. Saha
Professor
Department of Mechanical Engineering
Indian Institute of Technology Guwahati
Guwahati-781039, India

Acknowledgements

The journey of doctoral study is always a difficult and challenging task. I would never have successfully completed this thesis without the assistance of numerous people who I am indebted to. Their direction, advice, support and contributions have proved invariable along the way.

First and foremost, I would like to express my foremost and profound gratitude to my supervisors, Dr. Vinayak Kulkarni and Prof. Ujjwal K. Saha of Mechanical Engineering Department who have been a tremendous mentor for me. I appreciate their contributions of time, support, encouragement and active guidance to make my PhD experience productive and stimulating. A very special gratitude goes to them for encouraging my research.

I wish to express my heartfelt gratitude to Prof. Amarendra K. Das of Department of Design, IIT Guwahati for sharing in-depth knowledge in my field of research and assistance in turbine blade development. I offer my sincere thanks to my doctoral committee members, Prof. Pinakeswar Mahanta, Dr. Amaresh Dalal, Dr. Dipankar N. Basu and Prof. Rajib K. Bhattacharjya for their insightful comments and encouragement. I express my sincere gratitude to past and present HODs Prof. Anoop. K. Dass and Prof. Santosha K. Dwivedy for providing all the research facilities and financial support.

I am grateful to MHRD, Govt. of India, for providing me financial support through SERB to attend and present a technical paper in ASME 38th International Conference on Ocean, Offshore and Arctic Engineering (OMAE 2018) held at Madrid, Spain during June 17-22, 2018. I am also thankful to the Assam Power Generation Corporation Ltd, Assam, India, for funding a part of my research work.

A word of appreciation goes to all the staff members of Mechanical Engineering Department specially Mr. Mrinal Sarma, Mr. Dhaneswar Khaklary, Mr. Dilip Chetri, and Mr. Jiten Basumatary for extending their help in fabrication of experimental setups. I am very much thankful to my seniors and my colleagues Dr. Sukanta Roy, Dr. Bhaskor J. Bora, Mr. Shuvayan Brahmachary, Mr. Arif Sardar, Mr, Sarbindu Kumar, Ms. Dhanjita Medhi, Mr. Umang H. Rathod, Md. Nur Alom, Mr. Achinta Sarkar, Mr. Mirzaul Hussain, Mr. Subra S. Kalita, and Mr. Sibanand Mohanty for their support and friendship.

In this precious moment of my life, I would like to express my deep sense of gratitude to my beloved parents and elder brother for their continuous love, blessings and encouragement.

July, 2019
Guwahati, India

Parag Kamal Talukdar

Abstract

The rapid dwindling of oil reserves, growth of climate change, harmful environmental effects of conventional energy producing technologies and proliferation of energy demand encourage the researchers to look for harmless, reliable, cheaper, sustainable and clean energy production technologies. Such explorations and accessibility of electrical energy determines the economic growth and social living standards. Among the available renewable sources, hydro and wind power seem to be the optimum choices.

The absence of an efficient, low cost and environment friendly hydraulic energy converters suited for free-flowing water are still a major barrier to the exploitation of renewable energy source. Therefore, the present analysis is planned for understanding the feasibility of generating power by using a hydrokinetic turbine with emphasis on turbine design and performance. Advantageously, the hydrokinetic power generation system does not require a conventional dam and hence it is possible to reduce the construction costs, and at the same time to prevent the environmental pollution. Till date, hydrokinetic devices have not been extensively utilized in commercial power plants. Further, there are limited data available to estimate the turbine performance.

In view this, the present investigation is mainly focused on the performance analysis of hydrokinetic turbines (drag-based Savonius and lift-based helical-bladed turbines). The objective of the study is set to parametrically investigate the performances of Savonius and helical-bladed turbines in terms of power coefficient, torque coefficient and starting characteristics. Based on the literature review, the Savonius turbines are developed and tested by varying number of blades, and blade shape. Similarly, the helical-bladed turbines developed and tested by varying its solidity ratio and number of steps. The field tests have been conducted at various sites like open channel flow flume, irrigation sluice and river Brahmaputra. The experimental findings are further justified through unsteady CFD simulations using ANSYS Fluent.

Efforts are also extended to measure the output characteristics of the turbines at varying immersion levels as there can be an alteration in the associated water level due to seasonal changes. The experimental data for such conditions are not reported in open literature. At the same time, it is also important to review the relevance of solidity ratio and performance degradation due to change in immersion level. Besides this, the outcome of such explorations would reduce the scarcity of field data mostly required for validation of different computational algorithms for single and multi-phase flows or solvers of fluid structure interaction.

Contents

Nomenclature

A	swept area (m^2)
a	shaft diameter (m)
C	blade chord (m)
C_D	drag coefficient
C_L	lift coefficient
C_Q	torque coefficient
C_{QS}	static torque coefficient
C_P	power coefficient
$C_{P\max}$	maximum power coefficient
D	diameter of turbine (m)
D_o	diameter of end plate (m)
d	bucket diameter/chord length of blade (m)
e	overlap distance (m)
F_D	drag force (N)
F_L	lift force (N)
H	turbine height (m)
k	turbulence kinetic energy (m^2/s^2)
M	tension in tight side (kg)
m	blade camber
N	rpm of turbine
n	number of blades
p	location of blade camber
$P_{available}$	power available to turbine (W)
$P_{kinetic}$	power extracted by rotor (W)
r_p	radius of pulley mounted on the central shaft (m)
Re	Reynolds number
T	torque of turbine (N.m)
T_s	static torque of turbine (N.m)
S	tension in slack side (kg)
t	maximum thickness of airfoil (m)
V	incoming fluid velocity (m/s)
W	relative velocity (m/s)
y^+	dimensionless wall distance

Greek symbols

α	sectional cut angle (°)
β	overlap ratio
γ	azimuth angle (°)
θ	turbine angle/reference angle (°)
σ	solidity of turbine
ρ	density of fluid (kg/m^3)
ϕ	helix angle (°)
ν	kinematic viscosity (m^2/s)
ψ	blade pitch angle (°)
Ω	angular velocity of turbine (rad/s)
ω	specific rate of dissipation (1/s)

Abbreviations

ANN	Artificial Neural Network
AR	Aspect Ratio
CFD	Computational Fluid Dynamics
FVM	Finite Volume Method
HAT	Horizontal-Axis Turbine
HHT	Helical-Bladed Hydrokinetic Turbine
PISO	Pressure-Implicit with Splitting of Operators
TSR	Tip-Speed Ratio
SHT	Savonius Hydrokinetic Turbine
SST	Shear-Stress Transport
SWT	Savonius Wind Turbine
RANS	Reynolds-Averaged Navier-Stokes
VAT	Vertical-Axis Turbine

List of Figures

List of Tables

Chapter – 1

Introduction

Chapter Outline

Overview

To meet the future energy demands, the tapping of hydro and wind energy in sustainable manner is a promising concept to reduce the dependency on conventional energy sources. Of late, the power generation from hydrokinetic and wind energy becomes the area of research because of their enormous capability for small-scale power generation. Although the conventional dam-based hydro energy converters are more efficient as compared to hydrokinetic converters, the former types are mostly dominating the large-scale power production market and have several environmental side effects. In that context, the vertical-axis hydrokinetic and wind turbines can be the viable options for the off-grid power generation. Therefore, it is important to assess their potential to generate small-scale power. This chapter gives the overview of the present status of hydrokinetic and wind energy and the motivation behind the present investigations. In addition, this chapter includes the prime objective of the present study and the detailed roadmap in order to attain the same.

1.1 Energy Scenario

Conventional energy sources are depleting with time, hence, the harnessing of renewable energy sources is of utmost importance. The fossil fuels (coal, oil, natural gas) are the major source of energy but these are non-renewable in nature and causing greenhouse gas emissions which in turn results in climate change. Obviously, the reserve of all these fossil fuels is limited. The coal being the fastest-growing global source of energy is used to meet 47% of new electricity demand. However, there is a growing interest in introducing the carbon capture and storage (CCS) technology to achieve the climate change goals by 2020, which is difficult to achieve. Due to rapid economic growth and steep rise in world population, the projected consumption of energy is 739 Quadrillion British thermal units (BTU) in 2040 which has been 356 BTU in 1990. Further, Asia is projected to have the highest increase in consumption of energy among the Non-Organization for Economic Co-operation and Development (OECD) regions (Capuano 2018).

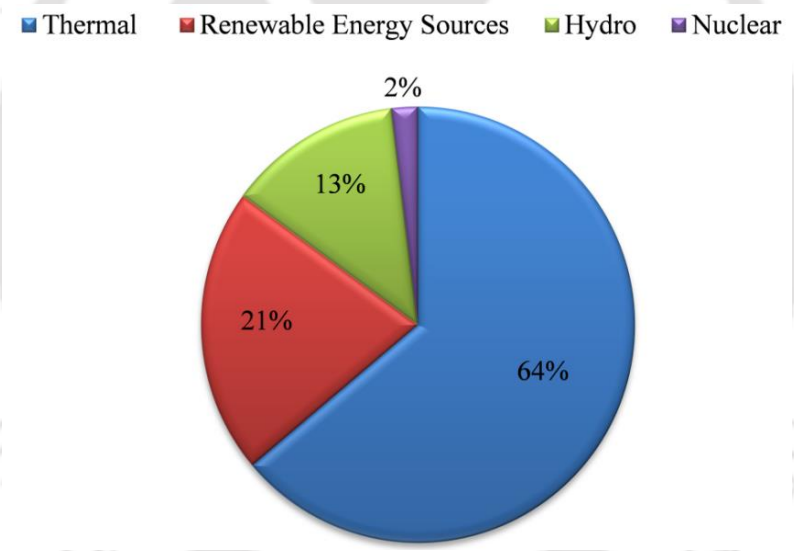

Figure 1.1: Sources of electricity in India by installation capacity

According to the report published by Central Electricity Authority of India, as on December 2018, the installed power generation capacity of India is 349288 MW of which 74081 MW is renewable energy based power. The installed power capacity in India corresponding to various sources of electricity, till December 2018, is shown in Fig. 1.1. Because of the rising greenhouse gas emissions and thus climate change, the dependency on power generation from conventional energy sources (coal, gas and diesel) has to be reduced by generating electricity from renewable energy sources (wind, solar, biomass and small-hydro). Among the renewable energy based sources, about 6% of power is produced from small-hydro power based plants, whereas, the wind contributes about 47% (CEA Report, 2018).

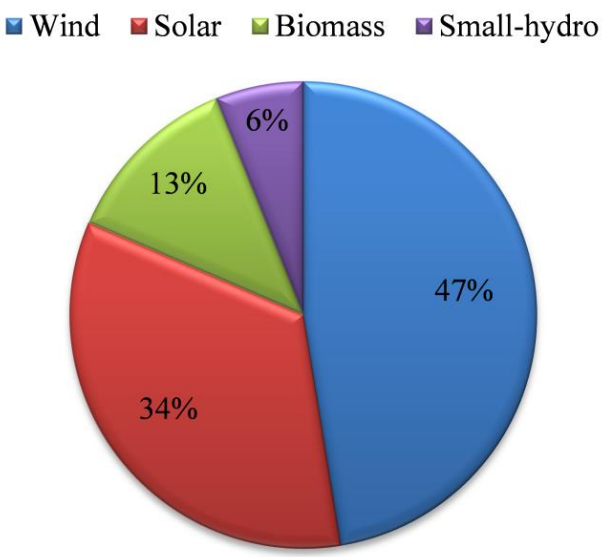

Figure 1.2: Installed electricity capacity in India based on renewable energy sources

Under these circumstances, it is essential to think of other alternative power sources such as hydro energy which is sustainable, clean, reliable, easily available and can offer significant benefits. It is the oldest form of renewable energy, and in the present time, has become one of the most important source of clean energy. It plays an important role to ensure energy supply to the growing demands of the masses and in the development of water resources. Hydropower is also the most effective way of generating electricity. Modern hydro turbines can convert up to 90% of the water potential energy into electricity. Conventionally hydropower has been harnessed by constructing dams on rivers. Although the installation costs are huge, such hydroelectric projects have low operational costs and long lifetime compared to other options of large-scale electricity generation. The water is renewable and does not depend on the market fluctuation costs. However, the development of huge artificial water reservoirs creates several major environmental and social problems like climate and wildlife change in the region, misbalancing of migration processes of some species. More recent studies of large water reservoirs created by hydroelectric dams have shown that the processes of decay of aquatic vegetation can lead to the emission of greenhouse gases (the formation and elimination of methane in the atmosphere) which are equivalent to the emissions from other electrical energy sources. Further, over the years, the construction of dams has had problems with huge numbers of residents being migrated from their native lands. Besides this, for remote community electrification, the grid extension has been reported to be uneconomical due to the low consumption and poor load factors (Vermaak *et al*. 2003).

1.2 Hydrokinetic Power

The natural power of a running river or a stream has been of interest for electricity production for many years. A more efficient use of hydro energy is the conversion of kinetic energy of free-flowing water into usable forms of energy rather than the flow being manipulated behind manmade structures (Guney and Kaygusuz 2010; Hall 2012). According to the Electrical Power Research Institute (EPRI) site selection criteria, a viable site for commercial power production normally requires peak currents of 1.5 m/s or greater (Hagerman and Polagye, 2006), although Owen and Bryden (2007) suggest this to be as low as 1.0 m/s. However, according to Thropton Energy (2010), hydrokinetic technology can be installed in any flow with a velocity greater than 0.5 m/s. The main advantage of this type of energy conversion systems is the relative simplicity and ecologically friendly (Anyi and Kirke 2010; Hydrovolts 2010). Based on the energy conversion methodology, the hydrokinetic energy converters can be broadly classified into two categories such as turbine type and non-turbine type. The working principle of turbine-type converter is based on its rotating motion, whereas the oscillating motion, torsional galloping phenomenon, buffeting phenomenon are the prime driving forces of non-turbine type converters (Fernandes and Armandei 2014, Fernandes and Rostami 2015). However, the turbine type converters are the primary choices for hydrokinetic energy conversion as non-turbine type converters are still at proof-of-concept stage (Khan *et al*. 2009). The kinetic energy of water is available during 24 hours a day, and therefore, the use of hydropower potential at a very small-scale is substantial in terms of its cost. In the case of mini-hydroelectric power, the negative environmental impacts associated with large hydroelectric power stations are also eliminated (Ellabban *et al.*, 2014). These mini-hydroelectric power plants can meet energy needs of consumers, particularly in rural areas (Lago *et al*. 2010; Yuce and Muratoglu 2015; Kumar and Saini 2016). Local industry should be encouraged to use this power for its sustainable development. There exists several concepts for harnessing the kinetic energy of the free flowing water of which turbine has been the widely accepted and proven one. Conceptually, the working principle of the hydrokinetic turbine is similar to that of a wind turbine. Since water is approximately 800 times denser than air, it implies that upon being subjected to equal velocity of wind and water, the amount of energy generated by a hydrokinetic turbine is much greater than that produced by a wind turbine. The hydrokinetic turbine is also called as water current turbine (Garman 1986), ultra-low-head hydro turbine (Radkey and Hibbs 1981), free flow/stream turbine (implying use of no dam, reservoir or augmentation), zero-head hydro turbine or in-stream hydro turbine (Gorlov 1998). For rivers or artificial waterways this turbine technology

is generally referred as River Current Turbines (RCT) or River Current Energy Conversion System (RCECS) and River In-stream Energy Converter (RISEC) and their capacity lies in the range of 1–10 kW (Dixon 2007). Similarly, in case of tidal applications, these converters are often termed as Tidal In-stream Energy Converter (TISEC). This is a low cost technology with enormous potential, with the help of which it is possible to exploit water resources to meet the needs of consumers in rural areas with little access to conventional sources of energy. According to Electric Power Research Institute (EPRI) reports, the hydrokinetic based technology may generate 13,000 MW of electricity in United States by 2025 (Dixon 2007). Under such expectations, a tidal power plant based on vertical-axis helical-bladed hydrokinetic turbine was installed in Uldolmok Strait, Korea in 2009. The plant was equipped with 1 MW capacity turbine system which generates 2.4 GWh of electricity annually (Kim *et al*. 2012; Whiting 2016). In the year 2011, additional 500 kW was commissioned and it was planned to expand its generation to 50 MW by 2018 (Whiting 2016). The various companies like Thropto Energy Services (UK), Alternative Hydro Solutions Ltd. (Canada), Lucid Energy Technologies (USA), Seabell Int. Co., Ltd. (Japan), Eclectic Energy Ltd. (UK) and Alternative Hydro Solutions Ltd developed and tested a range of prototype hydrokinetic turbines (Sornes 2010; Kumar and Saini 2017). Hydrokinetic or low head turbines are designed to be installed in a stream or current, extracting kinetic energy from the flow of water to power an electric generator without impounding or diverting the flow of the water. Considering this, the hydrokinetic turbines can be deployed in any water resource having sufficient velocity to drive. Water resources that could be harnessed using hydrokinetic systems include natural streams, tidal currents, ocean currents and constructed waterways such as channels. Installation of such systems is much simple and can be easily moved to another location or entirely removed from the waterway. However, the hydrokinetic power generation has certain advantages and drawbacks associated with it (Gorlov 1995, Kumar and Sarkar 2016, Laws and Epps 2016) as listed below:

Advantages:

- ✓ It doesn't require artificial water reservoirs to generate power.
- ✓ It can generate power at water velocity as low as 0.6 m/s.
- ✓ It has the potential to improve the power portfolio of remote locations.
- ✓ This kind of turbine can be installed in remote areas in the vicinity of rivers having little or no elevated flows to harness energy from water without using impoundment structures that cause environmental disruptions.
- ✓ The operation of this technology is free from greenhouse gas emission.

Disadvantages:

- ✓ Structures may obstruct movements/migrations of aquatic animals.
- ✓ Moving parts and mooring systems could affect bottom habitat during operation.
- ✓ Screens used to protect the machine or to reduce strike could themselves injure aquatic animals.
- ✓ On larger scales, extraction of energy from the currents may reduce the ability of streams to transport sediment and debris, cause deposition of suspended sediments and thereby alter bottom habitats
- ✓ It has relatively low efficiency.

1.3 Wind Power

Harnessing wind energy offers an immense scope like getting rid of the present reliance on fossil fuels (coal, oil, natural gas), reducing greenhouse emissions and generating local employment opportunities (Singh and Ahmed 2013; Kota *et al*. 2015). Similar to hydro energy, wind energy is also environment friendly and abundant in nature. Thus, in recent years the annual installation of wind energy converters have been increased remarkably on global, national and region levels. The first offshore wind farm having a capacity of 4.95 MW was built in Denmark in the year 1991. In the European Union (EU), a total wind capacity of 153.7 GW has been installed; out of which 12.6 GW is from offshore wind farms (Satir *et al.* 2018). The net global wind power capacity has increased from 24 GW in 2001 to 487 GW in 2016 and by 2021, it is expected to attain 817 GW. In 2016, a total of 54.6 GW wind power has been newly installed worldwide of which major contributors such as China, U.S and Germany contribute 42.8%, 15% and 10%, respectively. As per the most recent report of Global Wind Energy Council (GWEC), the wind energy market is experiencing a rapid growth globally in the marketplace against heavily subsidized conventional power generation technologies. In 2017, more than 52GW of clean, emissions-free wind power was added which brings the total installations of wind power to 539 GW globally. In 2017, Denmark received its 44% of electricity from wind, whereas, Uruguay has generated more than 30%. At the same time, wind power supplied more than 30% of electricity to the four US states, the state of South Australia, and a number of states in Germany. According to GWEC wind energy sector will gather dramatic growth in 2019 and will reach 60 GW milestone in 2020 (GWEC, 2017).

1.4 Scope of Research

Among the possible renewable energy sources, hydrokinetic and wind energies are the potential sources as they are abundant, efficient, sustainable and environment-friendly. Similar to wind power extraction systems, the hydrokinetic technologies can convert in-stream hydrokinetic power mainly from tidal currents, rivers, streams and ocean currents into useful electricity. Upon installation, these technologies can significantly impact the power portfolios of remote locations which do not have access to electricity. In that context, the drag-based vertical-axis Savonius turbines and lift-based helical-bladed turbines can be a good contender to extract hydrokinetic and wind energies for small-scale power generation. These technologies are simple to construct, omni-directional, require low installation and maintenance cost (Khan *et al.* 2009; Akwa *et al.* 2012).

It is perceived that the vertical-axis hydrokinetic or low head turbine can be a viable option for eco-friendly power generation. The performance of a hydrokinetic is influenced by several design parameters, and hence to get the maximum benefit out of this technology, the optimum design of the turbine is required. A host of researchers have been trying to improve the performance over the last few decades, but many areas of research need to be explored.

Though Savonius and helical-bladed turbine are used to harness power from hydrokinetic and wind energy, the flow fields around the hydrokinetic and wind turbines are expected to be different due to the basic difference between the wind flow and the open channel water flow. The wind flow is mainly governed by pressure difference, whereas water flow predominantly occurs due to gravity (Patel *et al.* 2017). Further, the higher power density of water has attracted the researchers to study the potential of Savonius hydrokinetic turbines (SHTs) and helical-bladed hydrokinetic turbines (HHTs).

Hitherto, a host of blade profiles have been developed and used in Savonius wind turbines (SWTs), however, SHTs have employed mostly semicircular blades (Kumar and Saini 2016). Thus, there is scope to study the influence of blade shape on the performance of the turbines. In this connection, a recently developed elliptical blade having more wind energy capturing capacity can be chosen for SHT in order to explore its performance due to basic difference in the flow field dynamics. In this connection, both experimental and computational studies can be pursued with semicircular-bladed and elliptical-bladed SHT.

Another research scope is to evaluate the performances of SHTs and HHTs at different immersion levels. Though this issue has not yet been addressed, such immersion level experiments are essential to provide the insight about the performance deviation of the turbines when there is a fluctuation in the water level because of the seasonal changes. The lack of such experimentation has led to scarcity of data required for validation of multiphase flow solver or solver that deals with fluid structure interaction.

Further studies can be made to compare the performance of SHT and SWT having an identical kinetic energy of the oncoming fluid (hydro/wind). Separate studies on the effect of different design parameters on the performance of SHT or SWT are reported in the literature. However, a comprehensive analysis of a Savonius design for known input kinetic energy but with a difference in the working fluid medium is rarely reported.

1.5 Organization of the Thesis

Chapter 1 provides the present energy scenario and motivation behind the work in the field of hydro energy/wind energy. **Chapter 2** introduces the design and performance parameters of Savonius and helical turbines. Extensive review of literatures on Savonius turbine and helical-bladed turbine has also been made. **Chapter 3** outlines the design specifications used for experimental setup, the testing sites and the experimental procedures. **Chapter 4** gives the computational methodology of the turbines under investigation. The unsteady simulations for both Savonius and helical-bladed turbines are reported. **Chapter 5** includes the experimental and computational observations related to Savonius hydrokinetic turbines (SHTs). Parametric studies of turbines based on number of blades and blade profile are also part of this chapter. **Chapter 6** contains the results of field experiments and numerical computations of the helical-bladed hydrokinetic turbines (HHTs). **Chapter 7** discusses the results of wind tunnel tests and computational analysis of Savonius wind turbines (SWTs). **Chapter 8** concludes the brief summary of the present research work and future scope of studies.

Chapter – 2

Basic Concepts and Literature Review

Chapter Outline

Overview

Due to the growing demand of clean energy, the hydrokinetic turbines are considered to be one of the most promising means of small-scale power generation. These turbines can harness energy from the free-flowing water and they have the low installation and maintenance costs. Since its inception a number of researchers have investigated the performance of drag-based Savonius hydrokinetic and lift-based helical-bladed hydrokinetic turbines. Over the years, various turbine designs have been evolved through experimental and numerical studies. However, in most cases, the performances are primarily estimated for the wind applications. The reported studies in the area of hydrokinetic turbines are very limited. This chapter gives a thorough review on various design issues and performance parameters of both the types of Savonius and helical-bladed turbines.

2.1 Hydrokinetic Turbines and Wind Turbines

Generally, hydrokinetic and wind turbines can be classified into two categories: the horizontal axis turbines (HATs), and the vertical axis turbines (VATs). Both of these turbines have their respective advantages and drawbacks. For small-scale power production of a few kW, the horizontal-axis turbines (HATs) are not cost effective. In that context, the vertical-axis turbine (VAT) serves as viable alternative which relies upon rotation about a vertical axis. Because of the following differences, a VAT is the preferable option (Akwa *et al*. 2012; VanZwieten *et al*. 2015; Kumar and Saini 2017).

- ✓ It demonstrates good self-starting abilities at slower fluid velocity and hence, it can generate power at this velocity condition.
- ✓ It does not need a yaw control system and thus, it can be installed in a more confined space than a HAT.
- ✓ Its design and manufacturing is simpler than HAT.
- ✓ It imparts less vibrational loads to the supporting structure due to its slow speed.

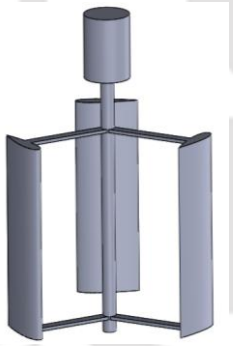

(a) Squirrel Cage Darrieus

(b) H-Darrieus

(c) Curved-Darrieus

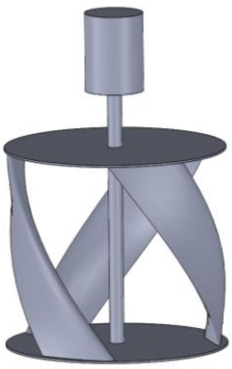

(d) Gorlov

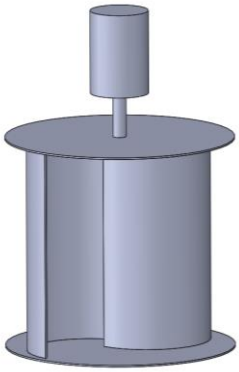

(e) Savonius

Figure 2.1: Vertical-axis turbines (Khan *et al.* 2009)

The VAT can be broadly grouped into two categories of designs: turbines based on Darrieus design and turbines based on Savonius design. Figure 2.1 shows a range of popular VATs with generators. Among these, the Gorlov (helical structured blades) and straight-bladed Darrieus turbines (H-type or Squirrel Cage type) are very common for hydro/wind applications. Further, depending upon aerodynamic force needed to rotate the blades of turbine VATs can be classified into drag-type and lift-type.

2.1.1 Drag-based Turbines

The typical drag force driven VATs are the Savonius rotor and the Sistan rotor (Faizala *et al.* 2010; Wong *et al*. 2017). These turbines possess a better self-start ability when compared to the lift-type VATs. Such turbines consist of a number of straight or concave cup shaped blades which utilize the push force of the incoming fluid to rotate the turbine. In a drag-type device, the primary motive force is the stagnation pressure of the fluid pushing against the profile of the turbine cup, paddle, or blade (Alam and Iqbal 2009). The Savonius rotors, the most popular type of VATs was developed and patented by a Finish engineer S. J. Savonius in 1920s (Savonius, 1931).

The Savonius turbine mainly consists of the rotating components like buckets/blades and endplates, which are mounted around a central shaft. A schematic diagram of the vertical-axis Savonius turbine is shown in Fig. 2.2. Its outlook resembles to an 'S' shape when viewed from the top. This turbine design is comprised of two semicircular shaped blades/buckets placed such a way that concave part of one blade faces the other but with a slight overlap in the middle (Fig. 2.2). In a two-bladed turbine design, one of the blades is termed as an advancing blade, whereas the other one is called a returning blade. In such system, turbine rotates mainly due to the drag force between the concave and convex side of the blades. In addition, the lift force also contributes to the net torque generation at different angular positions. In general, the advancing blade is subjected to more drag force than the returning blade to produce a positive torque. The negative torque on the returning blade due to drag force should be kept to a minimum. Unlike the HATs, the positive torque is not always developed when the incoming fluid stream interacts with the rotating blades of VATs. The negative torque that reacts in the counter direction reduces the overall performance of the VATs. The main drawbacks of the Savonius turbine lie with its low efficiency and with its difficulty to integrate with a generator because of its low operating speed (Alam and Iqbal, 2009; Akwa *et al.* 2012; Roy and Saha 2013; Jin *et al.* 2015). However, the advantages

include design simplicity, independency of fluid flow direction and good starting characteristics. Further, it is cost effective and has less vibrational load on the supporting structure (Altan and Atilgan 2008; Patel *et al*. 2017). Considering these advantages, Savonius wind and Savonius hydrokinetic turbines are studied both experimentally and numerically by the researchers across the globe.

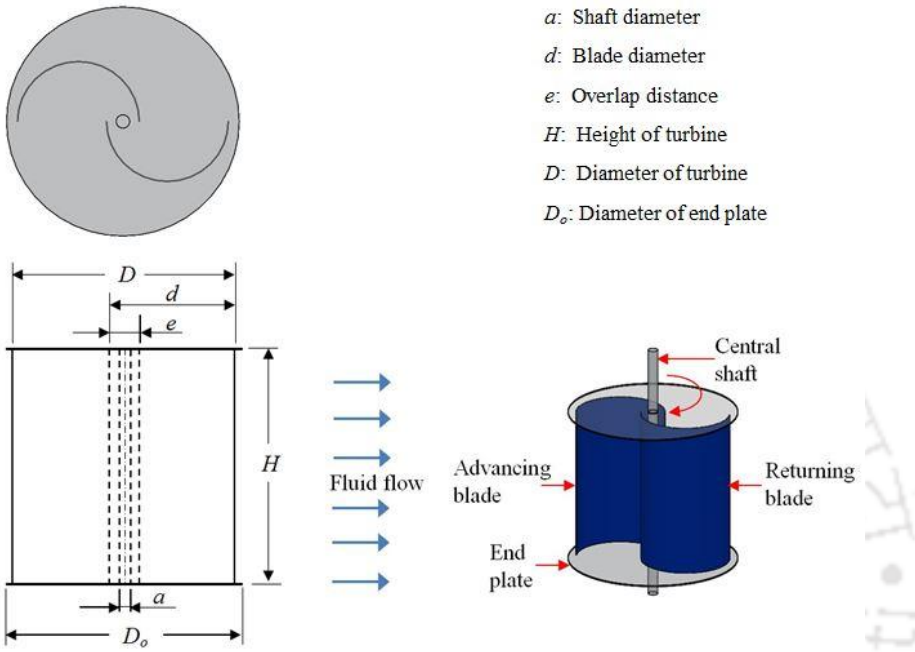

Figure 2.2: Vertical-axis Savonius turbine

2.1.2 Lift-based Turbines

The lift-type VATs that include the H-rotor and Darriues rotor are constructed with airfoil shaped blades (Fig. 2.3). As the water/wind flows over the blades, the turbine starts rotating due to the aerodynamic lift force. The lift-type VATs perform efficiently but they suffer difficulty in self-starting (Gorlov 1998; Shiono *et al*. 2002; Nguyen *et al*. 2015; Marsh *et al*. 2015). Darrieus first developed a vertical-axis straight-bladed hydro turbine integrated with a generator to produce electricity (Darrieus, 1931). Such straight-bladed turbines are not used extensively because of their poor self-starting characteristics and high torque fluctuation. Further, Alexander M. Gorlov in the year 1995 proposed a helical-bladed hydrokinetic turbine that operates at low or zero water head. As per Gorlov, a large mass of water with a relatively low velocity can produce high rotational speed and improved power output without significant vibration (Gorlov and Rogers 1997; Gorlov 1998). The main advantages of the helical-bladed turbine lie with its better self-starting characteristics together with its reduced torque oscillation as compared to straight-bladed turbine (Scheurich *et al.* 2010; Niblick

2012; Marsh *et al.* 2015). Hence, some researchers have suggested a hybrid VAT that combines both types of VATs to overcome their weaknesses (Jin *et al*. 2015).

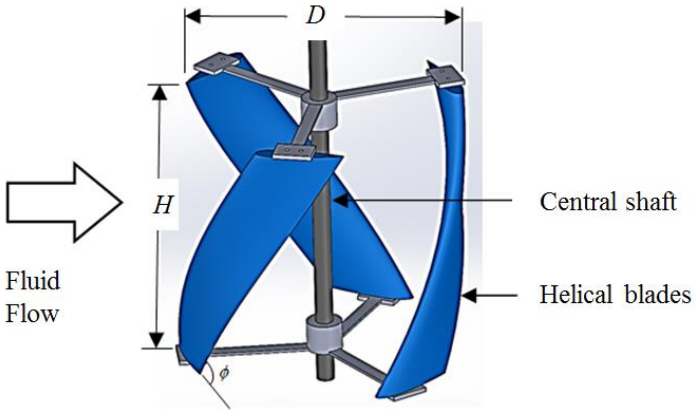

Figure 2.3: Lift-based vertical-axis helical-bladed turbine

For energy extraction using lift rather than drag, it requires specially shaped airfoil surfaces, like those used on airplane wings. The lift-based vertical-axis Darrieus and helical-bladed turbines are cross-flow devices. These turbines make use of lift force developed by fluid motion around an airfoil at an angle relative to the blade chord (known as the angle of attack) causing a pressure difference on one side of the blade as compared to the other. The lift force acts in a direction perpendicular to relative fluid velocity. In such lift-based devices, the drag force is also developed because of the fluid flow over airfoil and it normally opposes the rotation of turbine. However, the average tangential force developed by lift force overcomes the retarding drag force, and therefore the net tangential force acting at a radius of the turbine generates positive torque and power. Figure 2.4 depicts the aerodynamic forces acting on the drag-based and lift-based turbines.

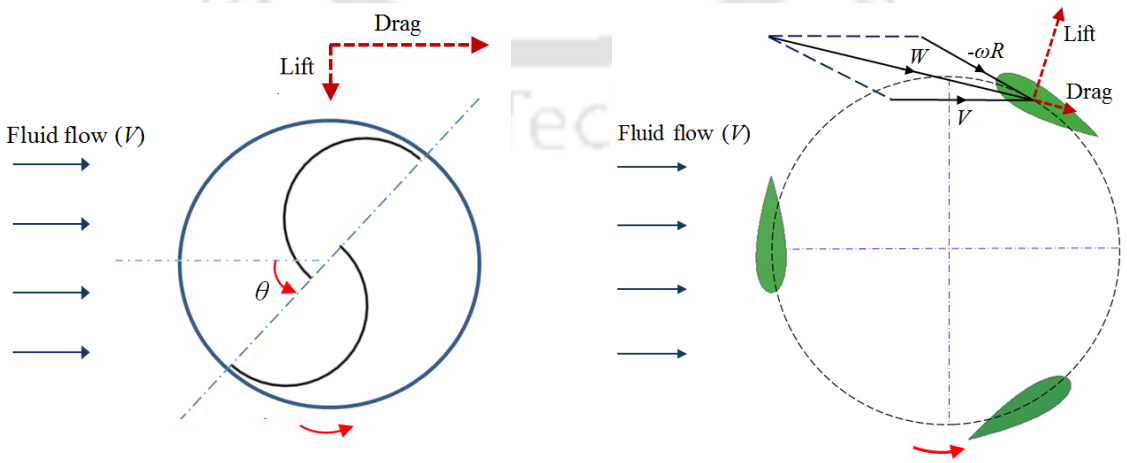

(a) Savonius turbine (b) Helical-bladed turbine

Figure 2.4: Aerodynamic forces acting on turbines

2.2 Performance Parameters

In this section, the basic performance parameters of vertical-axis drag/lift based turbines such as power coefficient (C_P), torque coefficient (C_Q), lift coefficient (C_L) and drag coefficient (C_D) are discussed (Kamoji *et al.* 2009; Roy and Saha 2013; Kumar and Saini 2017).

2.2.1 Power coefficient (C_P)

Power available in incoming water/wind depends up density of medium (ρ), fluid velocity (V) and projected area of turbine (A) and it is given by

$$P_{kinetic} = \text{Kinetic energy} \times \text{Mass flow rate}$$

$$P_{kinetic} = \frac{1}{2}\rho A V^3 \tag{2.1}$$

Because of the cubic relation fluid velocity mainly affects the available power. Swept area also has a direct impact on the available power since increase in available area increases the power. The power generated by the turbine is given by

$$P_{turbine} = \frac{2\pi NT}{60} \tag{2.2}$$

where T is the torque produced by the turbine rotor and N is the rotational speed of the turbine.

The power coefficient (C_P) of a turbine is represented as the ratio of power actually produced by the turbine ($P_{turbine}$) to the kinetic power available in the fluid ($P_{kinetic}$). Thus, the power coefficient of a turbine is given by

$$C_p = \frac{P_{turbine}}{P_{kinetic}} \tag{2.3}$$

2.2.2 Torque coefficient (C_Q)

Similarly, the torque coefficient is defined as the ratio of the torque generated by the device to the torque generated by the freestream fluid if all of the kinetic force is concentrated at the full radius. In case of turbines, the dynamic and static torques are used to analyze the performance. Dynamic torque is the net torque of the turbine at rotating condition and it is mainly responsible for the power producing ability of the turbine. Similarly, the static torque is defined as the net torque of turbine at static condition. A static torque coefficient, C_{QS} is

calculated by substituting rotating torque (T) with static torque, T_S. It is depicts the starting ability of the turbine.

The dynamic torque coefficient (C_Q) is given by

$$C_Q = \frac{T}{\frac{1}{2}\rho A V^2 R} \tag{2.4}$$

where R is the radius of turbine.

2.2.3 Lift coefficient (C_L)

Lift force (F_L) is defined to be force perpendicular to the direction of incoming air flow. The lift force is a consequence of the unequal pressure on the upper and lower surfaces of turbine blades. Lift coefficient (C_L) is given by

$$C_L = \frac{F_L}{\frac{1}{2}\rho V^2 C} \tag{2.5}$$

where C is the blade chord length and F_L is the lift force.

Jaohindy *et al*. (2013) conducted numerical investigation for a two-semicircular-bladed SWT and obtained the maximum C_L to be around 1.72 at turbine angle (θ) = 30° and 210°.

2.2.4 Drag coefficient (C_D)

Drag force (F_D) is usually to be parallel to the direction of the oncoming air flow. It is due to both the viscous frictional forces at the surface of the rotor and the unequal pressure on the rotor blade surfaces facing toward and away from the oncoming flow. Drag coefficient (C_D) is given by

$$C_D = \frac{F_D}{\frac{1}{2}\rho V^2 C} \tag{2.6}$$

Previous experimental work reported by Irabu and Roy (2011) indicated the maximum C_D for the two-semicircular-bladed SWT to be 1.56 at θ = 90° and 270°. Similarly, Jaohindy *et al.* (2013) conducted numerical investigation to analyze effect of C_D for a two-semicircular-bladed SWT and the maximum C_D is reported to be around 2.2 at θ in the range of 60°–70° and at tip-speed ratio (TSR) = 0.6.

2.2.5 Tip-speed ratio (*TSR*)

The tip-speed ratio or *TSR* for the turbines is the ratio between the rotational speed at the tip of a blade and the actual velocity of the fluid. The tip speed ratio is related to efficiency. Higher tip speeds result in higher noise levels and require stronger blades due to large centrifugal forces. It is given by

$$TSR = \frac{\Omega R}{V} \tag{2.7}$$

where, Ω is the rotational speed of turbine (rad/s).

2.2.6 Reynolds number (*Re*)

Reynolds number is defined as the ratio of inertial to viscous force in the flow regime of a turbine. Based on the turbine diameter it is expressed as:

$$Re = \frac{VD}{\nu} \tag{2.8}$$

where, υ is the kinematic viscosity of the fluid (m^2/s) and D is the diameter of the turbine (m).

Reynolds number (*Re*) plays a major role on the flow separation and boundary layer formation around the turbine blades. The numerical investigation on SWT by Akwa *et al* (2012) revealed an improvement of C_{QS} from 0.09 to 0.22 when the *Re* increases from 0.4×10^5 to 8.67×10^5. Kamoji *et al.* (2009) studied the effect of *Re* for a modified SWT (β = 0, *AR*= 0.7). The study demonstrated an increase in C_P value with the increase in *Re* and the C_P value was found to be increased by 19% as *Re* increases from 8×10^4 to 1.5×10^4. However, value of C_{QS} is found to unchanged for the same range of *Re*. Similar enhancement of C_P value with increase in *Re* for conventional semicircular bladed SWT has been reported by Shankar (1979) and Kamoji *et al* (2008).

2.3 Design Parameters of Savonius Turbine

In order to obtain optimum performance, several design parameters like overlap ratio, end plate diameter, number of blades and blade profile affect the performance of a vertical-axis Savonius hydrokinetic or wind turbines. In this section, detailed descriptions of design parameters are discussed.

2.3.1 Overlap ratio (β)

The selection of overlap ratio of Savonius turbine is crucial for achieving better performance. It is obtained by dividing the overlap distance between the turbines blades (e) by the blade diameter (D) and is expressed as:

$$\beta = \frac{e}{D} \tag{2.9}$$

The Savonius turbine with overlapping blades (Fig. 2.5a) has better starting abilities in comparison to a non-overlapping bladed design. Due to the overlapping flow between the blades, the negative torque generated by the returning blade reduces and hence, the average power of the turbine increases. However, large overlap distance may results in the reduction in torque output due to the generation of vortex in the overlapping region of the turbine. There is no consensus in the literatures regarding the optimum overlap ratio of a Savonius turbine. Blackwell *et al*. (1977), Fujisawa (1992, 1994), Kamoji *et al*. (2009), Nasef *et al*. (2013) have carried out experimental investigation and reported β of 0.15 for Savonius turbine.

Kamoji *et al*. (2009) investigated the effect of overlap ratio on modified and conventional Savonius turbine. In case of modified Savonius turbine, the increase in the β resulted in higher losses because of the generation of vortices which eventually lower the aerodynamic performance. Furthermore, for a conventional turbine, the loss due to vortices increases for β greater than 0.15. Thus, authors stated that conventional Savonius turbines show better performance at β of 0.15, whereas the modified Savonius turbines yield improved performance with no overlap between the blades. Yaakob *et al*. (2010) computational studied the effect of overlap ratio on SHT by taking β = 0.1 – 0.6 and found turbine (β = 0.21) to be best performing. Further, few researchers like Mahmoud *et al.* (2012) and Driss *et al.* (2012) revealed that the turbines with no overlap demonstrate superior performance. Mahmoud *et al.* (2012) experimentally investigated the performance of two-bladed SWT for a range of β like 0, 0.2, 0.25, 0.3 and 0.35 and reported enhanced power for turbine with β = 0. Thus, it is observed from the majority of literatures that turbine having β in the range of 0.15 – 0.25 is preferable in order to obtain enhanced performance.

2.3.2 Aspect ratio (AR)

The aspect ratio (*AR*) is a decisive non-dimensional parameter for satisfactory performance of a turbine. It is the ratio of height of the turbine blade (*H*) to diameter of turbine (*D*) as shown in Fig. 2.5b and can be expressed as:

$$AR = \frac{H}{D} \tag{2.10}$$

A low aspect ratio (<1.5) is often suitable for Savonius turbines for achieving structural stability. An increase in diameter of turbine results in increase of generated torque with simultaneous reduction in rotational speed. The aspect ratio of a turbine can also be adjusted according to the rotational rate of the electrical generator. With the increase of *AR*, the angular acceleration of turbine increases, with simultaneous decrement of moment and inertia of the turbine (Vance 1973).

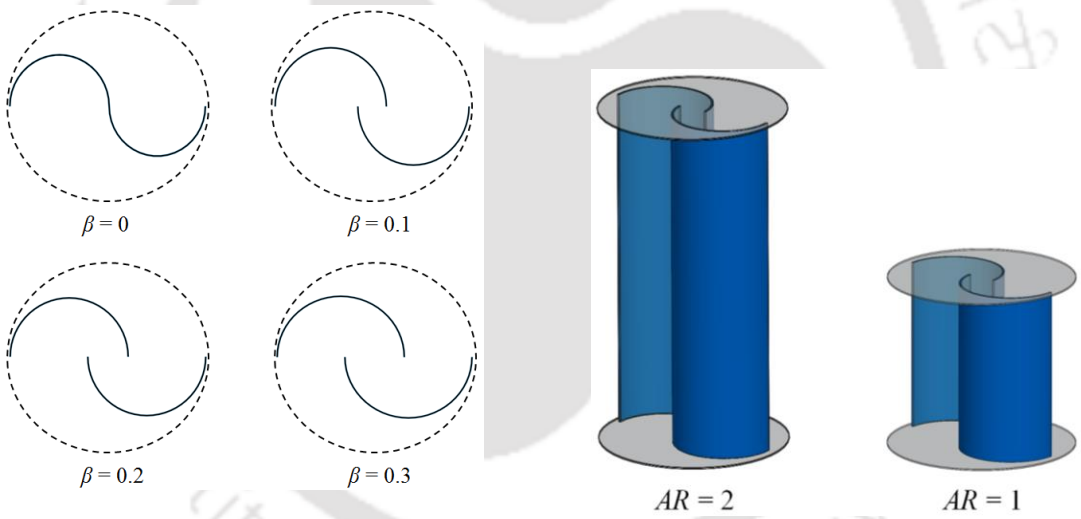

(a) Overlap ratio (b) Aspect ratio

Figure 2.5: Savonius turbine with different overlap ratios and aspect ratios

2.3.3 End plate

The end plates are used in order to hold the turbine blades in place. The addition of end plates to the Savonius turbine helps in achieving better power coefficient and higher tip-speed ratios (Alexander and Holownia 1978; Akwa *et al*. 2012; Jeon *et al*. 2015). The end plates help in preventing leakage of fluid from the concave side of the blades, thereby helping in maintaining uniform pressure along the height of the turbine.

Sivasegaram (1978) carried out an experimental investigation to study the effect of the end plate size and found optimum end plate diameter (D_o) as 1.1 times of turbine diameter (D). Ogawa and Yoshida (1986) analyzed the effect of shape of the end plates on the performance of the Savonius turbine and the study revealed significant improvement of power coefficient for simple circular shaped end plate, however, almost similar behavior of starting torque has been noticed for all the shapes. Therefore, there is a consensus in the literature regarding the optimal size of the end plate and the recommended size is equivalent to 1.1 times the rotor diameter to obtain better performance. Further, it should have negligible thickness, relative to the height of the turbine. It has also been noted that very high diameters for the end plates can dramatically increase the rotor inertia (Vance 1973; Alexander and Holownia 1978; Ushiyama and Nagai 1988; Saha *et al*. 2008).

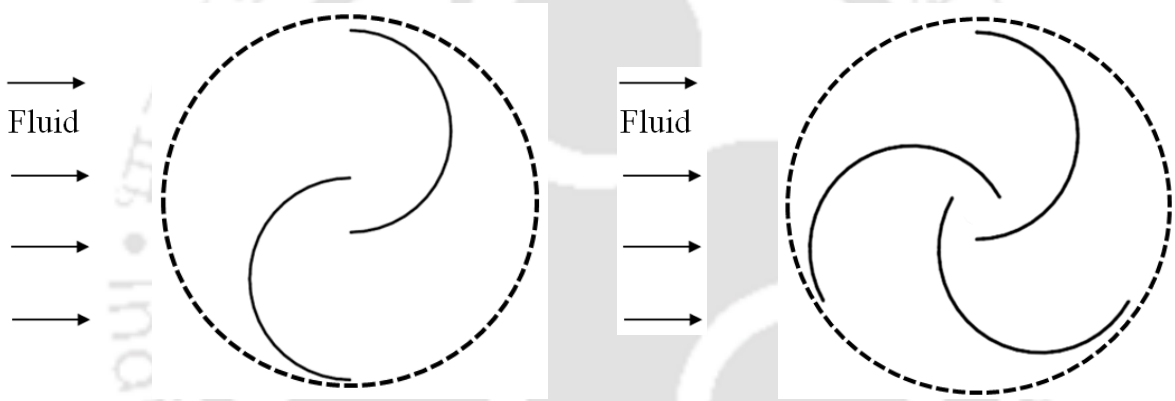

(a) Two-bladed turbine (b) Three-bladed turbine

Figure 2.6: 2D view of Savonius turbines with semi-circular blades

2.3.4 Number of blades (*n*)

The number of blades of a Savonius turbine (Fig. 2.6) plays a crucial role in achieving better performance of turbine. With the increase in number of blades, the pulsation of dynamic as well as static torque of a turbine is reduced along the various turbine angle or angular positions of the turbine blades. Emmanuel and Jun (2011) carried out 2D CFD analyses in order to improve the performance of Savonius turbine (AR = 2) by varying the number of blades between two to six. The study revealed improved a maximum power coefficient ($C_{P\max}$) of 0.30 for six-bladed turbine which is higher than the conventional two-bladed Savonius turbine. Wenehenubun *et al*. (2015) investigated the variation of performance for Savonius turbine (AR = 1.0, β = 0.15) with change in blade number from two to four. Authors concluded that three-bladed turbine has the best performance at high TSR and four-bladed turbine showed best performance at low TSR. Further, the four-bladed turbine demonstrated

high torque compared with two- or three-bladed turbine. Sheldahl *et al*. (1978) tested two- and three-bladed turbine having AR = 1.0 and β = 0.15. The two-bladed turbine showed better aerodynamic performance than for a three-bladed configuration. The authors obtained C_{Pmax} as 0.24 for two-bladed turbine whereas three-bladed turbine demonstrated $C_{P\max}$ of 0.15. According to Vance (1973), Blackwell *et al*. (1978) and Saha *et al.* (2008), the pulsation of static and dynamic moment of a Savonius turbine is reduced with simultaneous reduction in performance due the addition of extra blades along the angular positions of the advancing bucket. Further, Saha *et al*. (2008) and Hayashi *et al*. (2005) recommended the use of multi-stage turbine as a solution to reduce the moment fluctuations, without significant performance loss.

2.3.5 Blade profiles

The blade profile affects the performance of a Savonius turbine significantly. In addition to the traditional "S" shaped blade of Savonius turbine, several blade shapes developed by Bach (1931), Benesh (1988) and Mohamed (2011) are reported for wind turbine application. The 3D blade profiles such as twisted and helical blades are subsequently tested by Grinspan *et al.* (2001), Saha and Rajkumar (2006) and Saha *et al*. (2008). Furthermore, investigation of turbines with helical blades revealed smoother torque characteristics with marginal improvement in C_P (Kamoji *et al.* 2009; Zhao 2009; Damak *et al.* 2013).

Kamoji *et al.* (2009) reported positive static torque coefficient at all angular positions for helical-bladed Savonius turbine and such turbine (AR = 0.88; β = 0) without shaft demonstrated almost same C_P with semicircular-bladed turbine. Further, Damak *et al.* (2012) obtained C_{Pmax} of 0.20 and 0.16 for helical- and semicircular-bladed Savonius turbines, respectively. Tian *et al.* (2015) proposed a new blade profile and the results showed an improvement of a $C_{P\max}$ value by 10.98% for half-ellipse blades as compared to semicircular-blades.

2.4 Design Parameters of Helical Bladed Turbine

This section deals with major design parameters for helical-bladed hydrokinetic turbine (HHT).

2.4.1 Solidity ratio (σ)

Solidity is defined through an equation relating to the number of blades (n), chord length of blade (C) and turbine diameter (D). This variable represents the amount of circumference of

the turbine that is solid compared to the total circumference. It is defined by and expressed as in Eqn 2.11 (Shiono *et al*. 2002; Niblick 2012; Bachant and Wosnik 2015; Pongduang *et al.* 2015).

$$\sigma = \frac{nC}{\pi D} \tag{2.11}$$

The turbine with high solidity can easily self-start but it operates at a lower tip-speed ratio (*TSR*), whereas low solidity device suffers from difficulty of self-starting especially at low freestream flow (Twidell and Weir 2006). The lower solidity turbine offers less obstruction to the freestream flow which allows higher stream-wise velocity at the turbine blades and results in lower rotational speed. Shiono *et al.* (2002) conducted experimental investigation on effect on solidity ratio on performance of helical-bladed turbine. They revealed that C_P remains constant for σ = 0.20 – 0.40 and C_P value drops for σ = 0.50.

2.4.2 Number of blades (*n*)

Number of blades has direct relation with solidity. For any turbine, as the number of blades increases, the chord length of a blade must be decreased to maintain a desired solidity ratio. Conversely for constant chord length, as the number of blades increases the solidity of the turbine also increases. Increasing number of blades results in increased starting torque, a lower operating *TSR*. As the number of blades is increased, blade wake interference becomes a concern, where an advancing blade's performance gets altered by another blade's wake (Twidell and Weir 2006). Niblick (2012) compared the performance of three- and four-bladed HHT (*AR* = 1.36) with NACA 0018 profile and reported superior performance four-bladed HHT at same σ = 0.30. The former showed a $C_{P\max}$ of 0.10 while the later demonstrated $C_{P\max}$ = 0.16. Han *et al*. (2018) conducted wind tunnel experiments on four-bladed helical turbine (σ = 0.30, *AR* = 1.3) with NACA 0018 and obtained $C_{P\max}$ of 0.19 and 0.18 for wind speeds of 8 m/s and 9 m/s, respectively.

2.4.3 Aspect ratio (*AR*)

As mentioned in section 2.3.2, here as well, aspect ratio is referred to the ratio of blade height to diameter of turbine as in Eqn. 2.12 and Fig. 2.7. As the blade length increases blades may be subjected to deflection, vibration and stress. Again for the ease of installation and deployment one must consider size constraints.

$$AR = \frac{H}{D} \tag{2.12}$$

where, H is the height of the turbine.

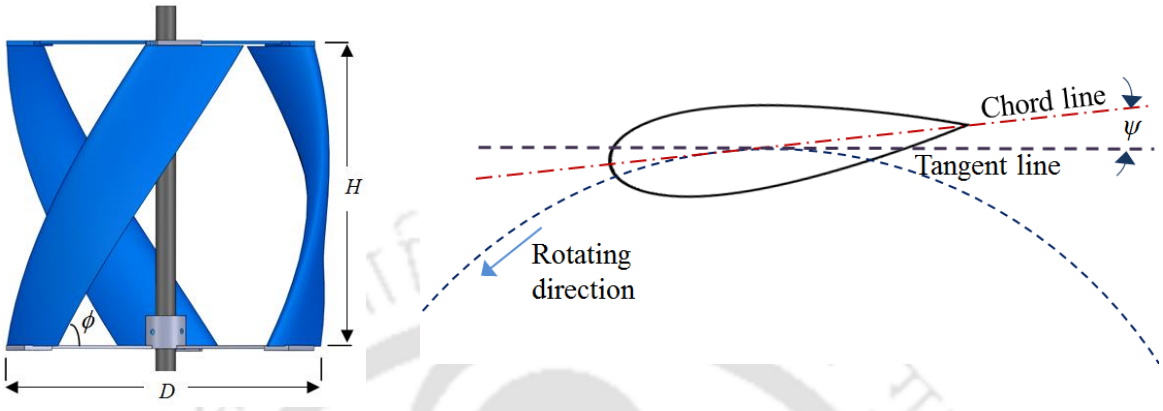

(a) (b)

Figure 2.7: The CAD model of HHT

2.2.5 Helix angle (ϕ)

For vertical-axis HHT, a helix angle (ϕ) is the angle that the blade makes with a horizontal plane (Fig. 2.7). The blades inclined to the flow, such as those on helical turbines can improve self-starting (Gorlov 1998; Shiono *et al*. 2002; Marsh *et al*. 2015). Shiono *et al*. (2002) investigated effect of ϕ ranging from 43.7° to 60° on performance of HHT and found that performance of the turbine improves with increase in ϕ. The testing revealed $C_{P\max}$ of 0.16, 0.18 and 0.21 for turbines having ϕ of 43.7°, 50° and 60°, respectively. Pongduang *et al*. (2015) carried out on-site testing on variants of three-NACA0020 bladed HHT with ϕ = 120°, 135°, and 150° and a better performance was reported at ϕ = 135°.

2.4.6 Blade Profile

Selection of hydrofoil/airfoil profile is the most critical factor in achieving better turbine performance. Blade profile has a significant impact on performance due to the forces developed when subjected to an incoming flow. The blade design parameters include chord length (C), leading edge profile, trailing edge profile, blade thickness-to-chord ratio, location of maximum thickness and blade camber (m). The chord line is simply a straight line connecting the leading edge to the trailing edge of the airfoil whose length is defined as the chord length. The blade camber refers to the position of the mean thickness of a blade along its length. So the camber line and the chord line are collinear for a symmetric uncambered blade. The NACA airfoils are developed by the National Advisory Committee for

Aeronautics (NACA) and shape of the NACA airfoils is depicted using a series of digits following the word "NACA". The NACA 4-series airfoil is expressed by a mean camber line and thickness distribution. In Fig. 2.8 the mean camber line is the dashed line that splits the airfoil in two halves. The maximum thickness (*t*) is located at 30% of the chord for NACA 4-series airfoil sections. A typical cambered NACA 6424 airfoil is shown in Fig. 2.8. The values of *m* and *t* are expressed as percentages of the *C*. This has a maximum camber of 6% located at 40% of the chord with a *t* of 24% of *C* located at 30% of *C*.

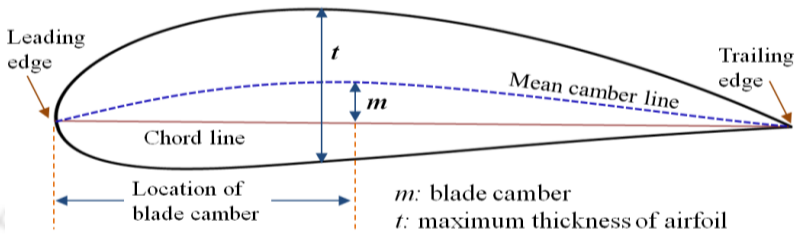

Figure 2.8: Cross section of NACA 6424 airfoil

The most common blade profiles used for vertical-axis Darrieus turbine are the symmetrical NACA airfoils whose thickness ranges from 12% to 21% (Tjiu *et al*. 2015). Nguyen *et al.* (2015) carried out computational analysis for vertical-axis Darrieus turbine having symmetric NACA airfoils with 12%, 15%, 18% and 22% thickness. The analysis revealed that the power coefficient is proportional to the thickness till *TSR* of 2, beyond which 15% and 12% thick NACA airfoils show improved performance. Although NACA 0012 gives a good performance at higher rotational speeds or *TSR*, its performance at lower *TSR* is quite low. Both NACA 0012 and NACA 0015 give better performance at higher rotational speeds or *TSR*, however, NACA 0022 shows the best overall performance as it performs well for high and low *TSR*s. Fiedler and Tullis (2009) also analyzed the performance of Darrieus turbines having NACA 0021 and NACA 0015 cross section over a wide range of *TSRs* and revealed improved performance of NACA 0021 in comparison to NACA 0015. Further, the effect of cambered airfoil on performance has also been studied, however, no remarkable difference in the performance has been achieved as compared to the turbine with symmetrical airfoil. This is because cambered airfoil causes an increase of tangential force in one half of the swept region with simultaneous decrement of force in the other half (Deglaire *et al.* 2009).

2.4.7 Blade pitch angle (ψ)

Blade pitch angle (ψ) refers to the angle between the airfoil chord and the line tangent to the circle of revolution of the turbine as shown in Fig. 2.7.

2.5 Computational Investigations

The flow field around the vertical-axis turbine is time dependent and complex in nature due to the flow separation and wake formation. It is difficult to capture this kind of complex unsteady flow physics using classical tools like stream tube model which is based on blade element momentum theory. Also, the soft-computing techniques like fuzzy logic, artificial neural networks (ANN) and genetic algorithms have the promising capability to predict the power factor of several energy systems. Further, the adaptive neuro-fuzzy inference system (ANFIS) has the effective methodology to estimate the power output over other soft computing techniques (Roy and Saha 2013; Wang *et al.* 2014; Olyaie *et al*. 2015).

The streamtube model which is based on the blade element theory is reported to be effective for the analysis of a Darrieus turbine at low *TSR* (Islam *et al.* 2008). At the same time, it fails to predict the performance of Savonius turbine (Paraschivou 2002; Biadgo *et al.* 2013). The large turbine area as compared to the flow swept area of Savonius turbine accounts for this behaviour. In addition, the staggered curved blades hinder the stream tube model to create the complete flow field as an isolated cross-sectional flow pattern and also to calculate the forces on the curved surfaces.

In the initial stages of analysis on Savonius turbines, the analytical calculations were carried out without taking into account the effect of flow separation which resulted in unrealistic performance prediction. However, these studies formed the baseline for the subsequent investigators (Wilson *et al.* 1976; Van Dusen and Kirchhoff 1978). Further, in the literature it has been reported that by dealing with the phenomenon like flow separation and vortex formation around the turbine, the discrete vortex method has the capability to predict the performance which considers the flow to be a blend of a finite number of discrete vortices (Ogawa 1984; Kotb and Aldoss 1991). The torque and power of a turbine are estimated here using pressure and velocity distrbution on both sides of the turbine blades.

For solving a wide range of industrial and non-industrial fluid flow problems, the computational fluid dynamics (CFD) is the most powerful tool at present. The three dimensional finite volume based solvers/ softwares such as ANSYS Fluent, CFX, ADINA, Star CCM+ and COSMOS-FloWorks have been used widely by the researchers at present to simulate the performance of Savonius and Darrieus turbines. In the finite volume method

(FVM), the selection of computational domain, grid size, turbulence model, capturing of boundary layer play a key role in obtaining accurate results.

The flow field around the Savonius or Darrieus turbines is generally turbulent in nature. Therefore, selection of suitable turbulence model is very important for obtaining the accurate results. However, each turbulence model has its own limitations. The Spalart-Allmaras (SA) model is a one-equation turbulence model, in which the near wall gradients of the transported variable are considerably smaller than the turbulent kinetic energy equation based (k–ε) models. Thus, this model is less sensitive in the near walls treatment around the blades of Savonius turbine (Roy and Saha 2013). In standard k–ε turbulence model, flow is assumed to be fully turbulent and neglects the effects of molecular viscosity for estimating the turbulent length and time scale while solving transport equations for k and ε. The standard k–ε model is the basic k–ε turbulence model and has given better results than SA model for turbine analysis (Pope *et al*. 2010; Ghasemian *et al*. 2017). The RNG k–ε turbulence model was obtained incorporating a statistical technique called ‘‘renormalization group” (RNG) theory. The RNG k–ε turbulence model considers the effects of rotation on the eddy viscosity and thus, an additional term is included in ε equation for rapidly strained flows. In addition, this turbulence model utilizes an analytical formula to calculate turbulent Pandtl numbers unlike constant values as in case of standard k–ε model. These features make the RNG k–ε turbulence model more accurate and reliable for a range of turbulence flows problems as compared to standard k–ε turbulence model. The realizable k–ε model uses modified turbulent viscosity and dissipation rate terms. As per literature, both the realizable and RNG k–ε models have found to be significantly improved models over the standard k–ε and SA models (Rogowski and Maronski 2015). This model demonstrates superior ability to capture swirling flows and the flows involving separation and recirculation. It was suggested in earlier studies (Castelli *et al.* 2011; Mohamed 2012, 2013; Mohamed *et al.* 2015; Chen and Lian 2015) that Realizable k-ε turbulence model is superior to simulate the rotating behavior of blades or airfoil, flow through the channel and separated flows. This model has two major differences from the Standard k–ε. It is comprised of a new formulation for the turbulent viscosity and a new transport equation for the dissipation rate ε, derived from an exact equation for the transport of the mean-square vorticity fluctuations. Further, this model does not rely on the assumed relationship between the Reynolds stress tensor and the strain rate

tensor. In the realizable k-ε model, the model constant (C_μ) is expressed as a function of mean flow and turbulence properties, unlike in the standard model, it is assumed to be constant.

The shear stress transport (SST) k–ω turbulence model is a two-equation eddy viscosity model combining the advantages of both k–ε formulation for free stream flow and k–ω formulation in the turbine boundary layer. Further, it exhibits less sensitivity to free stream conditions (far field) than other turbulence models. This SST k–ω turbulence model is utilized throughout the flow field as it is well suited for simulating flow in the viscous sub-layer (near wall) where a high boundary layer accuracy is required. This two-equation turbulence model effectively captures a wider class of flows like flow with adverse pressure gradients, flow over airfoils, rotating flows and low Reynolds number flows (Menter 1994; Roy and Ducoin 2016). Nasef *et al.* (2013) computationally compared the performance of SWT with experimentally obtained results. Different turbulence models viz k–ε, RNG k–ε, realizable k–ε and k–ω SST, and k–ω SST model were employed for simulations and good agreement with experimental data was noticed. The superior prediction capability of the SST k–ω turbulence model for 2D flow analysis over a Savonius wind turbine was widely reported (Abraham *et al.* 2011; Edwards *et al.* 2012; Jaohindy *et al.* 2013 and Roy and Ducoin 2013). Further, for 3D simulations, k–ω SST turbulence model had very good agreement with experimental results (Plourde *et al.* 2012; Alom and Saha 2018). Similarly, SST k–ω was also used by in case of performance simulation of HHTs. (Le *et al.* 2014; Tsai and Chen 2014; Marsh *et al.* 2015). The k–ω SST model has the ability to accurately model both free stream and boundary layer regions along with improved prediction of flow separation for adverse pressure gradients because of the inclusion of transport effects into the formulation of the eddy-viscosity. Therefore, the k–ω SST CFD turbulence model commonly used for vertical-axis turbine simulations (Dai and Lam 2009; Gretton 2009; Castelli and Benini 2012; Bruce 2014; Marsh *et al.* 2016).

The incompressible flow solvers can be employed as the Mach number for vertical-axis Darrieus turbine application is less than 0.30. There are many pressure-velocity coupling algorithms viz SIMPLE (Semi-Implicit Method for Pressure Linked Equations), PISO (Pressure-Implicit with Splitting of Operators) and COUPLED pressure-velocity coupling. The SIMPLE algorithm uses a relationship between velocity and pressure corrections to enforce mass conservation and to obtain the pressure field. It ensures a good solution stability through the pressure-velocity coupling (Roy and Ducoin, 2016). The SIMPLE scheme, on the

other hand, is computationally inexpensive and its convergence is faster in comparison to other schemes. Lanzafame *et al*. (2014) carried out 2D investigation on vertical-axis Darrieus turbine and obtained superior results using the PISO scheme, whereas SIMPLE scheme was reported to have inferior results at low tip-speed ratios. Further, the COUPLED scheme could not predict the flow physics for the flow over turbine blades. The Large Eddy Simulation (LES) is based on a scale separation and it is accurate, however, it is rather computationally expensive in order to simulate the performance of VAWTs (Ghasemian *et al*. 2017).

2.5.1 Simulation Methods

The computational fluid dynamics (CFD) simulation is frequently used as a numerical approach as an alternate to more expensive experimental studies in order to validate the performances of turbines. The power coefficient of the turbine can be estimated through two simulation methods. First method states a CFD simulation of turbine at a given *TSR* while the second method describes simulation of turbine with a given load.

Fixed *TSR* Simulation: The fixed *TSR* simulations are frequently used for studying the performance of a VAT. In such type of simulations, the sliding mesh is used for modelling the rotation of the turbine. In the sliding mesh technique, two or more cell zones are used where each cell zone is bounded by a one "interface zone" where it meets the adjacent cell zone. The interface zones of adjacent cell zones form a "grid interface" and the two cell zones move relative to each other along the grid interface. During the calculation, the cell zones slide i.e., rotates or translates, relative to one another along the grid interface in discrete time steps. In order to use the sliding mesh method, the computation domain is divided into two domains: stator body and rotor body. The outside domain, or the stator is comprised of domain boundaries while the inside domain, or the rotor includes the turbine. Between the stator and the rotor domains, there are interface conditions which are to be applied. In this method, the angular velocity of the rotor is varied to obtain simulation results in the tested range of *TSR*.

Flow Driven Simulation: Other kind of CFD simulation is with a given load which is called as flow-driven simulation. It is a method in which the rotational speed of the turbine axis is not fixed, but the turbine rotates at a certain rotational velocity because of the incoming fluid flow which exerts a force on the turbine blades i.e., it can start to rotate from standstill due to water flow acting on its blades (Le *at al*. 2014). Such an approach is convenient when investigations are required for whole turbine operation and not just some constant conditions.

Here, it is possible to predict and define all the other operating parameters (e.g. angular velocity at a certain load).

2.6 Objectives of the Present Thesis

The objective of the present study is set to evaluate the performance of Savonius and helical-bladed turbines through experimental and computational investigations. The performances of the turbines are expressed in terms of C_Q, C_P and *TSR*. In addition, the flow physics of the turbines at the various testing conditions are analyzed using ANSYS Fluent 14.5.

One of the major objectives of the present studies is to evaluate performance alteration of SHT with respect to its design parameters. There has been disagreement between the findings of the research groups upon the optimum number of blades for the SWT. As reported (Sheldahl *et al*. 1978; Mahmoud *et al*. 2012; Emmanuel and Jun 2011) the two-bladed configuration is found to be more effective than the three-bladed configuration. Contrarily, there are reporting about turbines having number of blades more than two being more effective (Emmanuel and Jun 2011; Wenehenubun *et al*. 2015). However, these are the findings of SWT and no such explicit data have been reported for SHT. Hence, it is necessary to inspect the impact of number of blades on performance alteration for SHT.

It is evident from the foregoing analysis that the very limited studies have been reported about the output characteristics of helical-bladed hydrokinetic turbines (HHTs). In view of this, helical-bladed turbines are developed by varying solidity ratio and number of steps. In the present investigation, the systematic measurements for torque and power are planned in order to obtain the output characteristics of the NACA- bladed helical hydrokinetic turbines.

Additionally, performance evaluation of the SHTs and HHTs at different immersion levels is the next extension of current investigations. The variation of performances with respect to various turbine design configurations is estimated for a range of immersion levels. The relevance of solidity ratio and performance fluctuation due to change in immersion level has also been studied. An attempt has also been made to compare the performance of SHT and SWT having an identical kinetic energy of the oncoming fluid (hydro/wind). In light of above, the following specific goals have been addressed in the present study.

(a) Development of Savonius turbines with varying blade number and blade profile are testing of these in an open channel water flume.
(b) Experimental analysis of the developed turbines at full immersion and partial immersion conditions

(c) Unsteady CFD simulations of the turbines for full immersion condition to support the experimental observations.

(d) Development of NACA 0020-bladed HHT with varying solidity ratios and testing it in an open channel and irrigational sluice.

(e) Measurement of the output characteristics of the turbine at varying immersion levels as there can be an alteration in the associated water level due to seasonal changes.

(f) Development and onsite testing of NACA 0022-bladed HHTs for single-step and double-step configurations at river Brahmaputra, Assam.

(g) Wind tunnel experiments of the SWTs at identical power with that of SHT.

The roadmap of the present investigation is shown in Fig. 2.9.

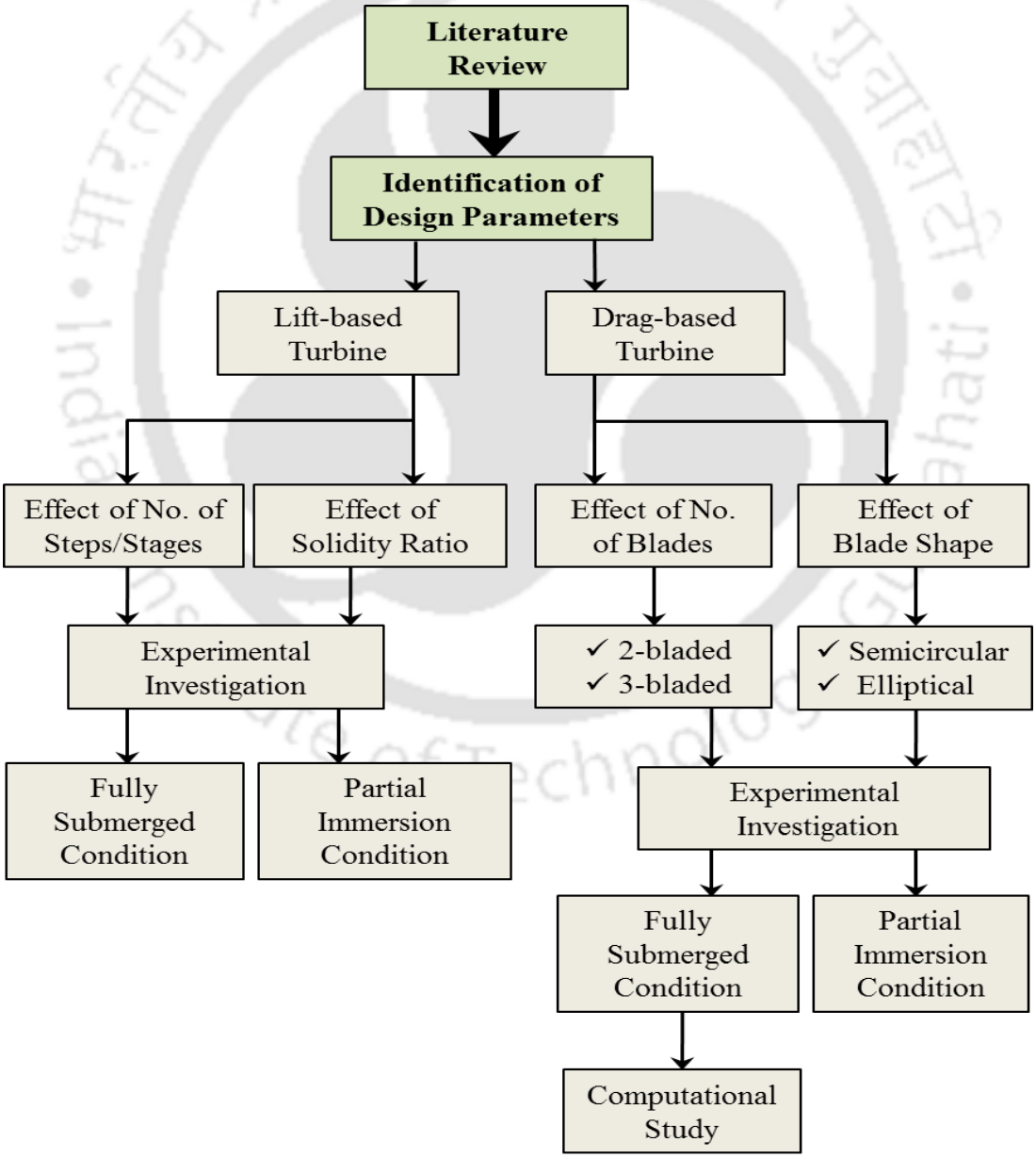

Figure 2.9: Roadmap of the present investigation

Chapter – 3

Turbine Designs and Test Facilities

Chapter Outline

Overview

In this chapter, the details of the vertical-axis turbine designs and their fabrication along with testing sites are discussed. Considering the various design parameters, Savonius hydrokinetic turbines (SHTs) and helical-bladed hydrokinetic turbines (HHTs) are designed accordingly. In case of SHTs, three models are developed to study the influence of blade profiles and number of blades. Similarly, three models of HHTs are designed to study the influence of solidity ratio on the turbine performance. The testing facilities such as the open channel water flow flume, and the irrigation sluice are described. Also, the test setup to find the effect of multi-staging of turbines in the river Brahmaputra is explained. Finally, the wind tunnel facility for testing the Savonius turbines is described.

3.1 Introduction

As experimental testing is the main focus of present study, therefore, based on the literature review and available facilities, several models of turbines are designed and developed. In order to design an efficient Savonius turbine, the two important design parameters viz. number of blades and blade shape are considered in the current study. The researchers have mostly carried out lab scale experimental investigation of SHTs and subsequently the turbines were tested by mounting it on wave tank with a towing carriage (Khan *et al*. 2009) and in an open channel flow flume (Golecha *et al*. 2009). Similarly in the present work, various designs of helical hydrokinetic turbines (HHTs) are developed by varying the solidity ratios and number of stages.

Previously, the researchers conducted lab-scale and full-scale experiments of HHTs in various testing facilities/sites like narrow channel on the Korean coastline (Han *et al*. 2013), test bed with turbine being mounted on carriage (Bachant and Wosnik, 2015), water flume (Niblick 2012), Uldolmok Strait in Korea (Kim *et al*. 2012), Kvichak river in USA (Johnson and Pride 2010). In the present study, the developed SHTs are tested in open channel flow flume, whereas the HHTs are tested in three different sites viz., open channel, irrigation sluice and river Brahmaputra.

In another set of experiments, SWTs are tested in a low speed subsonic wind tunnel. It is observed from literature that a torque sensor coupled with an electromagnetic brake or a rope brake dynamometer can be used for the measurement of mechanical torque and hence power. However, in the current investigation, a rope brake dynamometer, which is simple to install and less sensitive to its alignment to the turbine shaft, has been employed. Because of its good accuracy and lower cost, researchers have used it extensively (Kamoji *et al*. 2009; Golecha *et al*. 2011, 2012; Patel *et al*. 2017). In this chapter a detailed description on experimental facility and instruments used are presented.

3.2 Savonius Turbines

In the present investigation, three different configurations of Savonius turbines have been considered keeping the cross-sectional area (A) of the turbines fixed at 0.0625 m^2. The turbines with two-semicircular blades, three-semicircular blades and two-elliptical blades have been studied. The detailed specifications of the developed Savonius turbines are given in Table 3.1.

Table 3.1: Design specifications of Savonius turbines

Parameters	Two- semi-circular-bladed turbine	Three-semi-circular-bladed turbine	Two-elliptical - bladed turbine
Aspect ratio (*AR*)	1.0	1.0	1.0
Overlap ratio (β)	0.15	0.15	0.15
Turbine diameter (*D*)	250 mm	250 mm	250 mm
Chord length of bucket (*d*)	144 mm	144 mm	144 mm
End plate diameter (D_o)	277.2 mm	277.2 mm	277.2 mm
Central shaft diameter (*a*)	16 mm	16 mm	16 mm

The schematic diagrams of the two- and three-bladed turbines with semicircular shaped blades are shown in Fig. 3.1. Mild steel sheets of 1.2 mm thickness have been used to fabricate the blades/buckets of turbine. The study of elliptical-bladed Savonius turbine as hydrokinetic turbine has not been reported in literatures till date. The present study thus includes development and performance analysis of two-bladed elliptical turbine. The dimensions of major and minor axis are chosen for elliptical blade profile is taken as 262.5 mm and 175 mm so that the ratio of minor axis to major axis is 2/3. In the present study, the sectional cut angle (α) of 47.5° is chosen for the elliptical-bladed turbine since the SWT with this value of α has been reported by Alom *et al* (2016) to perform better than the semicircular-bladed SWT. The value α is selected in such a way that it would result a blade profile of chord length same as the semicircular blades. The sectional cut of an ellipse and elliptical shaped turbine are shown in Fig. 3.2 (a) and 3.2 (b) respectively. Further, the overall test set-up of turbine with mechanical dynamometer is shown in Fig. 3.3.

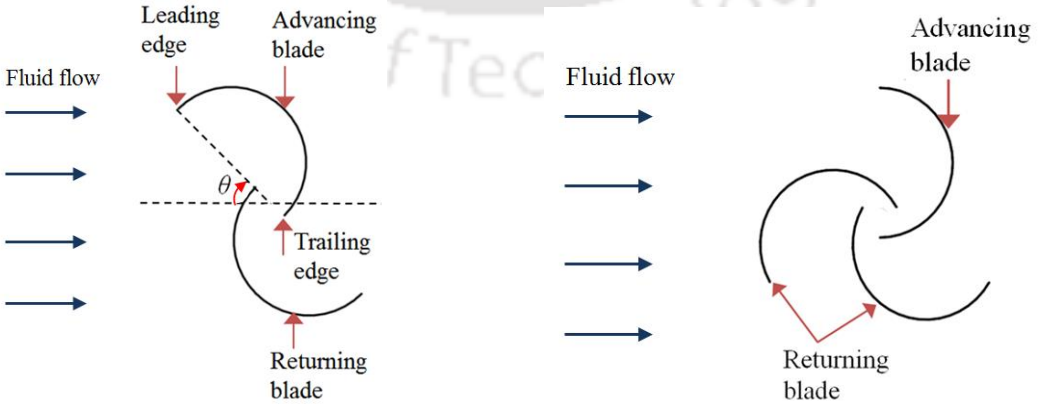

(a) Two-bladed turbine (b) Three-bladed turbine

Figure 3.1: Schematic diagram of semicircular-bladed Savonius turbines

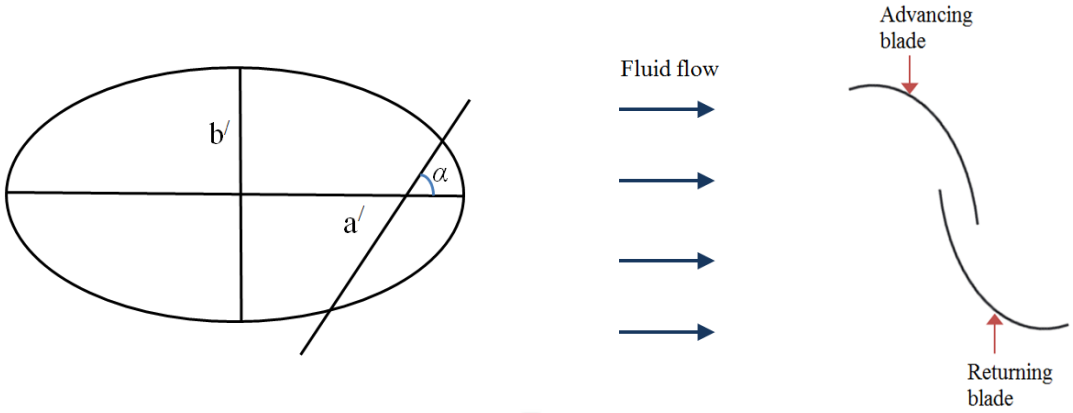

(a) Sectional cut of an ellipse (b) Elliptical shaped blades

Figure 3.2: 2D view of Savonius turbine with elliptical blades

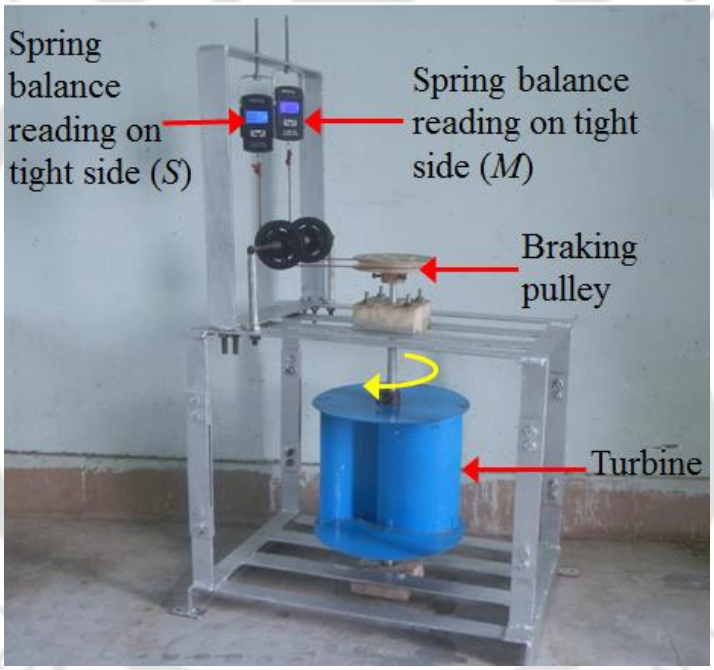

Figure 3.3: Developed experimental set-up for Savonius hydrokinetic turbine

3.3 Helical-bladed Turbines

3.3.1 Design of HHTs to analyze the effect of solidity ratio

In the present investigation, three turbine design configurations with different solidity ratios, as shown in Table 3.2, have been considered for testing. The HHTs with NACA 0020 blade profile and 0° blade pitch have been developed in order to compare the performances. In this study, because of the high durability and ease of manufacturing of a thick blade, NACA 0020 symmetric airfoil has been selected for blade design. Initially, wooden chips having a cross

section in the shape of a standard NACA 0020 airfoil are prepared to make a pattern. The chips are then arranged helically around the circumference of the cylindrical boundary and the positioning of each chip is done so that the tips of the individual chips are separated by a fixed distance from each other. This procedure is followed to ensure that the chips exactly cover a helix angle of 60° between the top and bottom surfaces of the blade. The chips are attached to each other with adhesives, and thereafter, synthetic putty is applied around the helical structure of the blade. The putty is then allowed to dry to obtain the desired pattern. A mould is then fabricated out of the pattern from which helical shaped blades are made. These fabricated three blades are shown in Fig. 3.4. These blades are connected to the turbine shaft of 0.025 m diameter with the help of two spoke arms made up of mild steel through a flange coupling welded to the spoke arm on either arm for the upper and lower bases. To connect the spoke arm system to the shaft, three holes on each flange are made for bolts.

Table 3.2: Designing parameters of helical-bladed turbines

Design	D (mm)	H (mm)	ϕ (°)	C	σ
I	300	300	60°	120	0.38
II	340	300	60°	120	0.34
III	370	300	60°	120	0.31

Figure 3.4: Fabricated helical fiberglass blades

The experimental set-up composed of the turbine with a central shaft, bearing housing, braking pulley fitted to the central shaft and two digital spring balances shown in Fig. 3.5 has been developed to evaluate the performance characteristics of the HHT. Bearings are used at the top and bottom of the shaft supported by nylon blocks, acting as bearing housing to

facilitate smooth rotation of the turbine. A double sealed ball bearing (6201ZZ) is used at the upper section of the turbine and a tapered roller bearing (2206) is used at the bottom section.

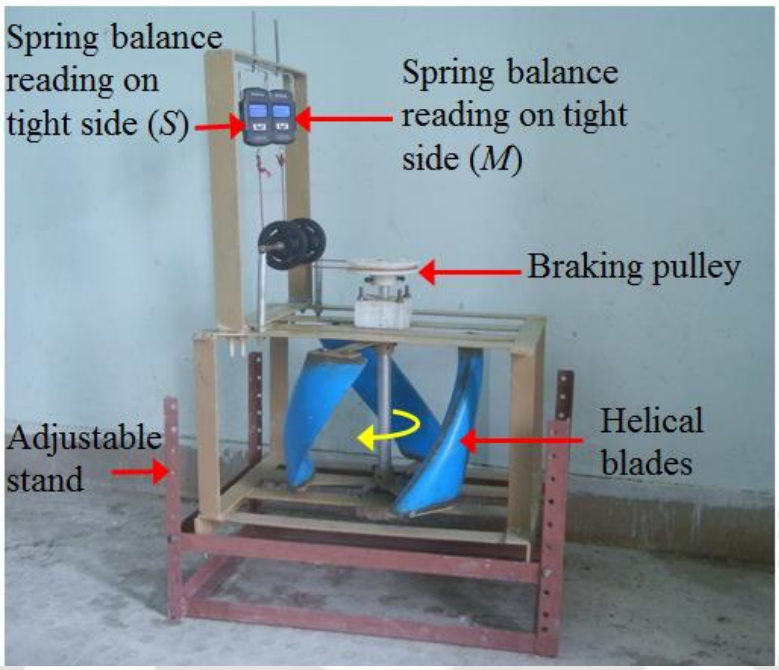

Figure 3.5: Test set-up of helical-bladed hydrokinetic turbine

3.3.2 Design of HHTs to analyze the effect of multi-staging

The present investigation deals with the in-situ experiments of a double-step three-bladed helical hydrokinetic turbine for possible electricity generation. Further, its performance is compared with that of a conventional single-step helical-bladed turbine. The helical NACA 0022 bladed turbines with σ = 0.20 have been developed. The design specifications used in this investigation are outlined in Table 3.3.

Table 3.3.Turbine design specifications

Parameter	Specifications
Diameter (D)	0.25 m
Height (H)	0.25 m
No. of blades (n)	3
Helix angle (ϕ)	43.7°
Solidity ratio (σ)	0.20
Aspect ratio (AR)	1:0

In the present design, the NACA 0022 blade profile has been selected considering the durability and ease of manufacturing due to its symmetric shape. In order to obtain the accurate blade profiles, a helical shaped blade is fabricated with the PA2200 material using selective laser sintering process which is a versatile and frequently used 3D printing technology. Using this blade as a pattern, the required number of helical shaped blades have been developed using fibre-glass resin composite material that offers high resistance to wear and indentation. The turbine blades are attached to the turbine shaft of 16 mm diameter with the help of spoke arms on either side of the blades. Figure 3.6 shows the CAD models of the single-step and double-step HHT. The turbine shaft is mounted on bearings at the top and bottom using bearing housings. The developed experimental set-up with two-step HHT and dynamometer is shown in Fig. 3.7.

Figure 3.6: CAD models of single-step and double-step helical-bladed turbines

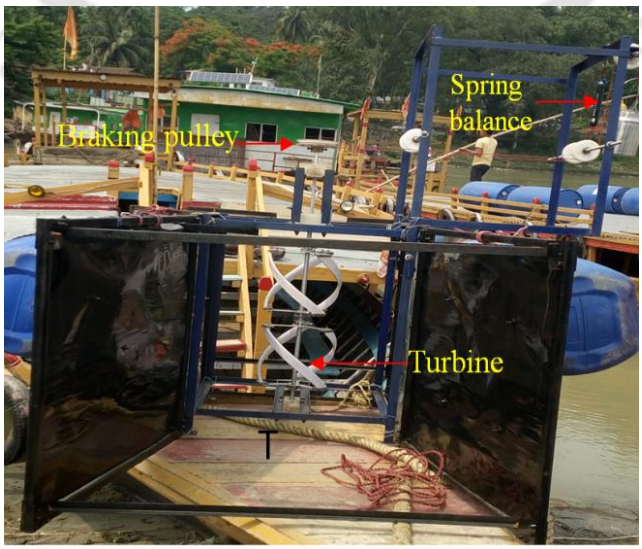

Figure 3.7: Assembled turbine set-up

3.4 Testing Facility for Hydrokinetic Turbines

3.4.1 Open channel water flume

The field testing of developed helical turbines was carried out in an open water channel at the water treatment plant, IIT Guwahati, India (Fig. 3.8). The flume consists of cemented walls of 1.0 m wide and 0.9 m in height. The turbine was mounted in the converging section of the flume as shown in Fig. 3.9.

A propeller-type current meter (model: Nixon 430, accuracy: ±1.5%) having operating range 0.6 − 3.0 m/s was used to measure the inlet water velocity at three locations of the open channel along the width in the inlet plane of the turbine. At each location, the velocity was measured at three different heights from the bottom surface of channel, such as 20%, 60% and 80% of total water depth. Thereafter, the arithmetic mean of all the readings was taken for further calculation. The water depth available at the site was 0.40 m.

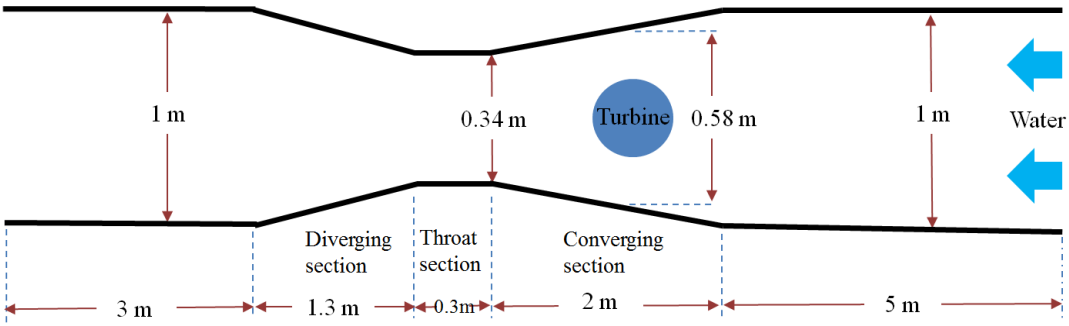

Figure 3.8: Schematic diagram of the open channel

a) Main parshall flume b) Converging section of the flume

Figure 3.9: Turbine testing site at IIT Guwahati

3.4.2 Irrigation sluice

The in-situ experiments of the helical-bladed turbines have been conducted in an irrigation sluice located at Mandakata (Lattitude: 26.34° N, Longitude: 91.78° E), Kamrup, Assam, India (Fig. 3.10). The water velocity at the sluice is measured with the help of a velocity meter (Make: Global Water, model: FP111) having an operating range of 0.1–6.1 m/s and least count of 0.1. A photograph of the velocity meter is shown in Fig. 3.11. The water velocity is measured at the inlet of the turbine at three different vertical positions across the turbine and the arithmetic mean of the readings is taken for further calculations.

(a) Zoomed view of the turbine set-up (b) Installed turbine at the irrigation sluice

Figure 3.10: Helical-bladed model turbine on the testing site at Mandakata, Assam

Figure 3.11: Water velocity meter

3.4.3 The Brahmaputra river

The field testing of the turbine has been carried out in the Brahmaputra river located at Guwahati (Latitude: 26.18° N, longitude: 91.66° E), Assam. Further, in order to maximize the power output, the turbine has been mounted in a venturi-shaped flume that can enhance the power produced by the turbine. The schematic of the venturi-shaped flume is shown in Fig. 3.12. Due to the venturi-shape, the flow accelerates inside the flume and therefore, the kinetic energy of flow striking the blades gets increased. However, this kind of augmentation technique requires large flow area as compared to turbine frontal area.

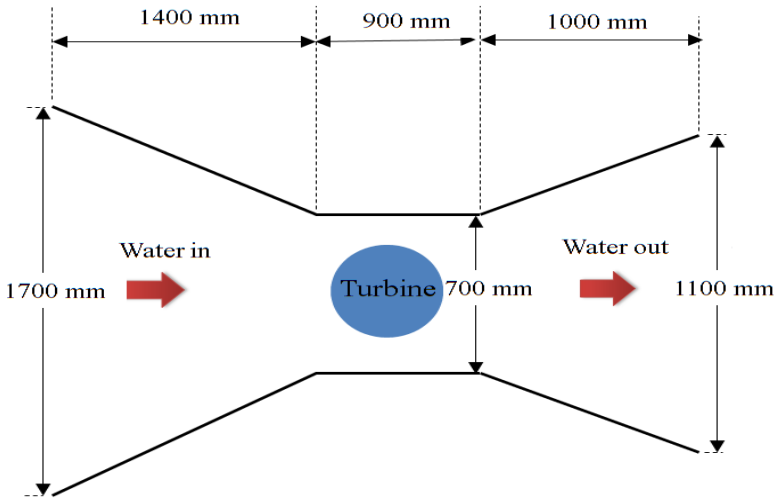

Figure 3.12: Schematic diagram of the venturi-shaped flume

The velocity of the water current at the site is measured with the help of a water velocity meter (Make: Global Water, model: FP111) with operating range of 0.1–6.1 m/s (least count of 0.1). The inlet velocities of water have been measured at the starting of the straight section (upstream of the turbine) of the flume.

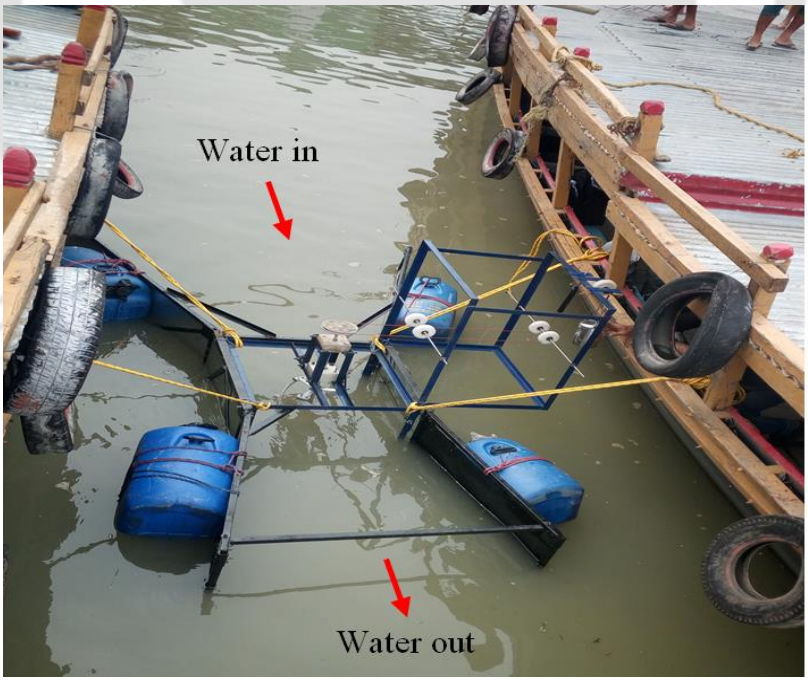

Figure 3.13: Turbine set-up on testing site

In order float the whole turbine assembly and venturi-shaped flume, the plastic drums of 50 kg capacity each are tied to the flume at four different sides. The whole structure is then held between two boats and the inlet of the flume is kept facing the incoming water flow. The mounted turbine set-up with all the accessories is shown in Fig. 3.13.

3.5 Wind Tunnel Test Facility

By keeping an identical kinetic energy (15.97 W) input to that of SHT, the performances of the SWTs have been evaluated in a low-speed open-circuit wind tunnel facility having closed test section. The schematic diagram of the wind tunnel is shown in Fig. 3.14(a). The wind tunnel facility of closed test section is employed for creating a uniform wind of known value in the test section. The facility is established for testing of various turbine models and to obtain their performance characteristics. The test section of size 2 m × 0.6 m × 0.6 m is equipped four perspex windows for viewing inside the test section. A wooden window at the top is used for mounting of turbine and the mounted turbine in the test section is shown in Fig. 3.14(b). The wind speed can be varied at the test section by adjusting the rpm of the fan. The fan is directly coupled to an AC motor whose speed can be varied using an AC motor controller. The wind velocity at the inlet to the turbine is measured using an inclined manometer. In the test set-up, a maximum wind speed of 45 m/sec can be achieved in the test section at about 1450 rpm.

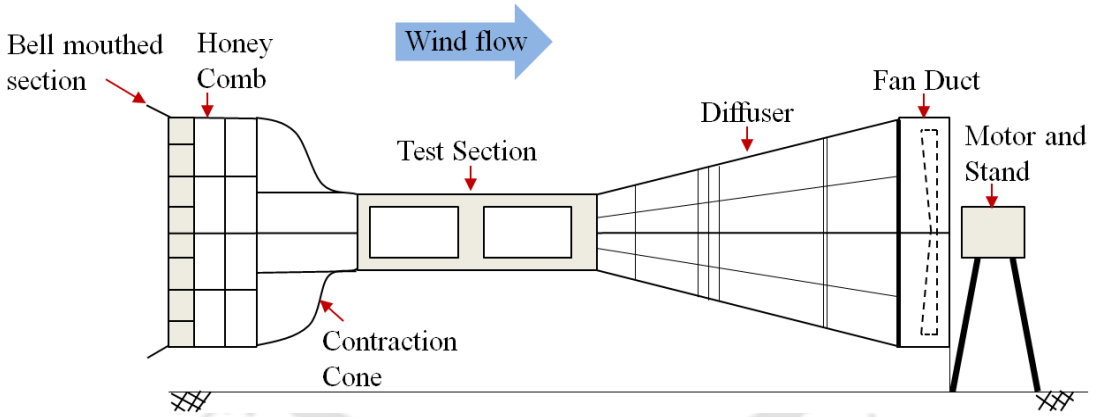

(a) Schematic of wind tunnel

(b) Mounted turbine set-up

Figure 3.14: Wind tunnel test facility

3.6 Torque and Power Measurements

The torque measurement procedure is followed according to the investigation reported by Roy and Saha (2014). As per this practice, the torque of the turbine is measured using a mechanical dynamometer composed of a braking pulley, two tension pulleys, a nylon rope and two digital spring balances. Initially, the turbine was allowed to rotate without any load so that it can rotate at its maximum rotational speed. The mechanical loads were then gradually applied with the help of load control mechanism. The torque is measured using the readings obtained from the digital spring balances (maximum capacity of 50 kg and 0.001 kg least count) on tight and slack side (Figs. 3.3 and 3.5). For a particular load, the readings on the tight side and slack side are denoted by M and S, respectively. The load ($M – S$) multiplied by the radius of rotating pulley attached to shaft (r_p) gives the torque (T) produced by the turbine. Hence, the torque measured by the mechanical dynamometer can be calculated by Eqn. 3.1.

$$T = (M – S) \times r_p \times g \tag{3.1}$$

Rotational speed (rpm) of the turbine was measured for each applied mechanical load using a tachometer. As the load increases, the rpm of the turbine decreases. This procedure is repeated to obtain several combinations of rpm and generated torque until the turbine is stalled. The load at which the turbine stops rotating is the maximum loading condition. From the experiments, a set of data points for torque and rpm is obtained at a particular fluid velocity from which the performance of the turbines at different *TSR*s is calculated.

3.7 Starting Torque Experiments

For measuring the starting torque of the HHT, the turbine is placed in the water stream of known velocity. The calculation of azimuth angle (γ) is shown in Fig. 3.15 and starting torque is evaluated at 20° interval of γ. Initially, the turbine is positioned at a particular γ at which the starting torque is to be evaluated. At this location, turbine is pre-positioned at maximum mechanical load. Now, the mechanical load is gradually reduced and at a particular load, the turbine starts rotating. This value of load depicts the starting torque of the turbine of that particular γ. The same procedure is repeated to find out the starting torque of the turbine at different values of γ.

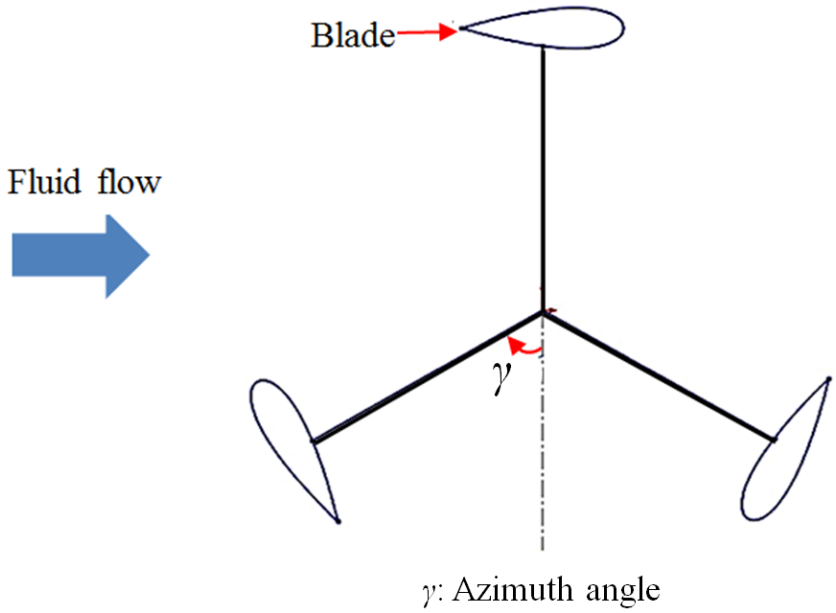

Figure 3.15: Azimuth angle of lift-based turbine

3.8 Summary

In this chapter, a detailed description of experimental facility and the instruments used in the present investigation is presented. The vertical-axis Savonius hydrokinetic turbines (SHT) are developed and subsequently tested in an open channel water flow flume located at water treatment plant, IIT Guwahati.

In another set of experiments, the Savonius turbines are tested in closed-type wind tunnel to evaluate the performance of SWT and SHT at an identical kinetic energy of the incoming fluid (wind/hydro). Further, the vertical-axis three-bladed helical turbines with varying solidity ratios have been fabricated and tested at two different sites viz., an open channel water flow at water treatment plant and an irrigation sluice. A mechanical dynamometer is designed and fabricated in order to measure the torque and hence power produced by the turbine. To measure the velocity of water, a propeller type current meter has been used. The turbines are tested at various mechanical loading conditions in order to find the variation of power coefficient at various tip-speed ratios, and hence to arrive at the optimum operating point of the turbine at a particular inlet water velocity.

Chapter – 4

Computational Methodology

Chapter Outline

Overview

This chapter overviews the computational methodology employed for the simulation of Savonius and helical-bladed turbines. In the present study, the symmetrical blades along the vertical axis are used and hence, the 2D planar simulations have been performed to investigate the performance of Savonius turbine which significantly lowers computational time without compromising the accuracy remarkably as compared to 3D simulations. However, for the helical-bladed turbine, 3D unsteady simulations have been incorporated. The unsteady RANS equations are incorporated in FVM based CFD software ANSYS-Fluent. To accurately predict the flow behaviour, the shear stress transition (SST) k-ω turbulence model is incorporated. In case of SHT, the inlet boundary condition is set as per the present experimental condition of water velocity, V = 0.8 m/s. Similarly, V = 1.1 m/s is set for analysis of HHT. In case of SWT, V = 7.4 m/s is used. The time independent torque coefficient (C_Q) is obtained through averaging of values of C_Q for a complete revolution of turbine after attaining quasi-steady state.

4.1 Introduction

Computational Fluid Dynamics (CFD) is an effective simulation tool to understand the fluid dynamics of engineering problems. As the blades of Savonius turbine are symmetrical along the vertical axis, hence, the two dimensional (2D) planar simulations have been performed to investigate the flow physics. Further, the two dimensional (2D) numerical studies cannot be incorporated for helical-bladed turbines because of the curved blade shape, and hence, the CFD studies of helical-bladed turbines are very limited.

In the present study, the three dimensional (3D) simulations have been carried out for the same. For the CFD simulations, commercial software, ANSYS-FLUENT 14.5 is employed. The validation of the proposed computational set-up is very important as it ensures the accuracy of the numerical methodology used to predict the performance of the turbine. Herein, the turbine has been modeled in SOLIDWORKS and then imported into ANSYS Workbench. The sliding mesh technique is used to model the rotation of the turbine and for this computational domain is divided into two domains. The finite volume based (FVM) moving/sliding mesh technique is commonly used for such transient flow problems. During the simulation, the cell zones rotate or translate relative to one another along the grid interface. This sliding mesh technique was used by researchers like Banerjee *et al.* (2014), Sarma *et al.* (2014); Tian *et al.* (2015), Alom *et al.* (2016), Roy and Ducoin (2016, Kumar and Saini (2017) to analyze the flow over vertical-axis Savonius and Darrieus turbines. The same computational technique has been used in the present study to simulate the flow field around the turbines. Thereafter, meshing is done in meshing module of ANSYS. The mesh file is then imported to FLUENT for solution setup, solutions and post processing.

4.2 2D unsteady Simulation for Savonius Turbine

The CFD simulation of a three-dimensional (3D) model of vertical-axis turbine is necessary when the turbine blade is not symmetrical along the vertical-axis. The turbine blades, in the present investigation, are symmetrical along the vertical axis, and hence, the two dimensional (2D) planar simulations have been performed to investigate the performance of SHTs. This simulation strategy favors lower computational time without remarkably compromising the accuracy as compared to 3D simulations which is computationally expensive (Tian 2015; Rogowski and Maronski 2015). The previous 2D studies have shown acceptable results for SHT/SWT (Altan and Atilgan 2008; Yang and Lawn 2011; McTavish *et al*. 2012; Kacprzak *et al*. 2013; Rosario *et al*. 2014). In addition, if the turbine aspect ratio (*AR*) is greater than or equal to unity, the 2D simulations can capture the flow physics adequately well (Abraham *et al*. 2011).

4.2.1 Description of computational domain

The computational domain for semicircular-bladed Savonius turbine is shown in Fig. 4.1. There are two distinct regions viz., (a) inner rotating region which includes turbine and (b) surrounding rectangular stationary region. The diameter of the inner rotating zone is assigned as thrice of the turbine diameter (3*D*), whereas the dimensions of the outer rectangular zone is given as 10*D* × 6*D*.

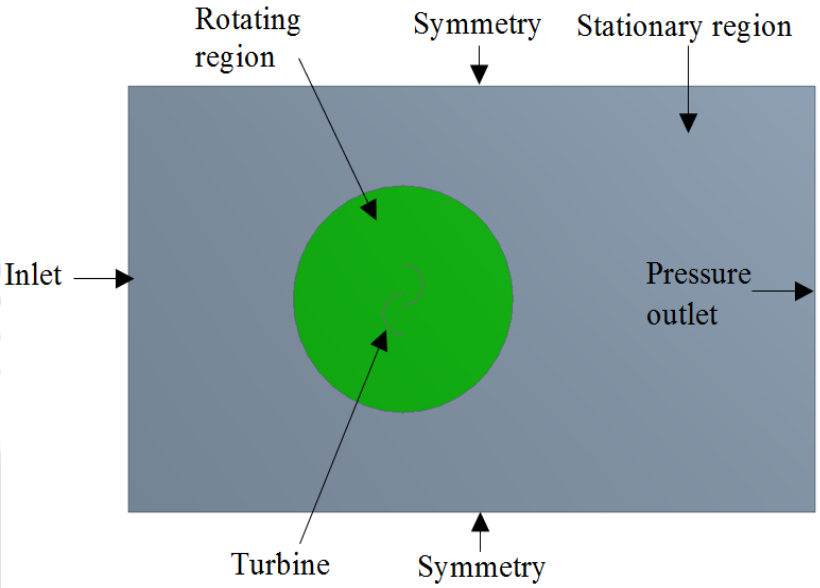

(a) Computational domain with boundary conditions

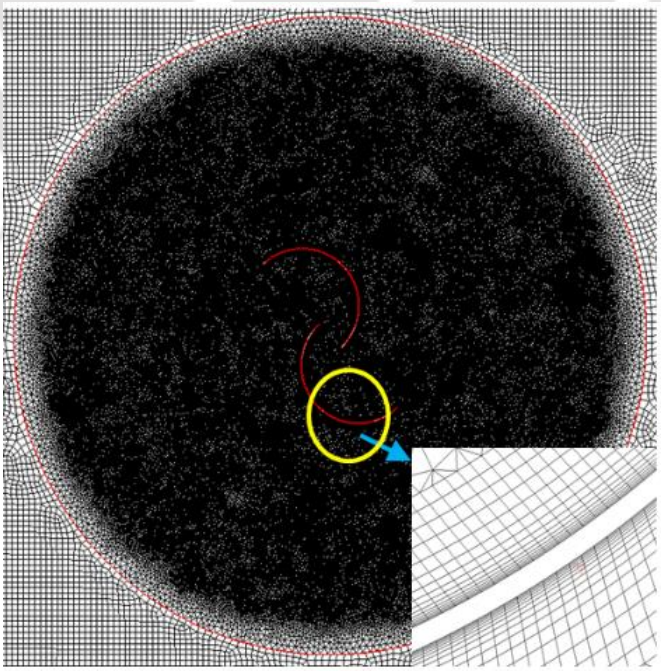

(b) Close up view of rotating region

Figure 4.1: Overview of computational domain

4.2.2 Details of problem set-up

The computational domain is discretized using unstructured volume elements with inflation layers near to the turbine wall surfaces to resolve the boundary layer for precise resolution of flow features (Fig. 4.1). A uniform velocity of $V = 0.8$ m/s is set at the inlet, which corresponds to a Reynolds number, $Re = 2.25 \times 10^5$, whereas the boundary condition at the outlet of the computational domain is specified as pressure outlet. These inlet conditions corresponds to the experimental tests performed in locations such as open channel. The top and bottom edges of the computational domain are assigned as symmetry boundary condition. This boundary condition allows the solver to avoid the wall effect and to accurately replicate the experimental lateral flow (Kacprzak *et al.* 2013; Roy and Ducoin 2016; Kumar and Saini 2017). The known rpm value is imposed on the inner zone of the computational domain for rotation of the turbine blades. The turbulence model incorporated for the present study is discussed in section 4.2.3.

4.2.3 Selection of turbulence model

For a realistic modeling of the flow field around a turbine, it is essential to account for turbulence. A large number of turbulence models are available for simulating the flow based on Reynolds number and turbine geometry. Among those, Spalart–Allmaras (SA) model, standard k-ε turbulence model, Realizable k-ε turbulence model, RNG k-ε turbulence model, Shear Stress transport (SST) k-ω model and standard k-ω model, anyone can be used for turbine related simulations (Zhou and Rempfer 2013, Kumar and Saini 2017). In case of studies associated with turbine, the standard k-ε model gives better results than SA model. Further, both the realizable and RNG k-ε models are found to be significantly improved models over the standard k-ε and SA models. The shear stress transport (SST) k-ω turbulence model is a two-equation eddy viscosity model combining the advantages of both k-ε formulations for free stream flow and k-ω formulations in the turbine boundary layer. Further, it exhibits less sensitivity to free stream conditions (far field) than other turbulence models. This SST k-ω turbulence model can be utilized throughout the flow field as it is well suited for simulating flow in the viscous sub-layer (near wall) where a high boundary layer accuracy is required. This two-equation turbulence model effectively captures a wider class of flows e.g., flow with adverse pressure gradients, flow over airfoils, rotating flows and low Reynolds number flows (Menter 1994; Nasef *et al.* 2013; Roy and Ducoin 2016). In view of this, the SST k-ω turbulence model is employed in the present study.

4.2.4 Details of flow solver

Unsteady simulations have been carried out to address the accelerating flow near the tip of the turbine blades and the turbulence after the blade. The pressure based unsteady Reynolds-Averaged Navier-Stokes (RANS) model has been employed using the SIMPLE (Semi-Implicit Method for Pressure-Linked Equations) algorithm for pressure-velocity coupling. This pressure-based solver deals the flow problem in a segregated or coupled manner. There are many pressure-velocity coupling algorithms as choice in ANSYS like SIMPLE, SIMPLEC, PISO and Coupled are available in FLUENT. The SIMPLE algorithm uses a relationship between velocity and pressure corrections to enforce mass conservation and to obtain the pressure field. It ensures a good solution stability through the pressure-velocity coupling (Roy and Ducoin 2016). The SIMPLE scheme, on the other hand, is computationally inexpensive and its convergence is faster in comparison to other schemes. The non-dimensional wall distance (y^+) value achieved is found to be less than 1. This is a necessary condition for the SST k-ω model for capturing the high levels of separation and adverse pressure gradients around the wall of the blades. Therefore, at the wall boundaries of the blades, the flow is resolved such that the dimensionless velocity is approximated as a linear function of y^+. The higher y^+ would result in reduced simulation accuracy as the ANSYS-prescribed wall functions cannot resolve the boundary layer flow. The time step size is taken here as 1° rotation of the turbine. The maximum iterations per time step are taken as 300. The simulation is carried out for 10 complete rotation of turbine. The criteria for stopping the simulation have been the convergence criteria which is 10^{-3}. The spatial discretization of the conservative equations is treated with second-order upwind scheme and the temporal terms of the conservative equations are discretized using second order fully implicit temporal scheme.

4.2.5 Calculation of power coefficient

As the simulations are conducted by considering unsteady flow assumption, the torque coefficients (C_Q) are time averaged to obtain a more accurate value. After the initial period, the variation of C_Q with time follows almost a cyclic path. The average C_Q is determined from last revolution of the turbine after attaining the quasi-steady state. The power coefficient (C_P) is obtained by multiplication of TSR and average C_Q over a revolution. The power coefficient (C_P) is directly computed from the coefficient of torque (C_Q) using Eq. 4.1.

$$C_P = C_Q \times TSR \tag{4.1}$$

4.3 3D Unsteady Simulation for Helical-bladed Turbine

4.3.1 Description of computational domain

The 3D computational domain, shown in Fig. 4.2, has been used to simulate the performance of helical-bladed turbine. The turbine model having D = 300 mm and H = 300 mm has been considered in this analysis. The computational domain has the gross dimension of 10D × 6D × 3D. Similar to the 2D simulation of Savonius turbines, overall computational domain consists of two zones: inner rotating zone cylinder and outer stationary zone. The cylindrical zone contains a helical-bladed turbine and it can rotate according to the specified angular velocity during computations. Further, the interface is created between stationary zone and rotating zone to ensure continuity of flow field.

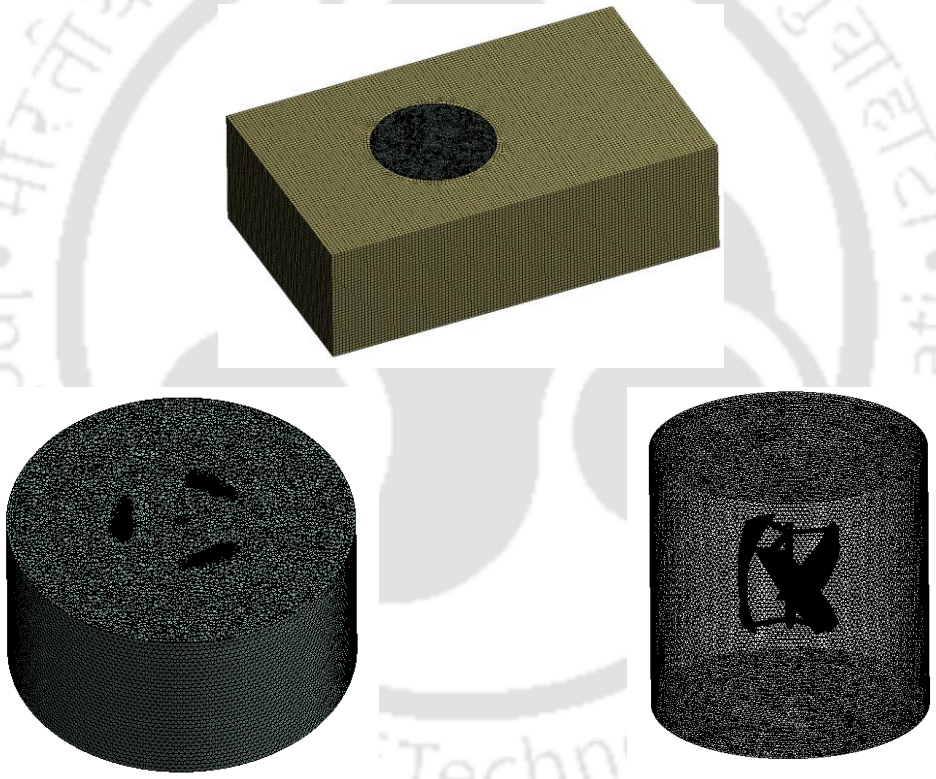

Figure 4.2: 3D mesh showing boundary layer and dense mesh in rotating zone.

4.3.2 Details of problem set-up

The flow domains are meshed in ANSYS Fluent 14.5 using unstructured grid. Further, the mesh density is refined by specifying body sizing, face sizing and cell curvature function on areas of interest The mesh density is increased near the blades and the central shaft. This is to fully capture the flow hydrodynamics, while the mesh density is decreased away from blades

to reduce the computational time (Fig. 4.2). The same boundary conditions as those mentioned in 2D flow are used for this 3D simulations as well.

4.3.3 Selection of turbulence model

In view of the better ability to capture the adverse pressure gradient and flow separation, the SST k-ω turbulence model is employed in the present study.

4.3.4 Details of the solver

The flow 3D flow solver with pressure based unsteady Reynolds-Averaged Navier-Stokes (RANS) model is used along with the SIMPLE (Semi-Implicit Method for Pressure-Linked Equations) algorithm for pressure-velocity coupling.

4.3.5 Calculation of power coefficient

In order to evaluate power coefficient from computational analysis similar procedure has been followed as mentioned in section 4.2.5.

4.4 Summary

In this chapter, the in-detail computational methodologies for Savonius turbine and helical-bladed turbine have been described. As the flow across the turbine is turbulent in nature, therefore unsteady turbulent model with RANS equation has been incorporated. In case of Savonius turbines, 2D simulations have been carried out as they provide very good agreement with experimental data. It requires less computational time as compared to 3D simulations. Further, 3D simulations have been performed for the experimentally best performing helical-bladed turbine.

Chapter – 5

Savonius Hydrokinetic Turbine (SHT) Results

Chapter Outline

Overview

This chapter details the experimental as well as computational results of the drag-based Savonius hydrokinetic turbines (SHT). As the performance of Savonius turbine is heavily depends on its design parameters, therefore, in the present study, a number of turbine designs with varying number of blades and blade shapes have been analyzed. The performance indices such as power coefficient and torque coefficient are estimated corresponding to a range of tip-speed ratios. The SHTs are tested at an inlet water velocity of 0.8 m/s at the open channel flume. The study reveals that the two-semicircular-bladed SHT demonstrates superior performance as compared to two-elliptical-bladed SHT and three-semicircular-bladed SHT under conditions of full immersion and partial immersion. In addition, the three-semicircular-bladed SHT shows better performance than two-elliptical-bladed SHT. Further, the performances of SHTs are found to decrease with the reduction in immersion level. The experimental observations for full immersion conditions further justified by using flow physics analysis carried out 2D CFD simulations.

5.1 Introduction

The drag-based Savonius hydrokinetic turbines (SHTs) have an enormous potential for small-scale power generation from free-flowing water and such turbines can be deployed especially at sites remote from existing electricity grids. The parametric studies of the Savonius hydrokinetic turbines (SHTs) based on number of blades, blade shapes and immersion level have been carried out. Considering various design parameters, the model turbines discussed in section 3.2 are developed and tested in an open channel water flow. The experiments are carried out at water velocity of 0.80 m/s. The measured test variables are torque, rotational speed, and inlet water velocity. The data presented here are in the form of C_Q and C_P as a function of *TSR*s. Furthermore, 2D CFD simulations are performed for the design variants to analyze the flow characteristics and aerodynamic performance of the turbines.

5.2 Effect of Number of Blades

5.2.1 Load characteristics experiments

A comparative assessment between two- and three-bladed SHTs with semicircular blades is carried out during the field tests. The variation of C_Q and C_P with *TSR* are shown in Fig. 5.1.

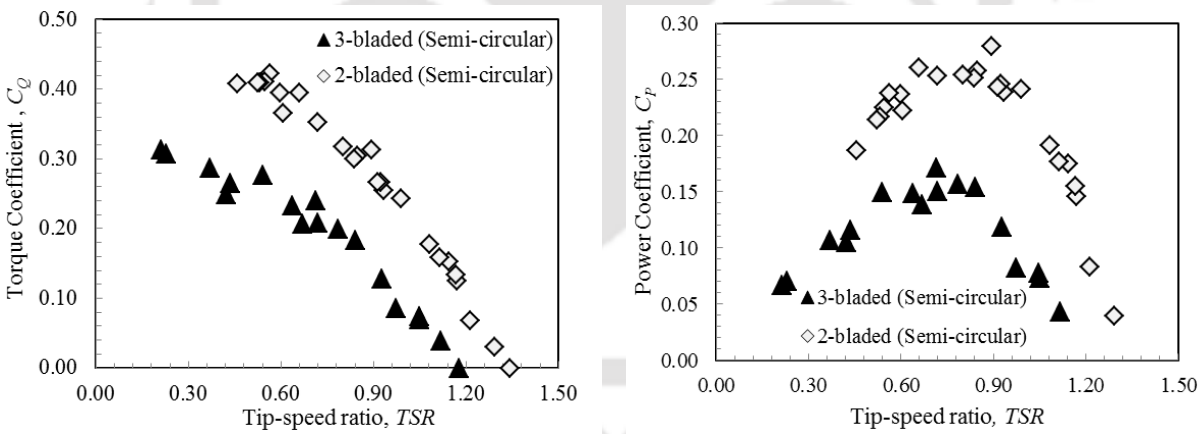

(a) C_Q vs *TSR* (b) C_P vs *TSR*

Figure 5.1: Performance characteristics curves (V = 0.80 m/s)

Initially, at no load condition, the two-bladed and three-bladed turbines are found to rotate at *TSR* = 1.34 and *TSR* = 1.18 respectively. Then, the mechanical loads are gradually applied and as mentioned in earlier section, torque, power and rotational speeds are recorded. It is observed (Fig. 5.1a) that the rotational speed of the turbine reduces with the increase in mechanical load, and this leads to an increment of C_Q with the decrease of *TSR*. The present

study also reveals that the two-bladed turbine produces more torque in comparison to the three-bladed turbine. Moreover, the two-bladed and three-bladed turbines stall at maximum braking load of 1.18 N.m and 0.91 N.m respectively. Thus, it is evident that the two-semicircular-bladed turbine shows better performance in comparison to the three-semicircular-bladed turbine (Fig. 5.1b). The maximum power coefficients ($C_{P\max}$) for two-bladed and three-bladed turbines are found to be 0.28 and 0.17 at corresponding optimum *TSR* of 0.89 and 0.71.

5.2.2 Grid refinement and comparison of computational model

The unsteady simulations are performed to understand the dynamics of water flow for two-bladed and three-bladed turbines and to obtain more insight about the experimental observations. The grid refinement study for two-semicircular-bladed SHT is carried out and simulation is repeated with different refinement levels of the mesh. As seen in Fig 5.2a, there is negligible quantitative change in the C_P beyond the computational domain having 3,00,925 number of elements. Therefore, the mesh size corresponding to 3,00,925 number of elements has been selected for further simulation. As an outcome of the present findings, the time variation of torque or moment coefficient for semicircular blades at *TSR* = 0.7 is shown in Fig. 5.2b. It can be seen here that the quasi-steady time convergence is attained after the initial starting fluctuations of around 4 secs. Such mesh independent simulations are used for further analysis. The convergence criterion for solving the continuity, momentum and the two transport equations of the turbulence model is taken as 10^{-3}, which is reported to be adequate for unsteady simulations with large flow separation (Tian *et al.* 2015; Kumar and Saini 2017).

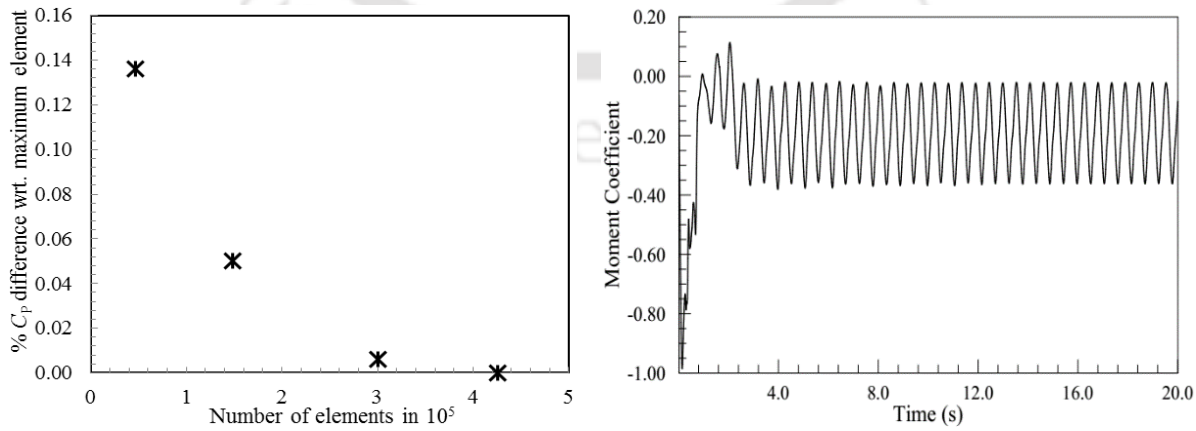

(a) Grid refinement (b) Quasi-steady convergence by time

Figure 5.2: Grid refinement and convergence study

The comparison of computational and experimental results for the two-semicircular-bladed SHT is shown in Fig. 5.3. The CFD results are found to follow the similar trend with the experimental results but with minor deviation. However, the C_P values obtained from experiments are higher than corresponding computational C_P values. The three dimensionality effect excluded in the CFD simulations may be accounted for this minor discrimination. The trends of computationally obtained C_P values show similar behavior (Fig. 5.3) with those of experiments. This clearly illustrates that the flow physics has been correctly captured well in the present simulations. The computational results are then considered for justifying the experimental observations (Fig. 5.3).

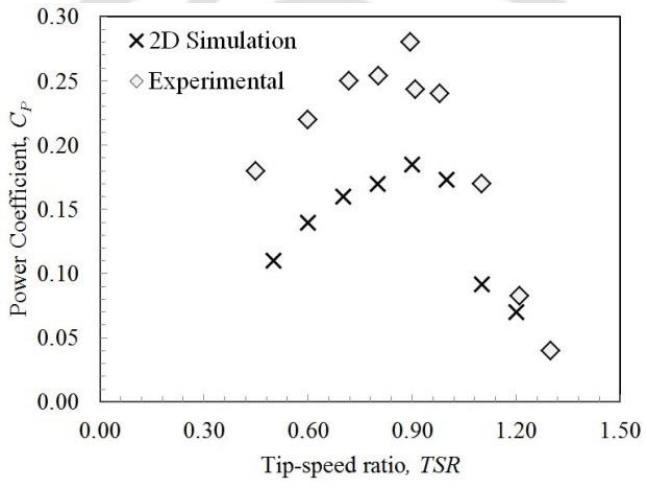

Figure 5.3: Model validation with experimental data

5.2.3 Flow physics analysis

For both the turbines, the streamline patterns for a particular orientation of blades are shown in Fig**.** 5.4. It is evident that, due to an extra blade there is an excessive deflection of water stream for the three-bladed turbine in comparison with two-bladed turbine. The deflected stream otherwise would have struck on the following blade. As a result of this, the Coanda-type flow at down-stream of the advancing blade gets destabilized due to generation of the large vortices in that region. This results in higher pressure at the downstream side of the advancing blade and thus lesser amount of energy available in flowing water is getting converted to mechanical energy by the turbine. Therefore, there are reduced maximum C_P and C_Q for the three-bladed Savonius turbine as compared to the two-bladed turbine. Some of the results reported on three-bladed Savonius wind/hydro turbine are shown in Table 5.1.

Table 5.1: Reported and present experimental data on three-bladed Savonius turbines

Investigators	Blade shape	C_{Pmax}	*TSR* corresponding to C_{Pmax}
Blackwell *et al*. (1977)	Semicircular (Wind)	0.15 (AR = 1.0, β = 0.17, Re = 8.67 × 10^5)	0.70
Khan *et al*. (2009)	Semicircular (Water)	0.038 (AR = 1.82, β = 0.20)	0.80
Sarma *et al*. (2014)	Semicircular (Water)	0.39 (AR = 0.65, β = 0, Re = 2.38 × 10^5)	0.77
Present study	Semicircular (Water)	0.17 (AR = 1.0, β = 0.15, Re = 2.25× 10^5)	0.71

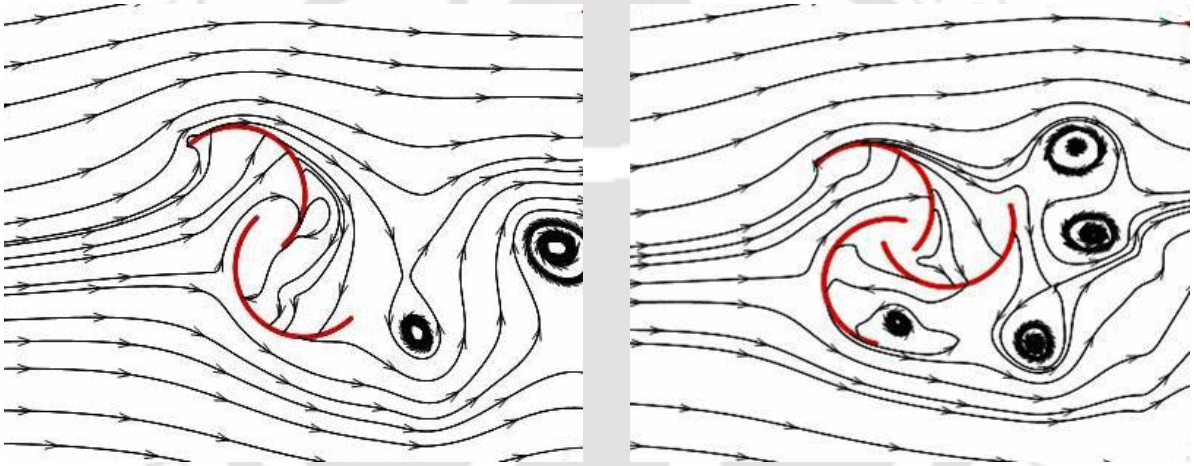

(a) Two-bladed turbine (b) Three-bladed turbine

Figure 5.4: Streamline pattern for two- and three-bladed SHTs

The pressure drop across the turbine blades can be examined since it can directly indicate the power extraction by the SHT. Hence, the pressure contours for two- and three-bladed SHT are compared in Fig. 5.5. The higher pressure zone at the concave side of the advancing blade and low pressure zone at the convex side of the advancing blade help in creating a pressure drop which affects the turbine rotation. Such pressure magnitude at the concave surface of the advancing blade is observed to be higher in case of two-bladed SHT as compared to three-bladed SHT. This results in a superior drag coefficient for the two-bladed semicircular SHT which in turn contributes to an improved overall performance. Thus, the present computational simulations not only compliment the experimental results but also help to justify them.

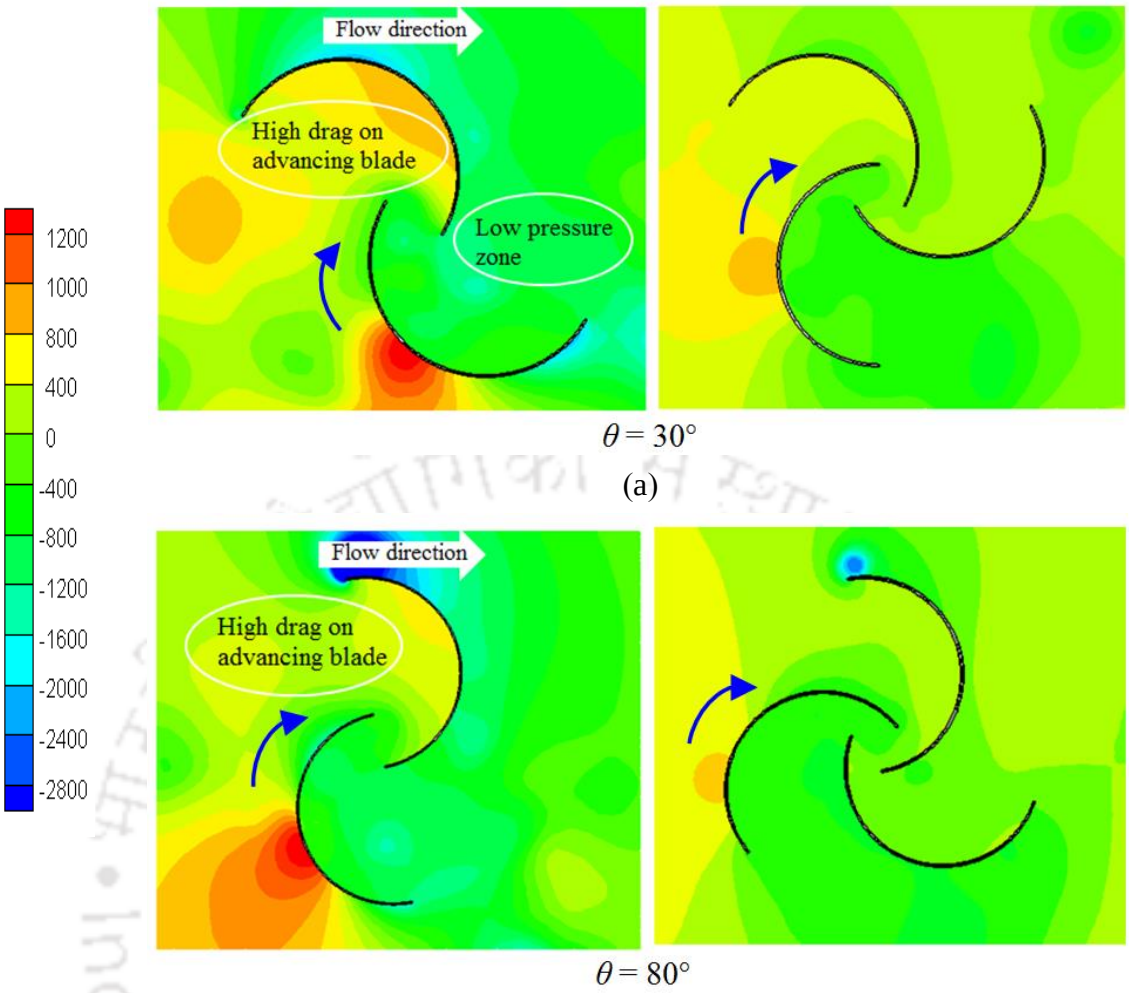

Figure 5.5: Pressure contour for two- and three-bladed SHTs

5.3 Effect of Blade Profile

5.3.1 Load characteristics experiments

In general, the conventional SHT suffers from low efficiency. Therefore, it is essential to improve the performance of the turbine either by implementing augmentation technique or by changing the blade shape. The alteration in blade shape has been proven to be effective for wind turbines (Banerjee *et al*. 2014; Alom *et al*. 2016). But no such efforts are reported for hydrokinetic turbines. Hence, in the present study, the effect of elliptical and semicircular shapes, on performance of the SHT, has been assessed. The two-bladed semicircular turbine, which demonstrates higher C_P than three-bladed turbine, is considered here as well. The performance parameters obtained experimentally are compared in Fig. 5.6. From the experimental investigations, it has been observed that semicircular-bladed turbine performs better in comparison to the elliptical-bladed turbine. At no load condition, the elliptical-

bladed turbine rotates at *TSR* = 1.1 whereas the semicircular-bladed turbine rotates at *TSR* = 1.34. The C_{Pmax} for elliptical-bladed turbine is found to be 0.20 at *TSR* = 0.77.

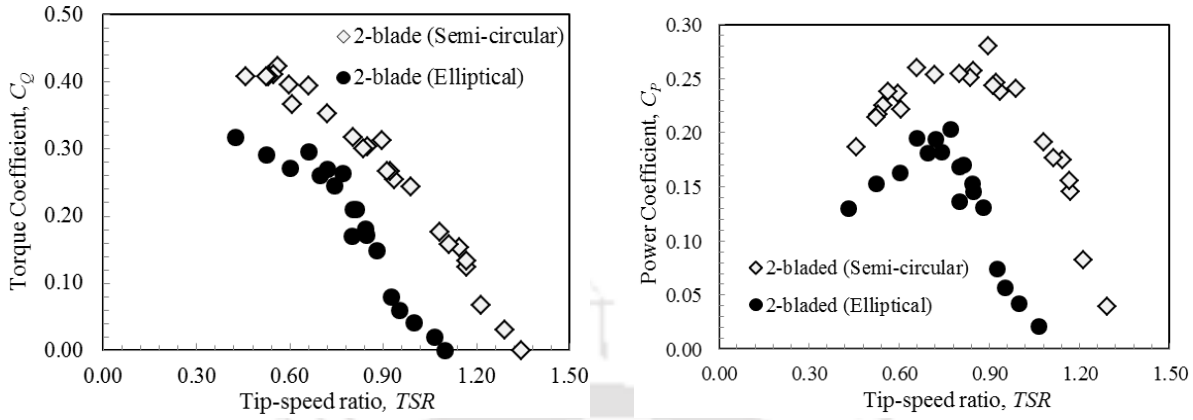

(a) C_Q vs *TSR* (b) C_P vs *TSR*

Figure 5.6: Performance characteristics curves

5.3.2 Flow physics analysis

In order to obtain the flow physics and reasoning behind the improved performance of the semicircular-bladed turbine over elliptical-bladed turbine, CFD simulations have been carried out for the experimental conditions. The velocity vector plots for both the turbines at *TSR* = 0.70 are presented at different angular positions in Fig. 5.7. The incoming water velocity is constant up to rotating zone consisting of the turbine. As the turbine rotates, two zones viz., (a) high speed zone around the tip of the turbine blade and (b) low speed or wake zone at the downstream of the turbine are observed. Similar trend has been reported by Kumar and Saini (2017) for SHT. At θ = 45°, a maximum flow velocities of 1.8 m/s and 2.4 m/s are obtained at tip of the advancing blade for semicircular and elliptical bladed turbines respectively. In case of elliptical-bladed turbine, highly aggravated sharp stream of velocity vectors depart from the tip of the advancing blade which in turn deteriorates the performance of the turbine (θ = 90° and 135°). Such streamline pattern is expected to have lesser momentum exchange between the waterstream and the turbine rotor. Such performance degradation due to sharp velocity vectors is also reported by Sarma *et al*. (2014). Further, at θ = 135°, the velocity vectors at the upstream are mainly responsible for generation of lift in the advancing elliptical-bladed turbine unlike semicircular bladed turbine. At θ = 90°, on the concave halves of the both advancing and returning blades are subjected to higher magnitude velocity vector for elliptical-bladed turbine. Hence, this accelerating flow produces low pressure on the concave side of blade and that degrades the positive moment generation on blades. Also in

the gaps between the trailing edge of the blades, overlapping type flow is more prominent in case of semicircular-bladed turbine compared to elliptical-bladed turbine. The flow helps in reducing negative torque generated by the returning blade. Therefore, the overlapping flow in case of semicircular bladed turbine results in more power output and torque coefficient.

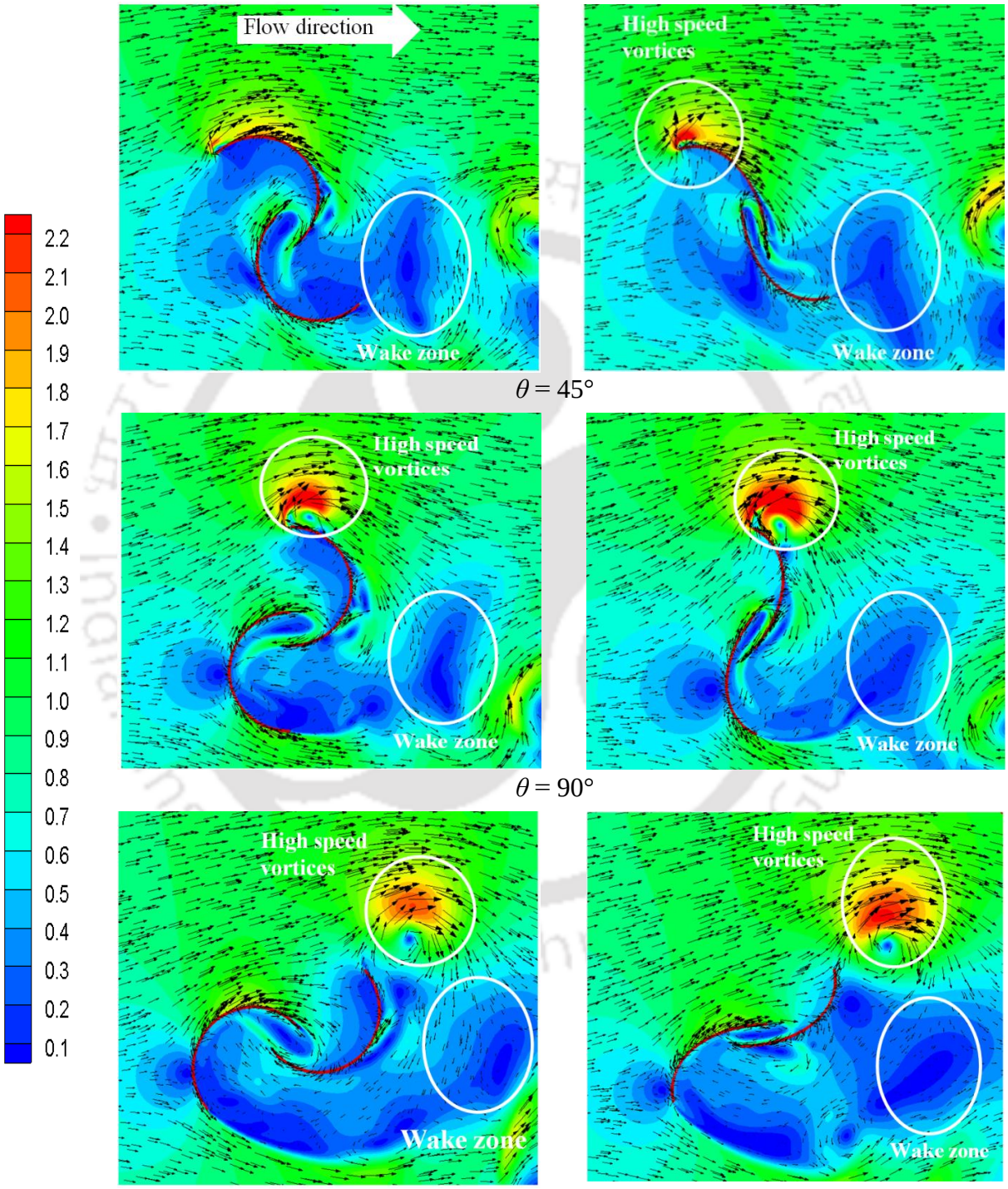

Figure 5.7: Velocity vector plots for semi-circular and elliptical bladed turbines

Further, in order to analyze the blade-wake interaction or vorticity distribution around the turbine blades, the vorticity contours (Fig. 5.8) of two-bladed semicircular and two-bladed elliptical SHTs at turbine position (θ) of 90° are generated. It is known that the vorticity denotes the spinning motion of fluid particles and it is expressed as curl of flow velocity (Mari *et al.* 2017). The identical type of wake structures can be seen around the blades of both the turbine geometries. However, it is observed that wakes of intense turbulence intensity is generated in case elliptical SHT in comparison to semicircular SHT especially at the tip of the blades, overlapping region between the blades and also at the downstream of turbine. This degrades the performance of the elliptical-bladed SHT as compared to semicircular bladed SHT.

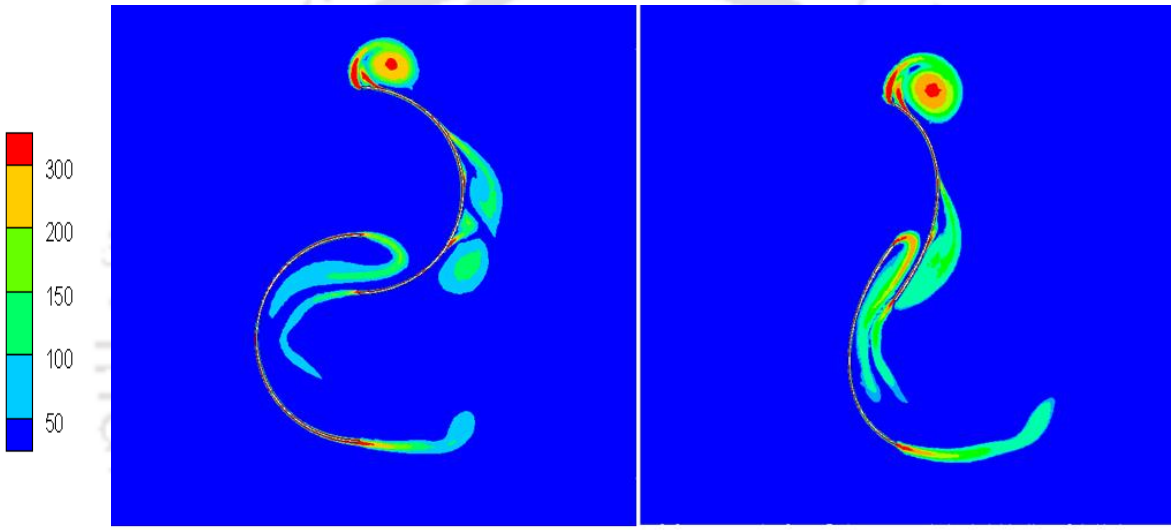

Figure 5.8: Vorticity contours for semi-circular and elliptical bladed turbines

Table 5.2 shows some of the reported results on two-bladed Savonius wind/hydro turbines. Further, the computational investigation carried out by Alom *et al*. (2016) states that elliptical-bladed turbine shows better performance than the semicircular-bladed turbine showing a $C_{P\max}$ of 0.32 and 0.27 at TSR = 0.80, respectively. However, in the present study the elliptical-bladed SHT shows a lesser C_P in comparison to semicircular-bladed SHT. It is worth mentioning that Alom *et al.* (2016) has carried out investigation taking overlap distance as 20% of the blade chord length. Therefore, further extensive parametric study on elliptical-bladed hydrokinetic turbine has to be carried out to arrive at an optimum configuration.

Table 5.2: Reported and present data on two-bladed Savonius turbines

Investigator	Platform	Blade shape	C_{Pmax}	Optimum *TSR*
Blackwell *et al*. (1977)	Experimental	Semicircular (Wind)	0.24 (AR = 1.0, β = 0.17, Re = 8.67×10^5)	0.90
Shankar (1979)	Experimental	Semicircular (Wind)	0.23 (β = 0.05)	0.85
Fujisawa and Gotoh (1994)	Experimental	Semicircular (Wind)	0.173 (AR = 1.0, β = 0.15)	0.90
Kamoji *et al*. (2009)	Experimental	Conventional semicircular (without shaft)	0.17 (AR = 1.0, β = 0.15, Re = 1.2×10^5)	0.78
		Modified blade (without shaft)	0.19 (AR = 0.70, β = 0, Re = 1.2×10^5)	0.72
		Modified rotor with shaft (Wind)	0.13 (AR = 0.70, β = 0, Re = 1.2×10^5)	0.61
Ali (2013)	Experimental	Semicircular (Wind)	0.21 (AR = 1, β = 0)	0.80
Chen *et al*. (2016)	Experimental	Wind tunnel (Wind)	0.21 (AR = 1.17, β = 0.17)	0.64
Sanusi *et al*. (2016)	Experimental	Semicircular (Wind)	0.24 (AR = 1.0, β = 0.15 =e/d)	0.78
Alom *et al*. (2016)	Numerical	Elliptical (Wind)	0.33 (AR = 0.7, β = 0.20 =e/d)	0.80
Patel *et al*. (2017)	Experimental	Semicircular (Water)	0.20 (AR = 1.096, β = 0.13)	0.55
Nakajima *et al*. (2008)	Experimental	Semicircular (Water)	0.25 (β = 0.36, Re = 1.1×10^5)	1.1
Golecha *et al*. (2012)	Experimental	Modified blade (Water)	0.14 (AR = 0.7, Re = 1.32×10^5)	0.70
Present study	Experimental	Semicircular (Water)	0.28 (AR = 1.0, β = 0.15, Re = 2.25×10^5)	0.89
Present study	Experimental	Elliptical (Water)	0.20 (AR = 1.0, β = 0.15, Re = 2.25×10^5)	0.77

AR = Aspect ratio
β =e/D=Overlap ratio
Re = Reynolds number
TSR = Tip-speed ratio

5.4 Immersion Experiments

From earlier sections, it has become evident that option of having two semicircular blades for a SHT is a better alternative than having three blades. Further, the semicircular blade shape is witnessed to have an edge over the elliptic shapes of the blade. But these conclusions are based on complete immersion of the turbine. Therefore, experiments with partial immersion are conducted mainly to forecast the degradation of performance with change in immersion level. All the three configurations viz. three-bladed semicircular, two-bladed semicircular and two-bladed elliptical turbines are studies. These turbines have been tested at 80% and 60% immersion level in addition to 100% or fully immersed condition at the same test site as discussed in section 3.2. It is known that the effective area of the turbine exposed to water stream is not the total cross sectional area of the turbine for partial immersion experiments. Therefore, the only immersed area of the turbine is taken for calculating power coefficients. From Fig. 5.9 through 5.11, it can be highlighted that the performance of a SHT drops drastically with the decrease in immersion levels.

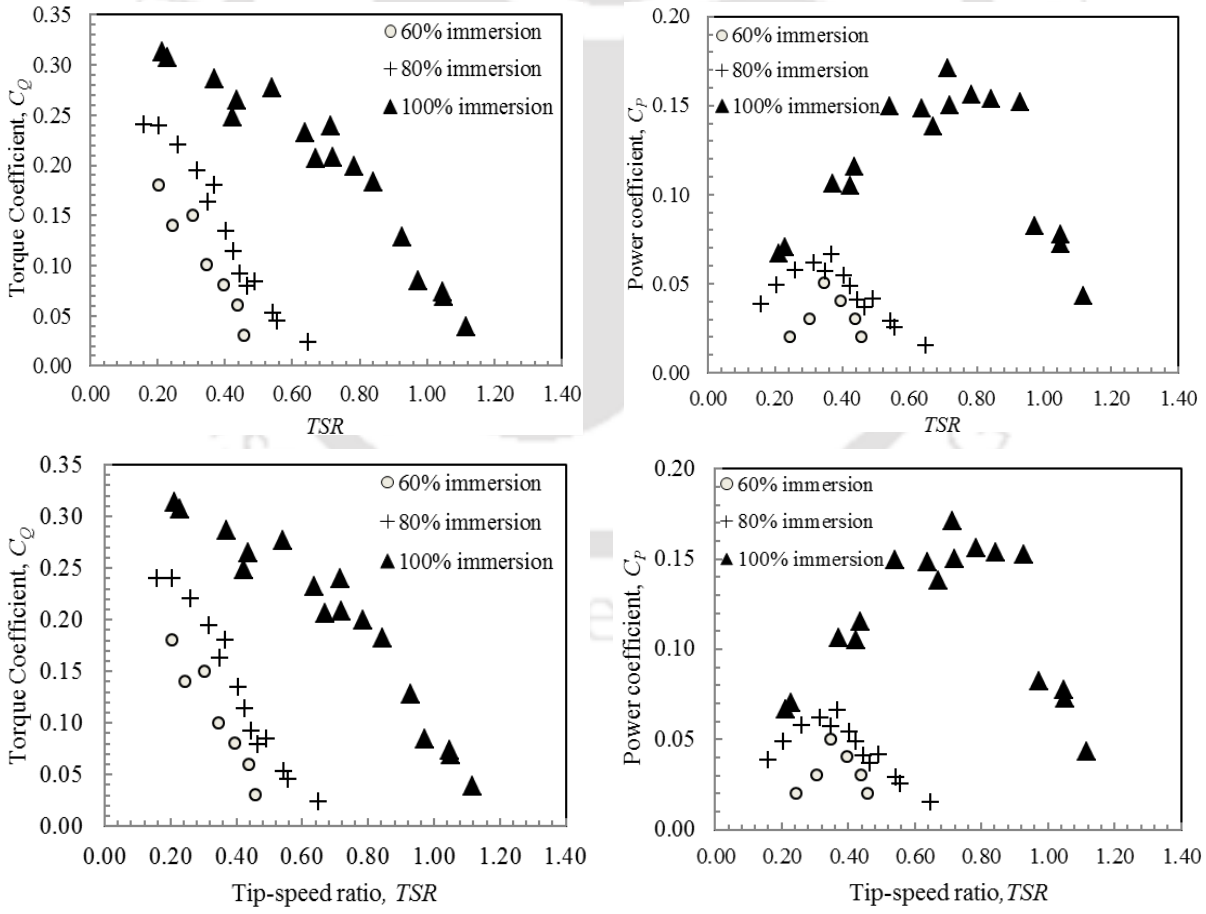

(a) C_Q vs *TSR* (b) C_P vs *TSR*

Figure 5.9: Performance characteristics of SHT with three semicircular blades

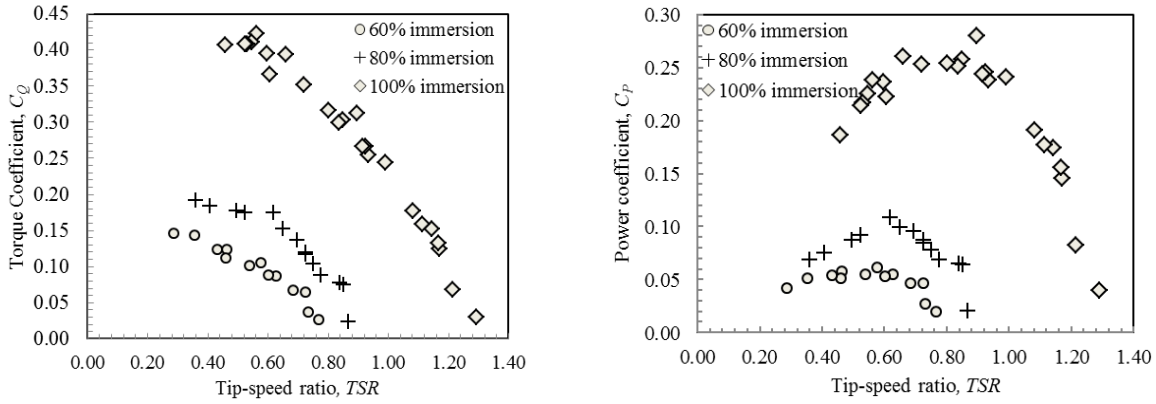

(a) C_Q vs *TSR* (b) C_P vs *TSR*

Figure 5.10: Performance characteristics of SHT with two semicircular blades

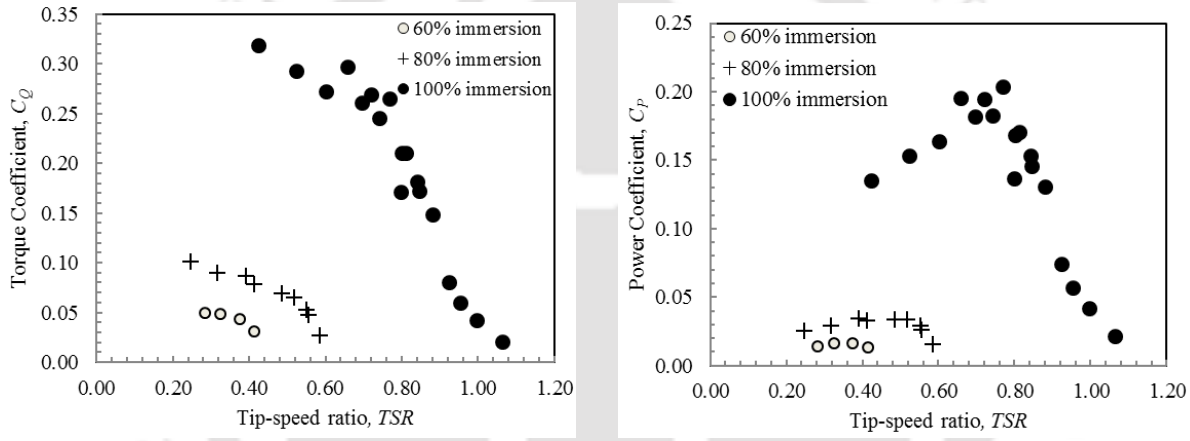

(a) C_Q vs *TSR* (b) C_P vs *TSR*

Figure 5.11: Performance characteristics of SHT with two elliptical blades

As observed, the C_P value drops suddenly and the point of optimum *TSR* also shifts towards the lower value with reduction in immersion level (Fig. 5.9 through 5.11). However, the trend of the C_P *vs TSR* curve remains the same at each level of immersion for all the turbines. This reduction in C_P is obtained to be more pronounced in case of elliptical-bladed turbine at each level of immersion. When the immersion level drop from 100% to 60%, the C_{Pmax} values of three-bladed semicircular, two-bladed semicircular and two-bladed elliptical turbines are decreased by 70%, 75% and 90%, respectively. In addition, when the immersion level is changed from 100 to 80%, the C_{Pmax} value drops by 58.8%, 64.2% and 80% for three-bladed semicircular, two-bladed semicircular and two-bladed elliptical turbines, respectively. The reduced values of *TSR* corresponding to C_{Pmax} are shown in Table 5.3.

Table 5.3: Variation of performance characteristics with immersion level

Immersion level	*TSR* corresponding to C_{Pmax}	C_{Pmax}	Torque coefficients corresponding to C_{Pmax}
Three-semicircular-bladed			
60%	0.31	0.05	0.15
80%	0.37	0.07	0.18
100%	0.71	0.17	0.24
Two-semicircular-bladed			
60%	0.57	0.07	0.10
80%	0.61	0.10	0.17
100%	0.89	0.28	0.31
Two-elliptical-bladed			
60%	0.37	0.02	0.04
80%	0.52	0.04	0.06
100%	0.77	0.20	0.26

Further, the braking torque of the turbines at different immersion levels are shown in Fig. 5.12 and it is observed that the peak braking torque of the three-bladed turbine is maximum at 60% and 80% immersion level. It is also evident that the three-bladed turbine shows better performance at partial immersion conditions in comparison to two-bladed elliptical turbine. Overall, the two-semicircular-bladed turbine demonstrates highest C_{Pmax} at all immersion levels along with higher *TSR* values compared to other turbine designs. Hence, a two semicircular-bladed turbine is better for implementation in a site where fluctuations in water level are high.

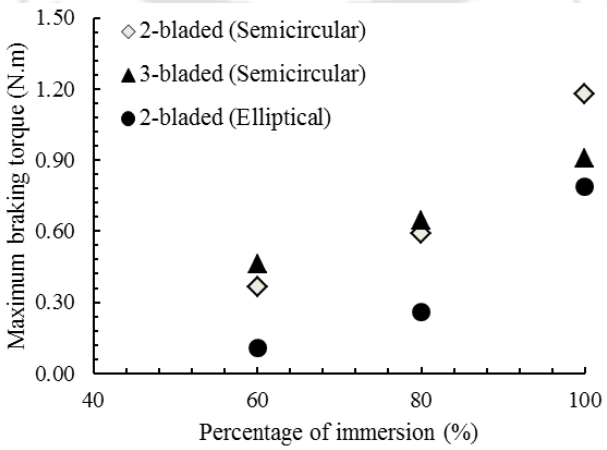

Figure 5.12: Variation of maximum braking torque with immersion level

5.5 Summary

In this chapter, a parametric study of the Savonius hydrokinetic turbines (SHT) based on number of blades, blade shapes and immersion level has been discussed. The performances of turbines with two-semicircular blades, three-semicircular blades and two-elliptical blades have been assessed at 100%, 80% and 60% immersion levels. The experimental observations of SHTs are further supported by 2D CFD simulations to analyze the flow characteristics and aerodynamic performance of the turbines.

The two-semicircular-bladed SHT (with β = 0.15, AR = 0.7 and D_o = 1.1D) shows an improvement of $C_{P\max}$ by 28.6% and 39.2% over two-bladed elliptical SHT and three-semicircular-bladed SHT, respectively. The CFD analysis indicates an improved flow characteristics of the semicircular-bladed SHT over the elliptical-bladed SHT. Furthermore, in case of three-semicircular-bladed turbine, the high pressure zone is being created at the downstream due to generation of large vortices. This results in lesser amount of available energy to be converted to mechanical power by the turbine. In the partial immersion experiment, the two-semicircular-bladed SHT demonstrates highest C_{Pmax} values at all partial immersion levels among all turbine designs. The two-semicircular-bladed SHT operates at higher optimum TSR values at all immersion levels as compared to other two turbine designs. Further, there is least percentage degradation of performance for the three-semicircular-bladed SHT whereas, the two-bladed elliptical SHT demonstrates the maximum degradation of performance at various immersion levels. At 60% and 80% immersion levels, the two-semicircular-bladed SHT indicates the highest $C_{P\max}$ followed by the three-semicircular-bladed and two-elliptical-bladed SHTs. The three-bladed turbine depicts an improved performances by 60% and 42.8% over the elliptical-bladed turbine at 60% and 80% immersion levels, respectively. At similar immersion levels, the two-semicircular-bladed SHT exhibits better performance than the three- semicircular-bladed SHT by 28.6% and 30%, respectively.

Chapter – 6

Helical-bladed Hydrokinetic turbine (HHT) Results

Chapter Outline:

Overview

This chapter focuses on the onsite experimental observations of HHT. In all the cases, the mechanical power measurement has been done using rope brake dynamometer and power coefficients are obtained for a range of mechanical loading conditions. In the initial set of experiments, the effect of solidity ratio on performance of HHT is evaluated along with the starting torque characteristics. Thereafter, the effect of immersion level on performance of the turbine has been estimated. The testing of turbines has been carried out in an open channel flow flume. Experimental results demonstrated a superior performance of the HHT having higher solidity under full and partial immersions. The effect of multi-staging of the HHT is studied at the river Brahmaputra. The experiments revealed better performance for single-stage turbine over double-stage turbine.

6.1 Introduction

The hydrokinetic (or zero head) vertical-axis helical turbine is lift-based and has immense potential for future small-scale power generation. In this part of the study, the effect of solidity ratio, immersion level and multi-staging on HHT has mainly been reported. Further, the starting torque experiments have been conducted for the turbine configurations in order to evaluate their starting characteristics at fully immersed condition. The three different sites viz. open channel flume, irrigational sluice and river Brahmaputra have been selected for the conduct of experiments.

6.2 Effect of Solidity Ratio

6.2.1 Experiments at open channel flume

Here, all the three in-house developed turbines (NACA 0020 bladed) of different solidity ratios are tested in fully immersed condition. Details of these turbines are given in section 3.3.1. However, the incoming water velocities (V) have had slight deviation while testing the turbines on different occasions. Thus, the velocities recorded are 0.87 m/s, 0.85 m/s and 0.80 m/s for turbines I, II, and III, respectively. The arithmetic mean of water velocities at three locations along the inlet plane is shown in Fig. 6.1 for three different heights from the bottom of channel. It has been observed that the velocity of water increases with the increasing distance from bottom surface.

Figure 6.2 shows the outcome of these experiments in the form of variation of torque characteristics for turbines I, II and III. A monotonic decrement in torque with the *TSR* is evident from this figure for all the turbines. During actual experiments, initially these turbines are found to rotate freely for no applied spring load. This state of turbine represents the maximum rotational speed or *TSR* and zero torque. Such maximum rotational speeds are noted to be 76.2 rpm , 73.2 rpm and 62.1 rpm for turbines I, II and III respectively. The increase in mechanical load on the turbine increases the torque at the cost of decrease in rotational speed or *TSR*. However, this trait is not continuous till the magnitude of *TSR* becomes zero. The lowest *TSR* as shown in Fig. 6.2 gives the magnitude of torque that is slightly less than the maximum braking torque at which the turbine stalls (*TSR* = 0). Hence, beyond this load, no measurement of *TSR*, and in turn, the power is possible. The present investigations thus are unlikely below *TSR* of around 0.70 since the turbines (Design I, II and III) stall beyond *TSR* = 0.70. Further, the critical values of load indicating maximum braking

torque are found to be 1.52 Nm, 1.69 Nm and 1.24 Nm for turbines I, II and III, respectively. The corresponding maximum torque coefficients are calculated to be 0.30, 0.31 and 0.23 for turbine I, II, and III, respectively.

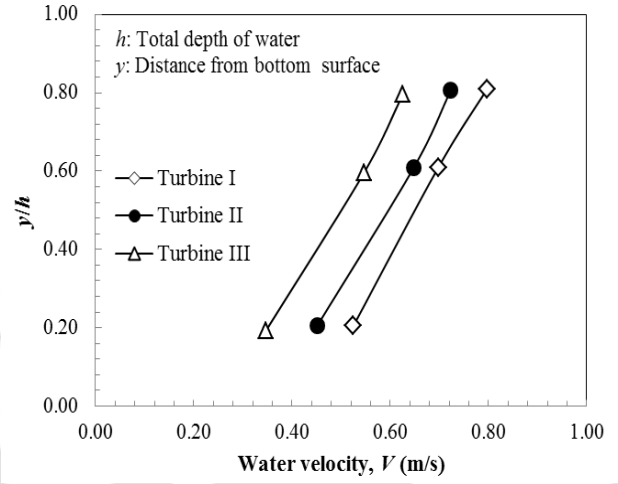

Figure 6.1: Inlet water velocity profile at different heights

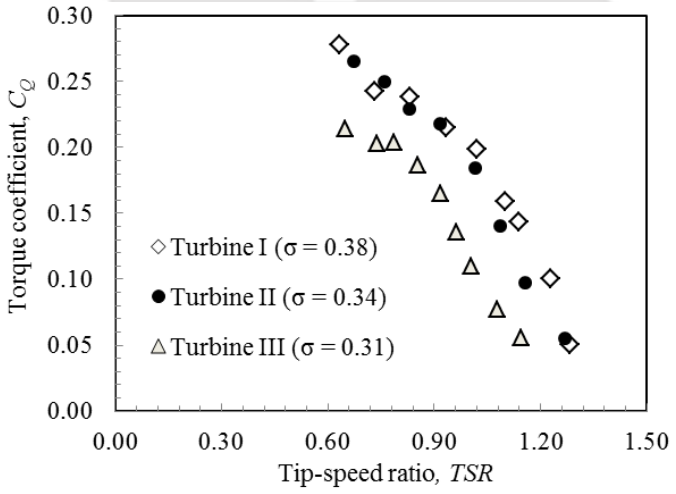

Figure 6.2: Variation of C_Q vs *TSR* for the tested turbines

Figure 6.3 shows the relationship between the C_P and *TSR* of the turbines. It can be observed from this figure that the C_P value initially increases with increase in *TSR* till an inversion point beyond which it starts decreasing with corresponding increase in *TSR* for all solidity ratios. The variation of C_P is analyzed with decrease in *TSR* since it resembles with the actual experimentation of all the turbines. At the starting of the torque measurement experiment, when turbine is unloaded, it rotates freely with maximum speed. At this no-load condition, the turbine acts more like a solid body in the flowing water, and hence, it cannot extract any

power. The extraction of partial power starts with an initial increase in mechanical load with a reduction in *TSR*. In this process, the power characteristic curve attains a peak that designates the maximum power output (product of rotational speed and the corresponding torque). Therefore, the turbine should run at this optimum *TSR* in order to extract maximum power. At V = 0.87 m/s, turbine I demonstrates $C_{P\max}$ = 0.20 at *TSR* = 1.02. Similarly for turbine II with V = 0.85 m/s, $C_{P\max}$ = 0.20 is obtained at *TSR* = 0.92. Moreover, turbine III at V = 0.80 m/s and *TSR* = 0.85 shows $C_{P\max}$ = 0.16. With further increase in applied load, the rotational speed (and hence *TSR*) of the turbine gets reduced below the optimum value leading to a decrement in power. At a particular load, the turbine stops operating causing least interaction with the flowing water. There has not been any change in C_{Pmax} when solidity reduces from 0.38 to 0.34 (turbine I to II). With further reduction in solidity ratio from 0.34 to 0.31 (turbine II to III) the $C_{P\max}$ gets reduced by 0.04. The present study demonstrates the $C_{P\max}$ to be weakly dependent on the alteration of solidity ratio in the range of 18% in the range of water velocity (0.80 – 0.87 m/s).

There are diverse observations from the investigations with helical hydrokinetic turbine of NACA 0020 blade profile. From one of his experimental studies, Gorlov (1998) reported a $C_{P\max}$ of 0.35, while the computational studies of Tsai and Chen (2014) showed a $C_{P\max}$ of 0.22 for the same turbine when tested at a slightly lower water velocity. Moreover, the $C_{P\max}$ obtained from present experiments and the one observed in computational results (Tsai and Chen 2014) have marginal difference. It is to be noted that the present $C_{P\max}$ lies in the range as reported by most of the researchers. Apart from this, the trend of C_P with *TSR* also agrees well with those of Niblick (2012) and Shiono *et al.* (2002) (Fig. 6.3). The use of airfoil shaped spoke arms is believed to be the reason for higher C_P in the experimental studies of Bachant and Wosnick (2015). The higher water velocity and hence the higher Reynolds number experienced by the helical turbine of Han *et al.* (2013) should actually lead to higher $C_{P\max}$ than the one noted by Gorlov (1998). But this turbine has a much lower solidity ratio thereby showing a lower peak C_P than that of Gorlov's turbine. As reported (Kumar and Saini 2017), the effect of Reynolds number for hydroturbine is found to have relevance for alteration in $C_{P\max}$ for the same turbine configuration. The present helical-bladed turbines have indicated nearly similar peak performances to those of the earlier tested turbines (Shiono *et al*. 2002; Tsai and Chen 2014; Marsh *et al*. 2015; Pongduang *et al.* 2015). The optimum *TSR* shifts towards a lower value with decrease in solidity ratio as evident in Fig. 6.3. The major reason for this shift is the increase in diameter of the turbines with a decrease

in solidity ratio for a fixed helix angle. As a result of this, the collective area spanned by the turbine blades around radial circumference decreases and creates void spaces between the turbine blades. This causes torque oscillation which in turn results in peak performance at lower *TSR*. It is worth mentioning that with the increase in diameter (and hence a reduction of solidity ratio) would increase the blockage in the experiments as observed in the present case due to confined water channel width. The blockage is thus marked as the reason for decrement in optimum *TSR* with increase in solidity ratio in the present experimental investigation. A comparison of studies performed on helical-bladed hydrokinetic turbine (HHT) has been shown in Table 6.1.

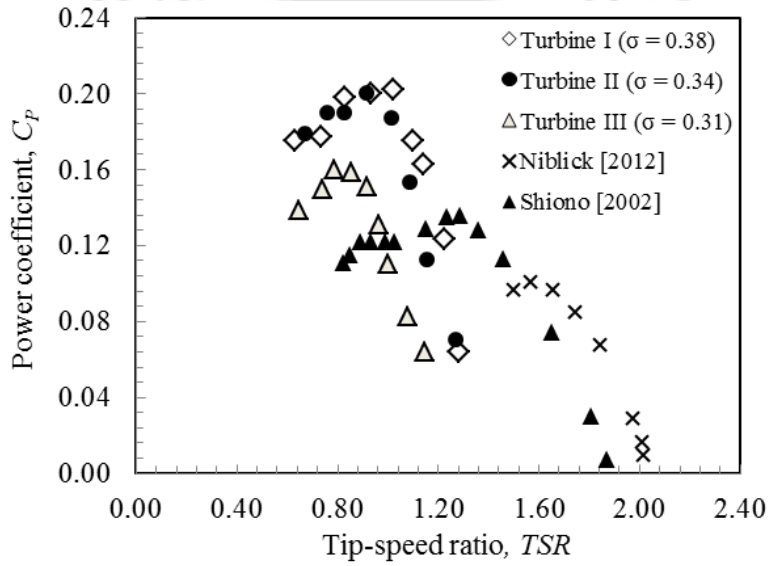

Figure 6.3: Variation of C_P vs *TSR* for the tested turbines

However, there is scope for improvement in their turbine performance either (a) by testing the turbines at higher water velocities, or (b) by using a frame and spoke arms constructed from extruded airfoil sections for minimizing the losses.

6.2.2 Immersion experiments

Another set of experiments were carried out in order to get an overall behavior of the turbine when it was fully and partially immersed in water. To ascertain the impact of partial immersion of turbines on its performance, experiments have also been carried out in the open channel flume. These tests include four different immersion levels of turbine viz. 100%, 86%, 73% and 60%. Since, in case of partial immersion experiments, the effective area of the turbine is not the total cross sectional area of the turbine in water, therefore, the only immersed area of the turbine is taken for calculating the power coefficient.

Table 6.1: Reported and present data on helical-bladed hydrokinetic turbines

Investigator	Platform	Dimensions D (m) × H (m)	ϕ (°)	σ	$C_{P\max}$	V (m/s)	Blade Profile
Gorlov (1998)	Experimental	0.61 × 0.86	60°	0.27	0.35	1.5	NACA 0020
Shiono *et al.*(2002)	Experimental	0.30 × 0.544	60°	0.40	0.17–0.24	0.6 – 1.4	NACA 63_3-018
Kirke (2011)	Experimental	1.0 × 1.25	--	0.13	0.25 to less than 0.10	2 – 5	NACA 0020
Niblick (2012)	Experimental	0.20 × 0.40	43.7°	0.30	0.11	0.80	NACA 0018
Han *et al.* (2013)	Experimental	2.20 × 2.50	65.3°	0.13	0.30	1.5 – 1.9	NACA 0020
Bachant and Wosnick (2015)	Experimental	1.00 × 1.32	--	0.14	0.36	0.5 – 1.4	NACA 0020
Tsai and Chen (2014)	Numerical	0.61× 0.86	60°	0.27	0.22	1.4	NACA 0020
Marsh *et al.* (2015)	Numerical	0.889 × 0.686	60°	0.07	0.12	1.5	NACA 63_4-021
Pongduang *et al.* (2015)	Experimental	0.50 × 1.25	150°	0.13	0.15-0.21	1.05 – 1.65	NACA 0020
		0.60 × 1.25	150°	0.11	0.10-0.17	1.28 – 1.57	
Present Study	Experimental	0.30 × 0.30	60°	0.38	0.20	0.87	NACA 0020
		0.34 × 0.30	60°	0.34	0.20	0.85	
		0.37 × 0.30	60°	0.31	0.16	0.80	

It is evident (Figs. 6.4 through 6.6) that as the percentage of immersion levels decrease the power output as well as C_P drops drastically and the point of optimum *TSR* also shifts towards the lower value. The percentage reduction of $C_{P\max}$ is found to be more pronounced in lower solidity turbines at each level of immersion. As the immersion level is decreased from 100% to 60%, $C_{P\max}$ value drops by 64%, 70.3% and 73.1% for turbine I, II and III, respectively. When immersion level is changed from 100 to 73%, the $C_{P\max}$ value drops by 42.50%, 56.31% and 60.81% for turbines I, II and III, respectively. In addition, when the immersion level has been changed from 100 to 86%, the $C_{P\max}$ value drops by 28.97%, 46.32% and 53.42% for turbines I, II and III respectively. It stands to reason that as the percentages of immersion decreases, the area of turbine blades exposed to water decreases. On the free surface, the water pressure equals the atmospheric pressure, however, at deeper water levels the water pressure increases. In case of partial immersion of turbines, the non-immersed part of the blades draw air into water which results in flow separation from the blade due to the adverse pressure gradient. This phenomenon of flow separation reduces the contribution of lift force to the net generating torque. This causes C_P and corresponding *TSR* to decrease with the decrease in percentage of immersion. Similar degradation of C_P due to partial immersion has been reported by Birjandi *et al*. (2013) for the Darrieus straight-bladed turbines. It is worth noting that the turbine III is the most affected turbine due to partial immersions at all levels of immersion. The performance of the helical-bladed hydro turbine with lower solidity ratio gets more aggravated with alteration in immersion level. This recommendation needs to be considered while designing a helical-bladed hydro turbine based power plant where seasonal fluctuations of water level are higher.

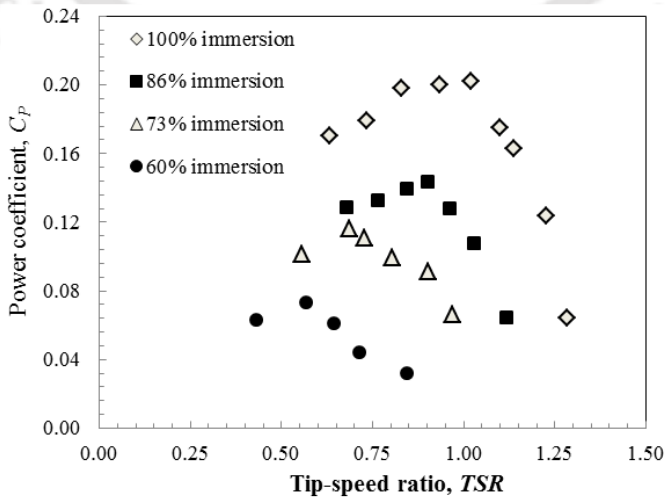

Figure 6.4: Variation of C_P vs *TSR* for turbine I (V = 0.87 m/s)

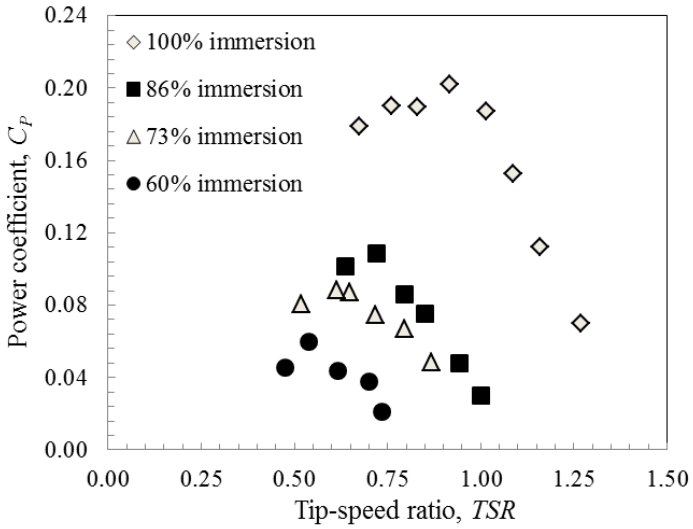

Figure 6.5: Variation of C_P vs TSR for turbine II (V = 0.85 m/s)

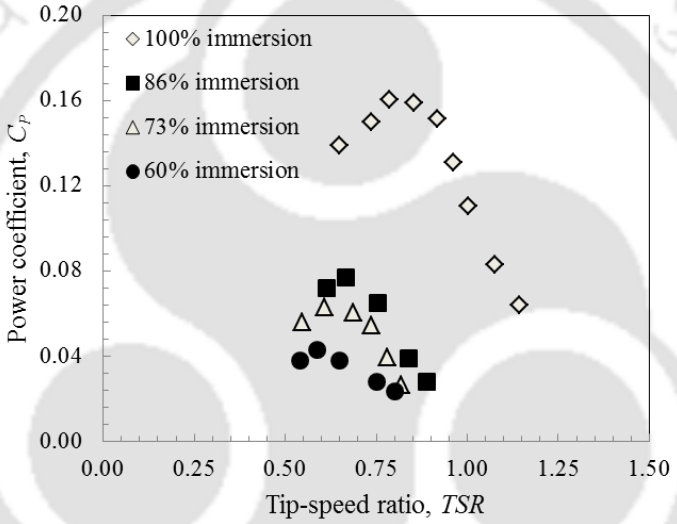

Figure 6.6: Variation of C_P vs TSR for turbine III (V = 0.80 m/s)

6.2.3 Starting torque experiments

In general, water or wind turbines are expected to have higher static torque which would showcase its self-starting ability. Therefore, estimate of static torque is highly essential since it is the characteristics of the turbine. However, limited attention for this measurement, in case of helical hydro turbines, has been observed in the literature. In view of this, presently designed and fabricated turbine is considered for starting torque measurement. Such static torque characteristics with respect to azimuth angles (γ) for turbines I, II and III are presented in Fig. 6.7. It is evident that the static torque of each turbine has attained three peaks in one complete revolution of the turbine. Maximum value of torque can be noticed as γ approaches 40°, 180° and 300° (Fig. 16). All the tested turbine configurations exhibit positive average starting torque coefficient (C_{QS}) over a complete 360° rotation which contributes towards

better starting ability of the turbines. The average C_{QS} of 0.22, 0.21 and 0.21 are observed from the experiments for turbines I, II and III respectively.

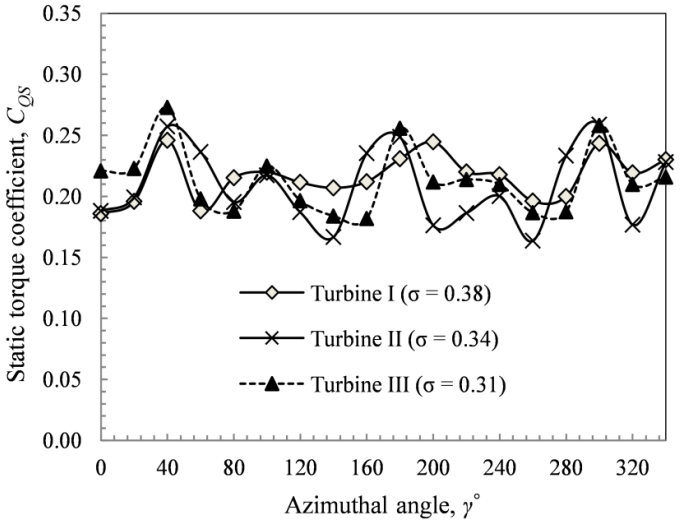

Figure 6.7: Variation of C_{QS} variation with azimuth angle (γ)

6.3 Load Characteristics Experiments at Irrigation Sluice

In this part of the analysis, the best performing HHT (σ = 0.38) mentioned in the section 6.2.1 and 6.2.2 has been field tested in an irrigation sluice located at Mandakata, Assam. The data of water velocity and rotational speed of turbine are recorded for the cases with and without mechanical loading conditions. This test reveals that at an inlet water velocity of 1.1 m/s, the maximum power coefficient of the turbine is found to be 0.16 at a *TSR* of 0.93. The variation of C_P and C_Q with *TSR* is shown in Fig. 6.8 and Fig. 6.9. The turbine rotates at 89.6 rpm for free-load condition and it stalls at maximum breaking load of 0.195 N.m.

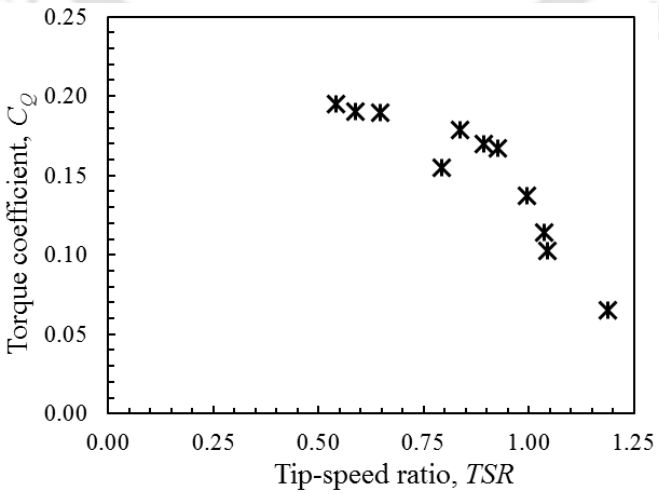

Figure 6.8: Variation of C_Q vs *TSR* (V = 1.1 m/s)

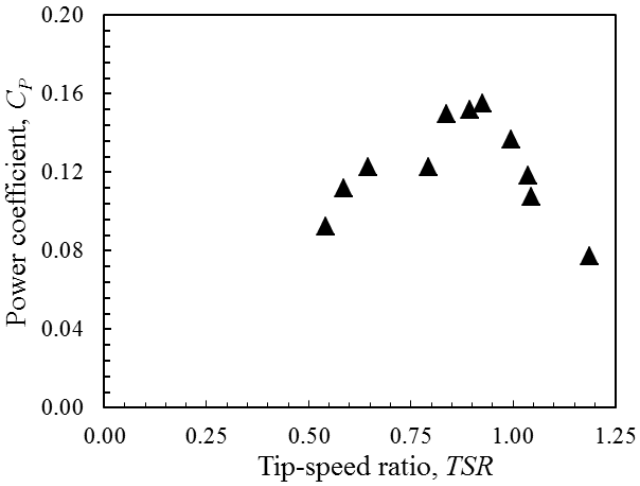

Figure 6.9: Variation of C_P vs *TSR* (V = 1.1 m/s)

6.3.1 Validation of computational model

The validation study has been carried out and the trends of simulation based results and the experimental results are found to be similar as seen in Fig. 6.10.

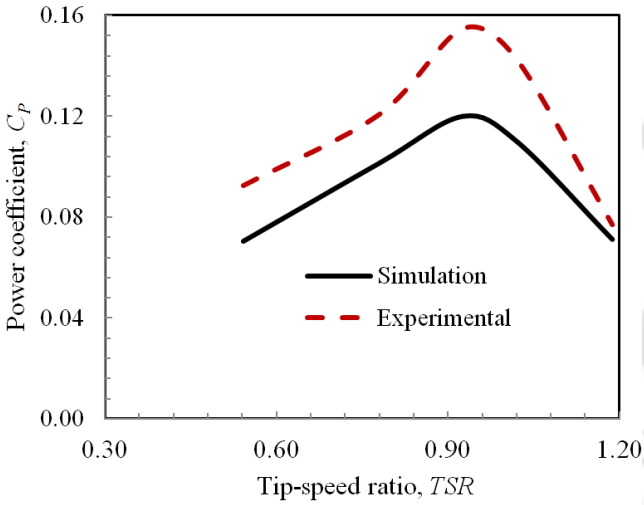

Figure 6.10: Validation study

Figures 6.11 and 6.12 show the generation of vortices at different angular positions of the helical turbine blades. The detached vortices have mainly been observed for HHT at 64.9 rpm, whereas at 38 rpm, the attached vortices have mostly been observed. It is also noticed that the generation and detachment of large vortices mainly occur at the upper half of turbine blades. It is also observed that the vortex generation is substantially higher in case of lower *TSR* (38 rpm) as compared to optimum *TSR* (64.9 rpm), which subsequently results in an inferior C_P value at lower *TSR*.

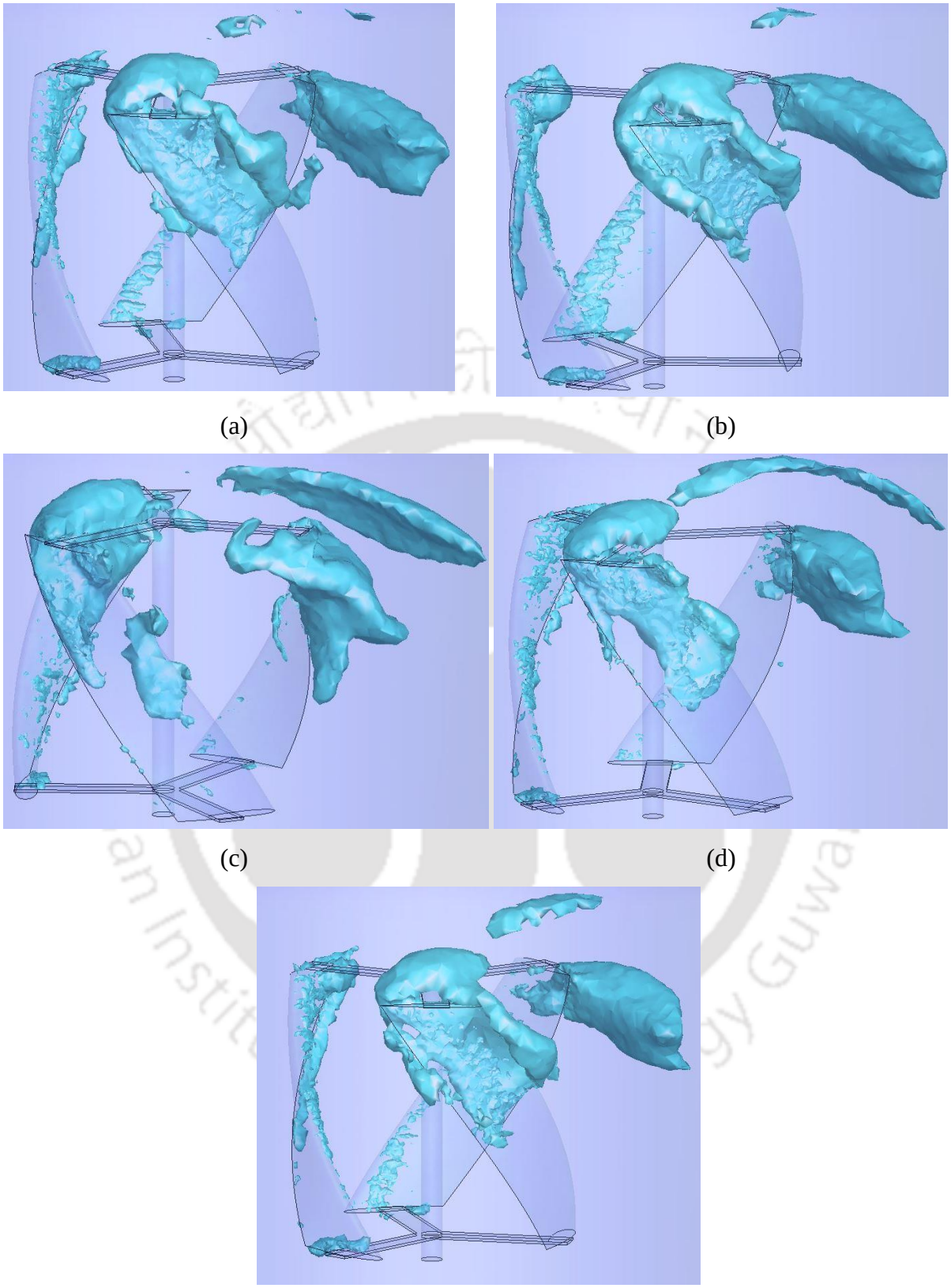

Figure 6.11: Turbulent kinetic energy contours (64.9 rpm)

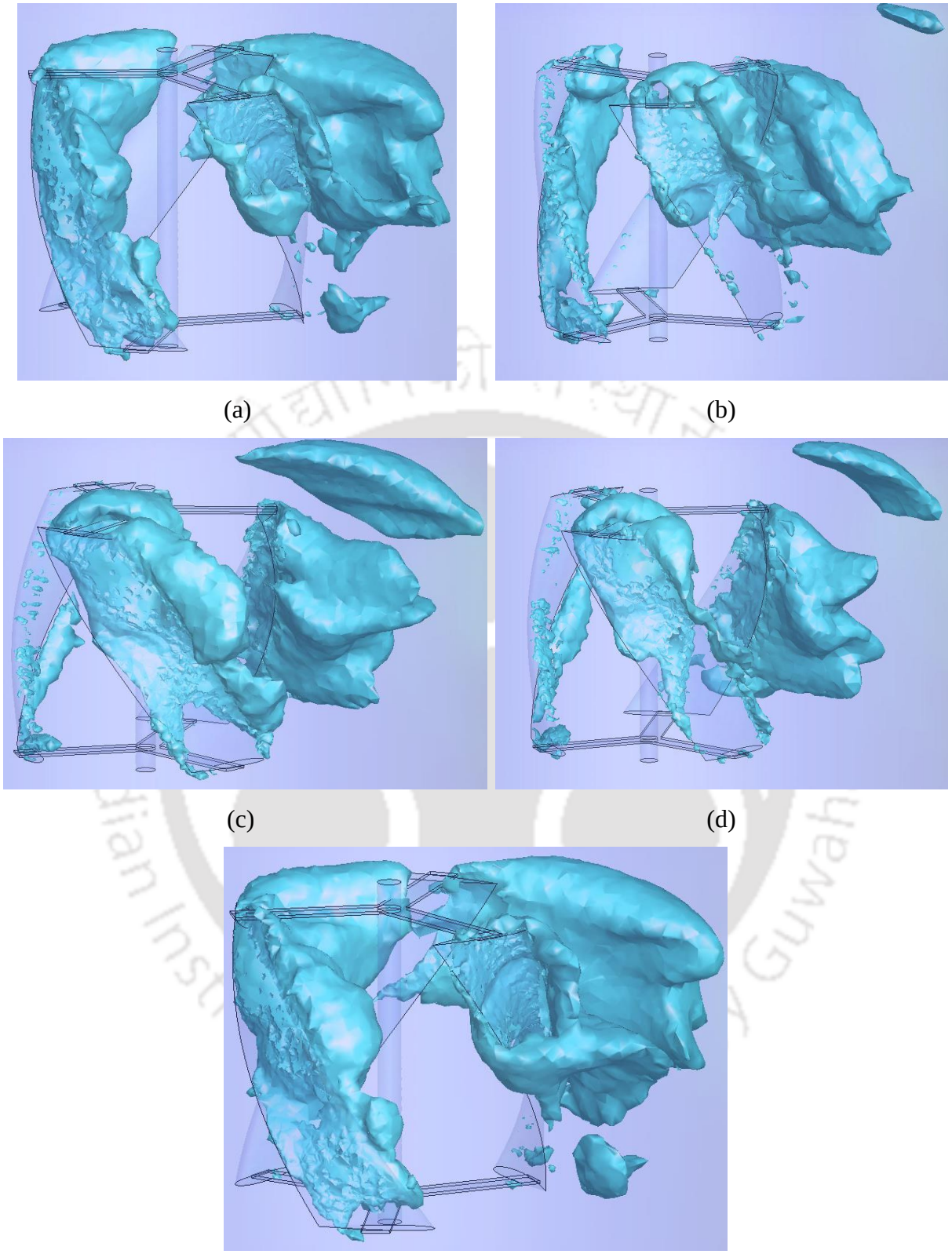

Figure 6.12: Turbulent kinetic energy contours (38 rpm)

Further, Fig. 6.13 and Fig. 6.14 show the total pressure contours of flow across a HHT at 64.9 rpm and 38 rpm. For the three-bladed HHT, a higher total pressure is observed outside the circular region at 64.9 rpm as compared the total pressure at 38 rpm. Also, the total pressure inside the circular region is very less in case of HHT at 64.9 rpm than at 38 rpm. Hence, there is a significant pressure drop for HHT at 64.9 rpm as compared to HHT running at 38 rpm. This indicates a higher energy extraction from the incoming fluid in case of HHT at 64.9 rpm. It can be also noticed that the recirculation is formed at immediate downstream of the blades at 38 rpm (Fig. 6.14a and 6.14b) which reduces the turbine performance. However, such recirculation is negligible in HHT at 64.9 rpm.

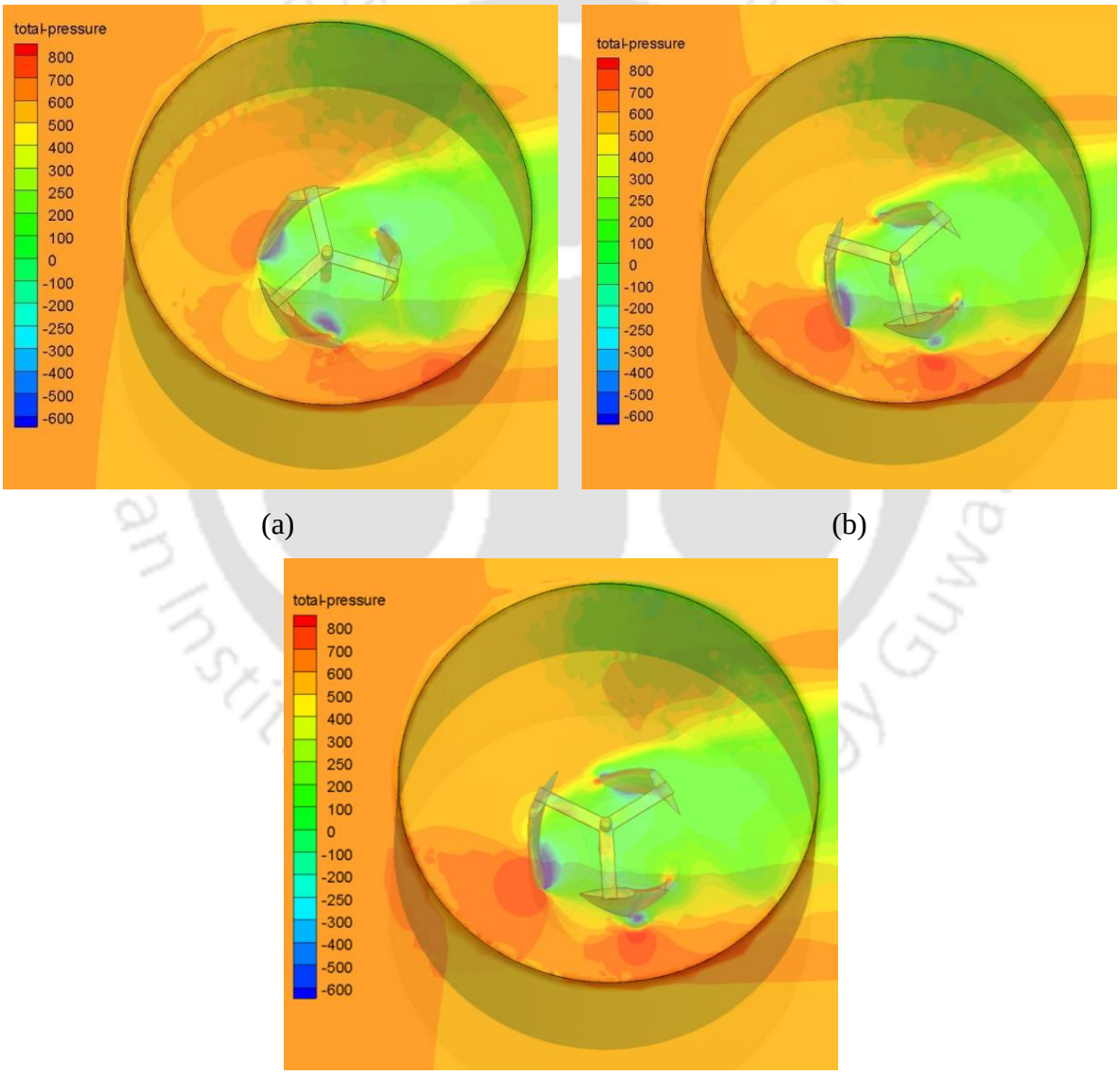

Figure 6.13: Total pressure contours (64.9 rpm)

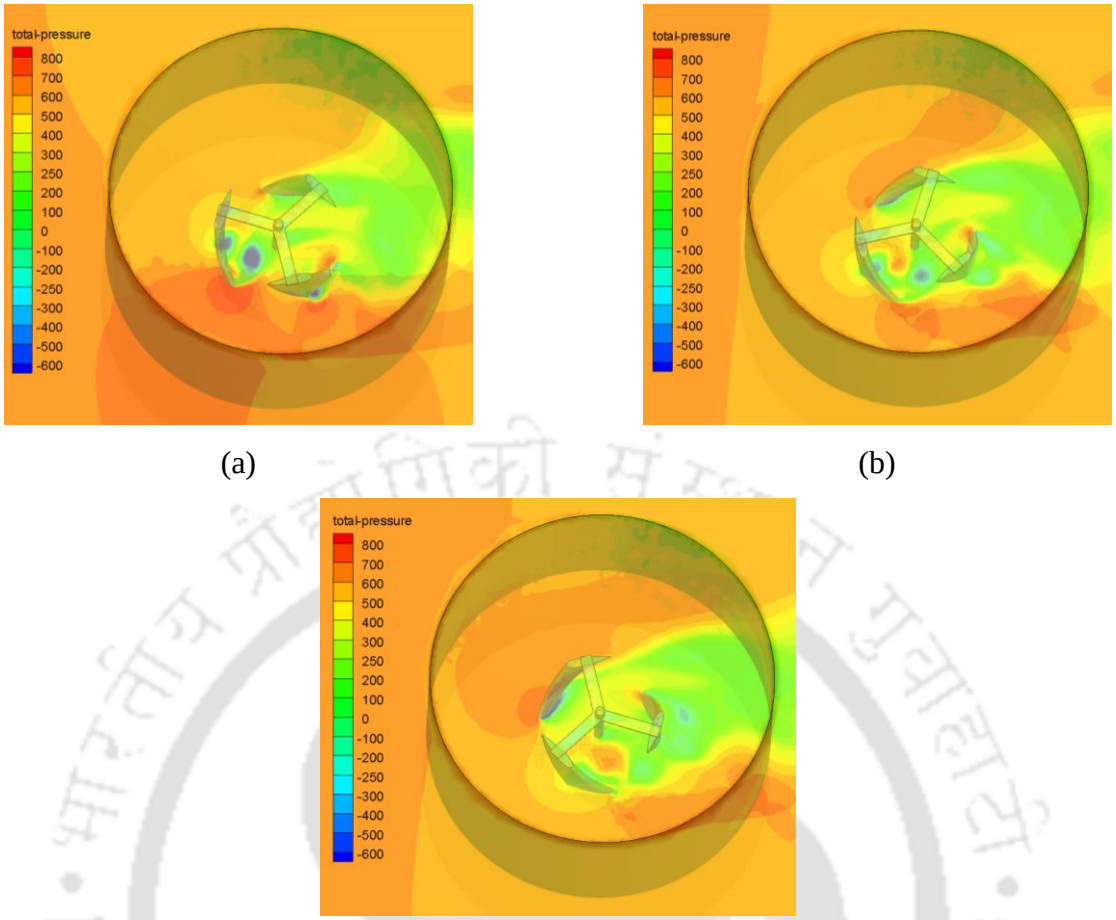

(a) (b)

(c)

Figure 6.14: Total pressure contours (38 rpm)

6.4 Effect of Multi-staging

The present investigation deals with the in-situ experiments of a double-step three-helical-bladed hydrokinetic turbine for possible electricity generation. Further, its performance is compared to that of a conventional single-step helical-bladed turbine. The turbines are tested in the Brahmaputra river and their performance characteristics are estimated at different mechanical loading conditions. Figure 6.15 shows the variation C_P of with *TSR* of the single-step and the double-step helical turbine configurations. It is worth mentioning that the inlet water velocity has had a slight deviation during testing of the single-step and double-step configurations and they are recorded as 1.3 m/s and 1.1 m/s, respectively. Both the turbine arrangements show initial increase in C_P with increase in *TSR*. At a particular *TSR*, the power output is recorded to be maximum. It is observed that the double-step configuration operates at high *TSR* in comparison to the single-step configuration. However, the $C_{P\max}$ obtained in the single-step and double-step configurations are 0.16 and 0.14, respectively at

corresponding *TSR* of 2.82 and 3.90. At no-load condition, the single-step turbine configuration is found to rotate at 486 rpm while the double-step turbine configuration rotates at 376 rpm. Further, the maximum braking torque obtained for single-step and double-step turbine configurations are 0.52 N.m and 0.41 N.m, respectively. Similar kind of experiment was carried out by Shiono *et al.* (2002) with σ = 0.20 and ϕ = 43.7° for single-step configuration. The study reported a $C_{P\max}$ of 0.13 at *TSR* = 1.9.

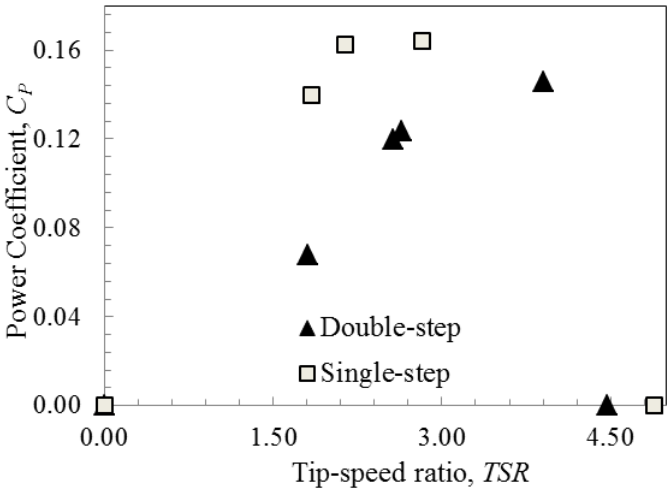

Figure 6.15: Variation of C_P vs *TSR*

6.5 Summary

In the present investigation, an attempt has been made to evaluate the performance of helical-bladed turbines at lower free-stream velocities. For this purpose, helical-bladed turbines with varying solidity ratios have been designed, developed and subsequently tested to arrive at an optimum design configuration. The investigation has also been extended to assess the performance of the turbines at different immersion levels in the water stream. Furthermore, the self-starting ability of the turbines has also been investigated. In order to compare the starting torque behavior of the turbines, the starting torque characteristics of each turbine has been evaluated experimentally at the fully immersed condition. The performance parameters such as C_P and C_Q are calculated over a range of *TSR*s. Experimental results indicate a $C_{P\max}$ of 0.20 at corresponding *TSR*s of 1.02 and 0.92 for turbines with solidity ratios of 0.38 and 0.31 respectively for *V* of 0.87 m/s and 0.85 m/s respectively. The C_P values of the turbines are observed to be reduced along with the optimum *TSR*s with decrease in immersion level of the turbines in the water steam. The starting torque experiment shows greater pulsation of static torque for turbine with solidity ratio of 0.31 in comparison to the turbines with solidity

ratios of 0.34 and 0.38. In similar line, the turbine with solidity ratio of 0.38 has been tested at an irrigation sluice. In another set of experiments, the performance of single-step and double- step turbines are compared. The maximum C_P obtained is found to be higher in case of single-step configuration than the double-step configuration. At no-load condition, the single-step turbine configuration is found to rotate at 486 rpm while the double-step turbine configuration rotates at 376 rpm.

Similarly, the experimental investigation of single-step and double-step HHT presents maximum C_P of the same order of magnitude. This study thus provides valuable guidelines on the onsite testing of hydrokinetic turbines. Conventionally, it is advisable to have multiple small turbine modules of equal swept area to be mounted on a common shaft for power generation instead of having a single larger turbine mounted on a shaft. However, in the presence of multiple turbines, the form drag due to spoke arms increases thereby reducing the performance of the overall system. In view of this, the present investigation recommends the use of a suitably designed multi-step hydrokinetic turbine for power generation with a converging channel for the velocity enhancement.

Chapter – 7

Savonius Wind Turbine (SWT) Results

Chapter Outline:

Overview

This chapter discusses the performance of Savonius turbines for a known input kinetic energy but with a difference in the working fluid medium. In that context, a comparison of performance for SWT and SHT having an identical kinetic energy of the oncoming fluid (wind/hydro) has been studied. In order to achieve these objectives, the wind tunnel experiments of SWTs have been carried out and the results are then compared with the results of the equivalent SHT testing. The study reveals almost similar performances for SWTs and SHTs at identical power input. The computational simulations are also performed to get a better insight of the flow physics. The lift and drag characteristics of the SWT and SHTs are evaluated and are found to complement each other.

7.1 Introduction

The wind flow is primarily governed by the pressure difference, whereas the gravity is predominantly responsible for water flow. The flow physics associated with them are therefore different. In the present analysis, an attempt has been made to compare the performance of SWT and SHT having an identical kinetic energy of the incoming fluid (wind/hydro). In order to keep the inlet kinetic energy (15.97 W) of the water to be identical to that of wind, the wind velocity is fixed at 7.4 m/s. Initially, the wind tunnel experiments with SWTs have been carried out and the results obtained are validated by 2D computational fluid dynamics (CFD) studies using ANSYS-Fluent. Further, the lift-drag characteristics of the SWT and SHTs are discussed to support the experimental observations.

7.2 Load Characteristics Experiments

From Fig. 7.1 through Fig. 7.3, it is evident that, at same kinetic energy of fluid, both trends of C_P vs *TSR* and C_Q vs *TSR* curves are seen to be similar for all the SWTs and SHTs. It is also observed that, the SWTs operate at slightly wider range of *TSR*s as compared to those of SHTs particularly towards increased value of *TSR* beyond optimum *TSR* in the plots of C_P vs *TSR*. The two-semicircular-bladed SWT demonstrates the $C_{P\max}$ = 0.25 at *TSR* = 0.87, whereas for SHT the $C_{P\max}$ = 0.28 is obtained at *TSR* = 0.89. Further, both three-semicircular-bladed SWT and SHT have shown same $C_{P\max}$ of 0.17 at *TSR*s of 0.72 and 0.71, respectively. The two-elliptical-bladed SWT and SHT have demonstrated $C_{P\max}$ = 0.20 at *TSR* of 0.78 and 0.77, respectively under similar condition. The two-semicircular-bladed SWT and SHT operate at maximum *TSR* of 1.44 and 1.34 for no-load condition. At similar condition, the three-semicircular-bladed SWT and SHT operate at *TSR*s of 1.35 and 1.18, respectively.

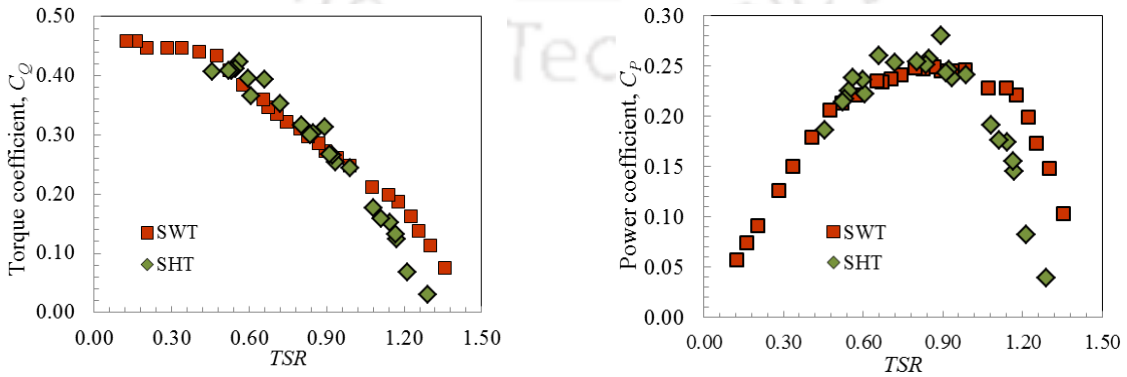

(a) C_Q vs *TSR* (b) C_P vs *TSR*

Figure 7.1: Performance comparison of two-semicircular-bladed Savonius turbine

Similarly, two-elliptical-bladed SWT and SHT run at *TSR* of 1.31 and 1.10 respectively under same condition. Again, the maximum braking loads leads to the braking torque of 0.13 N.m and 1.17 N.m for two-semicircular-bladed SWT and SHT, respectively. Similarly, for three-semicircular-bladed SWT and SHT, the maximum braking loads leads to the braking torque of 0.085 N.m and 0.91 N.m, respectively.

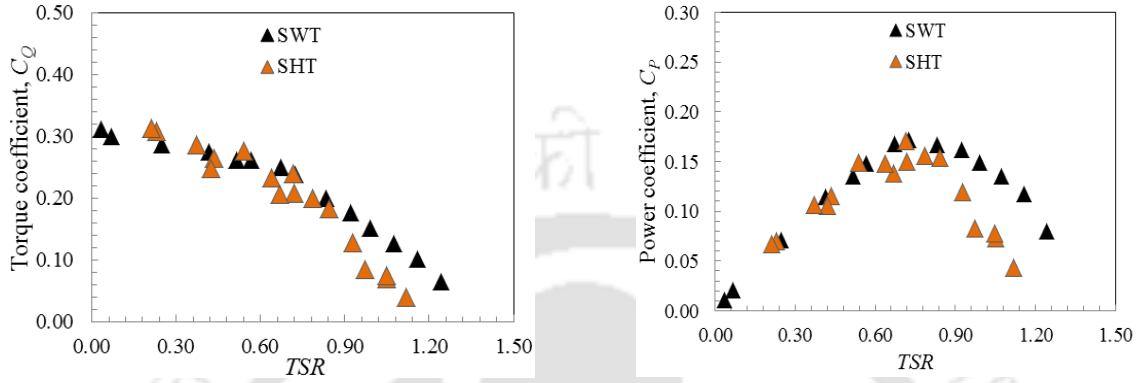

(a) C_Q vs *TSR* (b) C_P vs *TSR*

Figure 7.2: Performance comparison of three-semicircular-bladed Savonius turbine

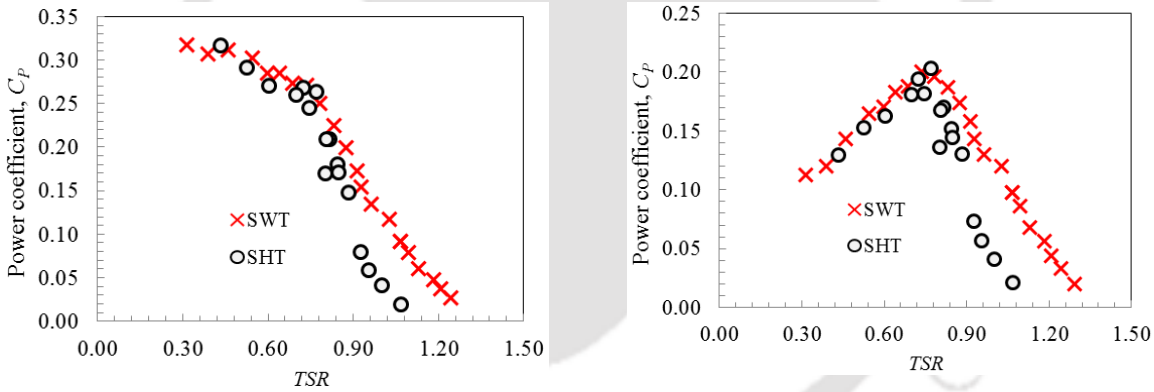

(a) C_Q vs *TSR* (b) C_P vs *TSR*

Figure 7.3: Performance comparison of two-elliptical-bladed Savonius turbine

7.3 Computational Analysis

The computationally obtained polar presentation of lift coefficient (C_L) and drag coefficient (C_D) with respect to turbine angle (θ) is presented in Fig. 7.4 to compare the performance of SWTs. The trend of C_D curve for the two-bladed SWT is found to be gradually increasing up to θ = 67° before gradually decrease up to θ = 162°, while following similar pattern afterwards. The two-elliptical-bladed SWT demonstrates similar lift and drag characteristic pattern to the two-semicircular-bladed SWT, however, it shows reduced magnitude of lift and drag as that of the latter. On the other hand, in case of three-bladed SWT, three peaks of C_D at

36°, 152° and 273° can be observed because of the additional blade. The mean values of C_D are obtained as 1.22 and 1.17 for two-bladed and three-bladed SWTs, respectively. In similar lines, the trend of C_L curve for the two-bladed SWT is found to be gradually increasing up to θ = 20° before gradual decrease up to θ = 120°, while following similar pattern afterwards. For three-bladed SWT, the polar plot shows three peaks values of C_L at 7°, 127° and 247°. Similarly, the mean values of C_L are observed as 1.32 and 1.14 for two-bladed and three-bladed SWTs, respectively. Thus, it is quite evident that the two-semicircular-bladed SWT demonstrates better drag and lift characteristics, as compared to two-elliptical-bladed SWT and three-semicircular-bladed SWT.

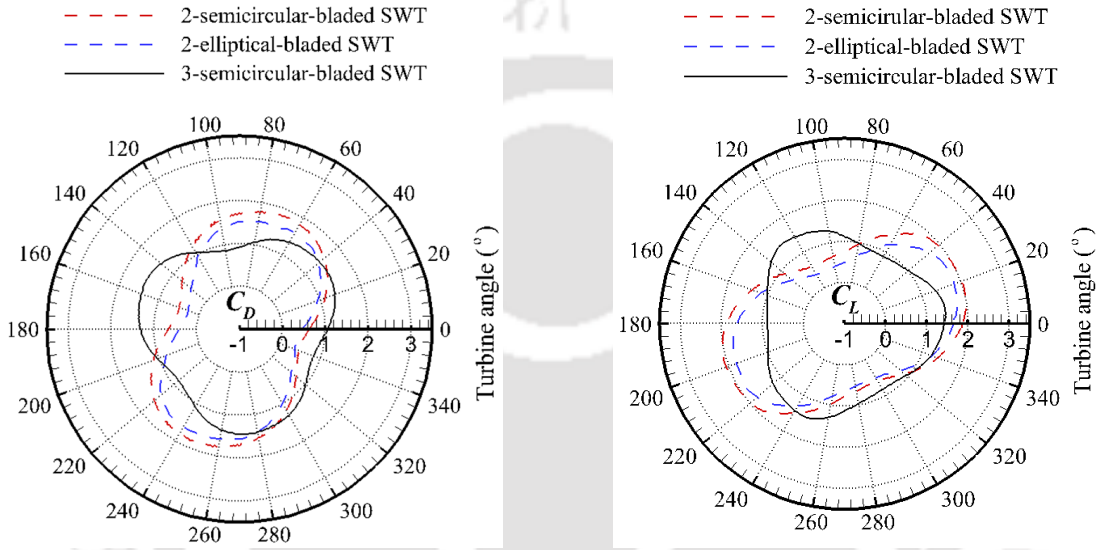

(a) C_D vs θ (b) C_L vs θ

Figure 7.4: Variation of lift-drag characteristics of turbine with angular positions

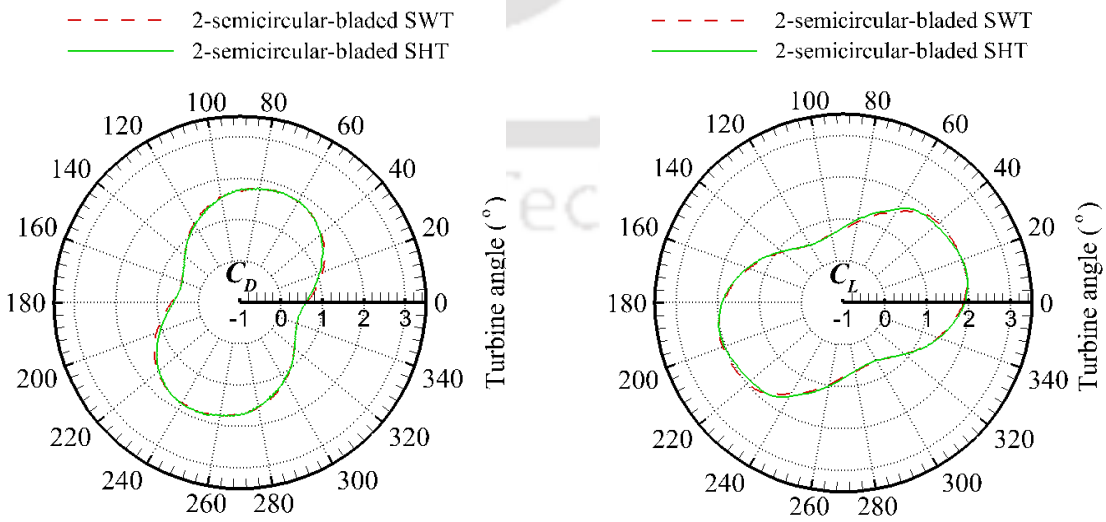

(a) C_D vs θ (b) C_L vs θ

Figure 7.5: Comparison of lift-drag characteristics for two-semicircular-bladed turbines

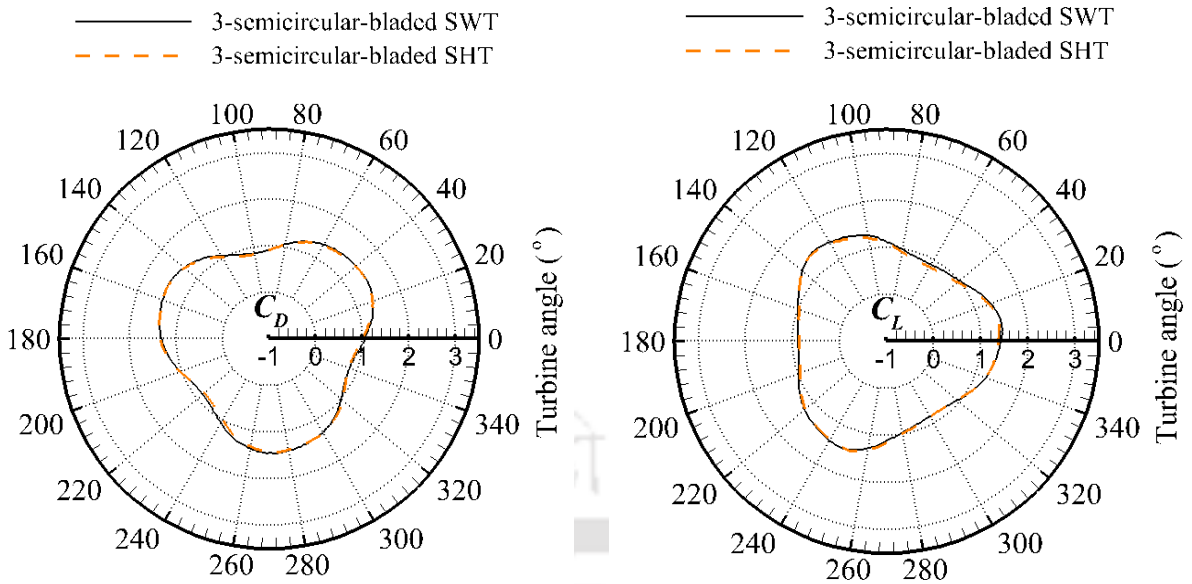

(a) C_D vs θ (b) C_L vs θ

Figure 7.6: Comparison of lift-drag characteristics for three-semicircular-bladed turbines

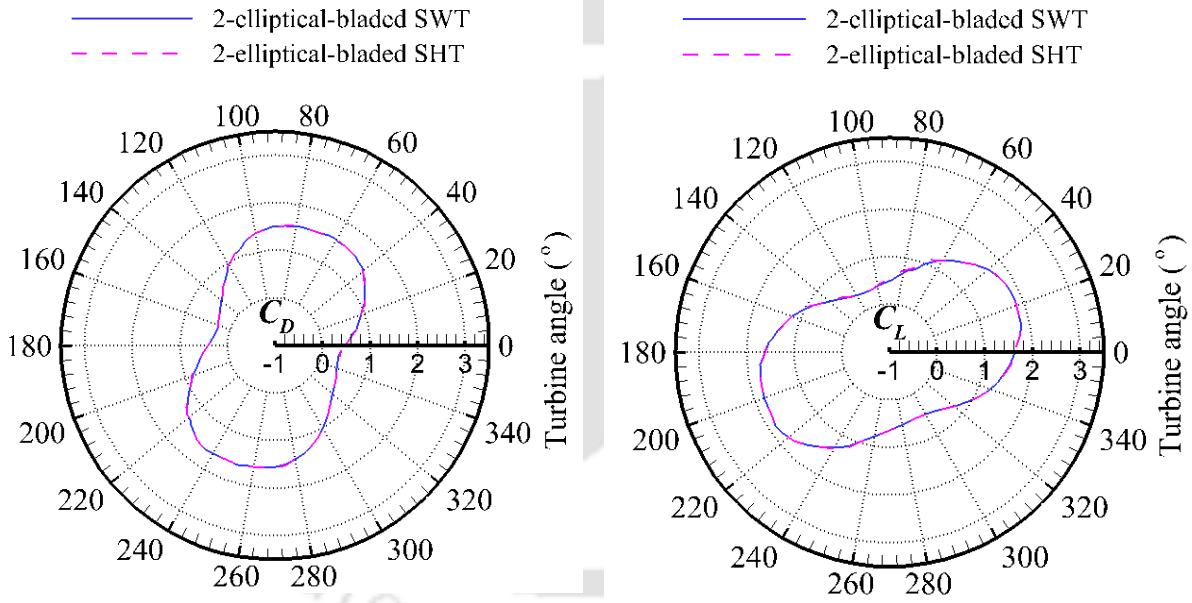

(a) Drag characteristics (b) Lift characteristics

Figure 7.7: Comparison of lift-drag characteristics for two-elliptical-bladed turbines

In similar lines, comparisons of lift-drag characteristics for SWT and SHT are presented in Figs. 7.5 through 7.7. It is evident that the SWT and SHT show almost same lift-drag characteristics. Therefore, it can be concluded that irrespective of the fluid (wind/water) medium, the vertical-axis Savonius turbine generates approximately same lift-drag characteristics for a given inlet power. Thus noticed similarity in the trend of load characteristic curves is consistent for two- and three-bladed SHTs and SWTs.

7.4 Summary

The vertical-axis Savonius turbine has the potential for small-scale electric power generation especially in rural areas. In this chapter, a comparison of performance between SHT and SWT has been done through experimental and 2D CFD investigation. In that context, Savonius turbine designs have been considered and tested under similar input power conditions of the fluids. The data of SWT and SHT are obtained through wind tunnel and open channel testing for identical input power condition of 15.9 W. All the SWTs have demonstrated almost same value of $C_{P\max}$ as that of SHTs. Again, the SWTs are found to operate at slightly wider ranges of *TSR*s than those of SHTs particularly towards increased value of *TSR* beyond optimum *TSR*. From the 2D CFD analysis, the lift and drag characteristics of the SWTs have been analysed. The improved performance of the two-semicircular-bladed SWT from the experimental study has been confirmed here. The variation of C_D with angular positions clearly indicates the higher magnitude of drag for the two-semicircular-bladed SWT over the two-elliptical-bladed and three-semicircular-bladed SWTs. Such observations have already been found for SHTs. At identical input power, the SWTs and SHTs demonstrate similar lift-drag characteristics which justify the fact that a turbine produces approximately the same power output for a given input power irrespective of the type of fluid. The present research reveals the working of Savonius turbine with change of fluid medium (hydro/wind). The study highlights the superior performance of two-bladed turbine as compared to the three-bladed turbine.

Chapter – 8

Conclusions and Future Scopes

Chapter Outline:

Overview

The present study attempts to parametrically evaluate the performance of hydrokinetic turbines. The performance of the vertical-axis drag-based and lift-based turbines are investigated through onsite testing and expressed in terms of torque and power coefficients. In addition, in order to obtain the aerodynamic behaviour and flow physics around the turbine blades, CFD simulations have been performed. The drag-based SHTs are analysed with variation in number of blades, blade shape and immersion level. Further, in case of HHTs, the performances are evaluated for effect of solidity ratio, immersion level and number of stages. In another set of experiments, a comparison of performance for SWT and SHT having an identical kinetic energy of the oncoming fluid (wind/hydro) has been done. In order to achieve this, initially, the wind tunnel experiments with SWTs have been carried out and results are then compared with the equivalent SHT testing. In addition, the lift-drag characteristics of the SWT and SHTs are estimated to further verify the experimental observations.

8.1 Contribution of the Present Work

It is only during the past decade that the research on hydrokinetic technologies has taken a quantum leap. The high power density of water has attracted the researchers to study the potential of hydrokinetic turbines as a low-cost energy conversion device. There exists several reported findings related to wind turbines, however, very limited studies on SHT and HHT have been reported in open literature. The present study is devised to evaluate the performance alteration of SHT/HHTs with respect to its design parameters. Additionally, the need for testing of SHTs has been felt to address the effect of different immersion levels on its efficiency. Though this issue has not yet been addressed, such immersion level experiments are essential to provide the insight about the performance deviation of the turbines when there is a change in the water level because of the seasonal changes. The lack of such experimentation has led to scarcity of data required for validation of multiphase flow solver that deals with fluid structure interaction. The key findings of the present investigation are summarized in the subsequent sections.

8.1.1 Savonius Hydrokinetic Turbine (SHT)

The influence of blade shape and number of blades on performance of SHT is analyzed through experimental and computational investigation. In the initial part of the experiments, two- and three-semicircular-bladed SHTs have been analyzed and thereafter, a comparison of performance between two-semicircular-bladed SHT and two-elliptical-bladed SHT has been carried out. The results are summarized in the following key points:

- ✓ The two-semicircular-bladed SHT (with β = 0.15, AR = 1.0 and D_o = 1.1D) results in highest $C_{P\max}$ of 0.28 at TSR = 0.89 as compared to two-elliptical-bladed SHT and three-semicircular-bladed SHT.
- ✓ The two-semicircular-bladed SHT shows an improvement of $C_{P\max}$ by 28.6% and 39.2% over the two-elliptical-bladed turbine and three-semicircular-bladed turbines, respectively.
- ✓ The CFD analysis also indicates an improved flow characteristic of the semicircular-bladed SHT over the elliptical-bladed SHT. In case of three-bladed turbine, the high pressure zone is being created at the downstream due to generation of large vortices. Thus, a lesser amount of available energy is being converted to mechanical power by the turbine.

- ✓ At different partial levels of immersion, the two-semicircular-bladed SHT demonstrates superior performance as compared to three semicircular-bladed SHT and two elliptical-bladed SHT. On the other hand, the three-semicircular-bladed SHT shows the least percentage degradation of performance; while the two-elliptical-bladed SHT demonstrates the maximum degradation of performance at various immersion levels.
- ✓ At 60% and 80% immersion levels, the two-semicircular-bladed SHT indicates the highest $C_{P\max}$ followed by the three-semicircular-bladed and two-elliptical-bladed SHTs. The three-bladed turbine shows improved performances by 60% and 42.8% over the elliptical-bladed turbine at corresponding immersion levels of 60% and 80%, respectively. At similar immersion levels, the two-semicircular-bladed SHT exhibits better performance than the three-semicircular-bladed SHT by 28.6% and 30%.
- ✓ The two-semicircular-bladed SHT operates at higher optimum *TSR* values at all immersion levels as compared to other two Savonius turbine designs.

8.1.2 Helical-bladed Hydrokinetic Turbine (HHT)

A series of experiments on various testing sites have been carried out to analyze the performance of HHTs. The influence solidity ratios (0.31 – 0.38) and immersion levels (60% –100%) on performance of HHT are studied. Also, the effect of staging on performance of HHT has been estimated. The salient points are briefly mentioned below:

- ✓ In-house design of HHTs of different solidity ratios and on-site testing of such instrumented turbines is performed. From the full immersion experiments, the $C_{P\max}$ of 0.20 is achieved for turbine I (σ = 0.38) and turbine II (σ = 0.34) at corresponding *TSR*s of 1.02 and 0.92.
- ✓ Efforts are extended to analyze the performance of the HHT for its partial immersion in the water stream. It has been observed that C_P drops drastically as the percentage of immersion of turbine in water decreases. Turbine I exhibits the least percentage degradation of C_P with the decrease in immersion level. The $C_{P\max}$ value drops by 64% for turbine I when the immersion level decreases from 100% to 60%.
- ✓ The point of optimum *TSR* also falls towards lower value as the percentage of immersion decreases.
- ✓ To estimate the self-starting ability of the HHTs, starting torque characteristics of each turbine has also been evaluated experimentally at different azimuth angles for fully

submerged condition. The starting torque coefficient is observed to be maximum for turbine I with solidity ratio 0.38.

- ✓ In another set of experiments, the comparison of performance between single-step and double HHTs has been investigated. The field testing has been conducted in river Brahmaputra, Guwahati, and the testing reveals a superior performance of single-step turbine by 12% as compared to double-step turbine.

8.1.3 Savonius Wind Turbine (SWT)

The performance of SHTs is compared with SWTs for identical input power condition of 15.9 W through wind tunnel experiments and 2D unsteady simulations. The key observations are as follows:

- ✓ The SWTs are found to operate at slightly wider ranges of *TSR*s than those of SHTs particularly towards increased value of *TSR* beyond optimum *TSR*
- ✓ The SWTs and SHTs demonstrate almost similar $C_{P\max}$ at the same input power.
- ✓ At identical input power, the SWTs and SHTs are found to demonstrate similar lift-drag characteristics which justify the fact that a turbine produces approximately the same power output for a given input power irrespective of the type of fluid (hydro/wind).

8.2 Application Potential

The hydrokinetic technology can serve as a backbone to remote locations to generate decentralized small-scale standalone power stations which can be used to generate electrical power for the household applications. Further, the hydrokinetic turbines can be deployed in free- flowing water of rivers, manmade channels and irrigation canals. Thus, it can produce electricity to operate water pumps, charging batteries, powering telecommunications and several other low power applications. Of late, the hybrid vertical-axis turbine designed by mounting Savonius- and Darrieus hydrokinetic turbines (with straight blades and helical blades) on a single shaft are found its application. This is because this hybrid design can combine the excellent starting torque of Savonius turbine with the high rotational speed of the Darrieus turbine.

8.3 Scope of Future Work

In the present experimental investigation, the in-house developed SHTs have been tested at only one particular water velocity, V=0.8 m/s. This study, therefore, can be extended to

analyze the performance of the turbines over a range of Reynolds number (*Re*). At the same time, 3D CFD simulation can also be taken up to undertand the 3D flow physics. Further, as a future scope of study, effect of venting on performance of Savonius hydrokinetic turbine (SHT) can be investigated.

The investigation undertaken for HHT can further be extended to find the variation in performance by changing the blade profiles as well the helix angle at different free-stream velocities. Further, there is scope for improvement in turbine performance either (a) by testing the turbines at higher water velocities, or (b) by using a frame and spoke arms constructed from extruded airfoil sections for minimizing the losses.

According to few literatures, there is a disagreement on superior type of turbine between straight-bladed turbine and helical-bladed turbine based on the power output. Some literatures mention that although straight-bladed hydrokinetic turbines are subjected to more torque oscillation and they possess lower starting torque, however, they give superior power coefficient as compared to helical-bladed hydrokinetic turbines. Thus, detailed computational as well as experimental studies can be carried out in this aspect.

Further, in the present CFD analysis of SHT/HHT, the unstructured grids were used. Thus, to order to have more accurate results, the structured grids can be used.

References

Abraham JP, Plourde BD, Mowry GS, Sparrow EM, and Minkowycz WJ, (2011), Numerical simulation of fluid flow around a vertical-axis turbine, *Journal of Renewable and Sustainable Energy*, Vol. 3, Article no. 033109.

Akwa JV, Vielmo HA, and Petry AP, (2012), A review on the performance of Savonius wind turbines, *Renewable and Sustainable Energy Reviews*, Vol. 16, pp. 3054–3064.

Alam MJ, and Iqbal MT, (2009), Design and development of hybrid vertical axis turbine, *Canadian Conference on Electrical and Computer Engineering*, CCECE, 3-6 May, St. John's, Newfoundland, pp. 1178–1183.

Alexander AJ, and Holownia BP, (1978), Wind tunnel tests on a Savonius rotor, *Journal of Wind Engineering and Industrial Aerodynamics*, Vol. 3, No. 4, pp. 343–351.

Ali MH, (2013), Experimental comparison study for Savonius wind turbine of two and three blades at low wind speed, *International Journal of Modern Engineering Research*, Vol. 3, No. 5, pp. 2978–2986.

Alom N, Kolaparthi SC, Gadde SC, and Saha UK, (2016), Aerodynamic design optimization of elliptical-bladed Savonius-style wind turbine by numerical simulations, Paper No. OMAE2016-55095, *ASME 2016 35th International Conference on Ocean, Offshore and Arctic Engineering*, June 19–24, Busan, South Korea.

Alom N, and Saha UK, (2018), Performance evaluation of vent-augmented elliptical-bladed Savonius rotors by numerical simulation and wind tunnel experiments, *Energy*, Vol. 152, pp. 277–290

ANSYS Inc, (2009), ANSYS Fluent Theory Guide 12.0.

Anyi M, and Kirke B, (2010), Evaluation of small axial flow hydrokinetic turbines for remote communities. *Energy for Sustainable Development*, Vol. 14, pp. 110–116.

Bachant P, and Wosnik M, (2015), Performance measurements of cylindrical and spherical-helical cross-flow marine hydrokinetic turbines with estimates of exergy efficiency, *Renewable Energy*, Vol. 74, pp. 318–325.

Bachant P, and Wosnik M, (2015), Performance measurements of cylindrical and spherical-helical cross-flow marine hydrokinetic turbines, with estimates of exergy efficiency. *Renewable Energy*, Vol. 74, pp. 318–325.

Bahaj AS, and Myers LE, (2003), Fundamentals applicable to the utilisation of marine current turbines for energy production, *Renewable Energy*, Vol. 28, No. 14, pp. 2205–2211.

Bahaj AS, Batten WMJ, and McCann G, (2007), Experimental verifications of numerical predictions for the hydrodynamic performance of horizontal axis marine current turbines, *Renewable Energy*, Vol. 32, No. 15, pp. 2479–2490.

Banerjee A, Roy S, Mukherjee P, Saha UK, (2014), Unsteady flow analysis around an elliptic-bladed Savonius-style wind turbines, *ASME Gas Turbine India Conference*, Paper No. GTINDIA2014-8141, December 15–17, New Delhi, India.

Biadgo AM, Simonovic A, Komarov D, and Stupar S, (2013), Numerical and analytical investigation of vertical axis wind turbine, *FME Transactions*, Vol. 41, pp. 49–58.

Birjandi AH, Bibeau EL, Chatoorgoon V, and Kumar A, (2013), Power measurement of hydrokinetic turbines with free-surface and blockage effect, *Ocean Engineering*, Vol. 69, 9–17

Blackwell B, Sheldahl R, and Feltz L, (1977), Wind tunnel performance data for two- and three-bucket Savonius rotors, *Sandia Labs*, Albuquerque, NM (USA).

Bruce ER, (2014), Numerical modelling of a Gorlov cross flow tidal turbine, *3rd Oxford Tidal Energy Workshop*, April 7–8, Oxford, UK, pp. 9–10.

Capuano L, 2018, EIA, International Energy Outlook 2018. (Accessed on February 26, 2019)

Castelli MR, and Benini E, (2011), Effect of blade inclination angle on a Darrieus wind turbine, *Journal of Turbomachinery*, Vol. 134, No. 3, pp. 1–10.

CEA Report, (2018), http://www.cea.nic.in/reports/monthly/installedcapacity/2018/installed capacity-02.pdf.

Chauvin A, and Benhrib D, (1989), Drag and lift coefficients evaluation of a Savonius rotor, *Experiments in Fluids*, Vol. 8, No. 1, pp. 118–120.

Chen L, Chen J, and Zhang Z, (2018), Review of the Savonius rotor's blade profile and its performance, *Journal of Renewable and Sustainable Energy*, Vol. 10, pp. 1–20.

Chen L, Chen J, Xu H, Yang H, Ye C, and Liu D, (2016), Wind tunnel investigation on the two- and three-blade Savonius rotor with central shaft at different gap ratio, *Journal of Renewable and Sustainable Energy*, Vol. 8, pp. 1–15.

Dai YM, Gardiner N, Sutton R, and Dyson PK, (2011), Hydrodynamic analysis models for the design of Darrieus-type vertical-axis marine current turbines, *Proceedings of the Institution of Mechanical Engineers, Part M: Journal of Engineering for the Maritime Environment*, Vol. 225, No. 3, pp. 295–307.

Dai YM, and Lam W, (2009), Numerical study of straight-bladed Darrieus-type tidal turbine, *ICE-Energy*, Vol. 162, pp. 67-76.

Darrieus GJM, (1931), Turbine having its rotating shaft transverse to the flow of the current. US Patent No. 1.835.018.

Deglaire P, Engblom S, Agren O, Bernhoff H, (2009), Analytical solutions for a single blade in vertical axis turbine motion in two-dimensions, *European Journal of Mechanics - B/Fluids*, Vol. 28, pp. 506–520

Dixon D, (2007), Assessment of waterpower potential and development needs. Technical Report, *Electric Power Research Institute (EPRI*), Palo Alto, CA.

Driss Z, Damak A, Karray S, and Abid MS, (2012), Experimental study of the internal overlap ratios effect on the performance of the Savonius wind rotor, *Journal of Engineering and Technology*, Vol. 1, pp. 15–21.

Ellabban O, Abu-Rub H, and Blaabjerg F, (2014), Renewable energy resources: Current status, future prospects and their enabling technology, *Renewable and Sustainable Energy Reviews*, Vol. 39, pp. 748–764.

Emmanuel B, and Jun W, (2011), Numerical study of a six-bladed Savonius wind turbine, *Journal of Solar Energy Engineering*, Vol. 133, pp. 044503-1–044503-5.

Faizala M, Ahmed MR, and Lee YH, (2010), On utilizing the orbital motion in water waves to drive a Savonius rotor, *Renewable Energy*, Vol. 35, pp. 164–169.

Fernandes AC, and Armandei M, (2014), Low-head hydropower extraction based on torsional galloping, *Renewable Energy*, Vol. 69, pp. 447–452.

Fernandes AC, and Rostami AB, (2015), Hydrokinetic energy harvesting by an innovative vertical-axis current turbine, *Renewable Energy*, Vol. 81, pp. 694–706.

Fernando MSUK, and Modi VJ, (1989), A numerical analysis of the unsteady flow past a Savonius wind turbine, *Journal of Wind Engineering and Industrial Aerodynamics*, Vol. 32, pp. 303–327.

Fiedler A, and Tullis S, (2009), Blade offset and pitch effects on high solidity vertical axis wind turbines, *Wind Engineering*, Vol. 33, No. 3, pp. 237–246.

Fujisawa N, and Gotoh F, (1992), Visualization study of the flow in and around a Savonius rotor, *Experiments in Fluids*, Vol. 12, No. 6, pp. 407–412.

Fujisawa N, and Gotoh F, (1994), Experimental study on the aerodynamic performance of a Savonius rotor, *Journal of Solar Energy Engineering*, Vol. 116, No. 3, pp.148–152.

Ghasemian M, Ashrafi ZN, and Sedaghat A, (2017), A review on computational fluid dynamic simulation techniques for Darrieus vertical axis wind turbines, *Energy Conversion and Management*, Vol. 149, pp. 87–100

Garman P, (1986), Water current turbines: a fieldworker's guide, UK: *Intermediate Technology Publishing*, ISBN 0946688273.

Golecha K, Eldho TL, and Prabhu SV, (2011), Influence of the deflector plate on the performance of modified Savonius water turbine, *Applied Energy*, Vol. 88, pp. 3207–3217.

Golecha K, Eldho TI and Prabhu SV, (2012), Performance study of modified Savonius water turbine with two deflector plates, *International Journal of Rotating Machinery*, Article ID 679247.

Gorlov A, (1995), Unidirectional helical reaction turbine, U.S. Patent No 5,451,137, Trademark Office.

Gorlov AM, and Rogers K, (1997), Helical turbine as undersea power source, *Sea Technology*, United States.

Gorlov A, (1998), Development of the helical reaction hydraulic turbine, Final technical report (DE-FGO1-96EE 15669), DOE/EE/15669-TI.

Gorlov AM, (1998), Helical turbines for the Gulf Stream: Conceptual approach to design of a large-scale floating power farm, *Marine Technology*, Vol. 35, No. 3, pp. 175–182.

Gretton GI, (2009), The hydrodynamic analysis of a vertical axis tidal current turbine, PhD Thesis, The University of Edinburgh.

Guney MS, and Kaygusuz K, (2010), Hydrokinetic energy conversion systems: A technology status review, *Renewable and Sustainable Energy Reviews*, Vol. 14, pp. 2996–3004.

Hagerman G, and Polagye B, (2006), Methodology for Estimating Tidal Current Energy Resources and Power Production by Tidal In-Stream Energy Conversion (TISEC) Devices, Report: EPRI – TP – 001 NA Rev 3.

Hall TJ, (2012), Numerical simulation of a cross flow marine hydrokinetic turbine, *Master's thesis*, University of Washington.

Han SH, Park JS, Lee KS, Park WS, and Yi JH, (2013), Evaluation of vertical axis turbine characteristics for tidal current power plant based on situ experiment, *Ocean Engineering*, Vol. 65, pp. 83–89.

Han D, Heo YG, Choi NJ, Nam SH, Choi KH, and Kim KC, (2018), Design, fabrication, and performance test of a 100-W Helical-blade vertical-axis wind turbine at low tip-speed ratio, *Energies*, Vol. 11, No. 1517, pp. 1–17.

Holman JP, (2007), Experimental methods for engineers, *Tata McGraw Hill Publications*, 7th edition.

Hydrovolts, (2010), http://www.hydrovolts.com/MainPages/Hydrokinetic%20Turbines.htm.

Irabu K, and Roy JN, (2011), Study of direct force measurement and characteristics on blades of Savonius rotor at static state, *Experimental Thermal and Fluid Science*, Vol. 35, No. 4, pp. 653–659.

Islam M, King D, and Fartaj A, (2006), Aerodynamic models for Darrieus-type straight-bladed vertical axis wind turbines, *Renewable and Sustainable Energy Reviews*, Vol. 12, No. 4, pp. 1087–1109.

Jaohindy P, McTavish S, Garde F, and Bastide A, (2013), An analysis of the transient forces acting on Savonius rotors with different aspect ratios, *Renewable Energy*, Vol. 55, pp. 286–295.

Jeon KS, Jeong JI, Pan JK, and Ryu KW, (2015), Effects of end plates with various shapes and sizes on helical Savonius wind turbines, *Renewable Energy*, Vol. 79, pp. 167–176.

Jin X, Zhao G, Gao K, Ju W, (2015), Darrieus vertical axis wind turbine: basic research methods, *Renewable and Sustainable Energy Reviews*, Vol. 42, pp. 212–225.

Johnson JB, and Pride DJ, (2010), River, tidal, and ocean current hydrokinetic energy technologies: status and future opportunities in Alaska, *Technical report, Alaska Center for Energy and Power*.

Kacprzak K, Liskiewicz G, and Sobczak K, (2013), Numerical investigation of conventional and modified Savonius wind turbines, *Renewable Energy*, Vol. 60, pp. 578–585.

Kahn MH, (1978), Model and prototype performance characteristics of Savonius rotor windmill, *Wind Engineering*, Vol. 2, pp. 75–85.

Kailash G, Eldho TI, and Prabhu SV, (2012), Performance study of modified Savonius water turbine with two deflector plates, *International Journal of Rotating Machinery*, Article ID 679247, pp. 1–12.

Kamoji MA, Kedare SB, and Prabhu SV, (2008), Experimental investigations on single stage, two stage and three stage conventional Savonius rotor, *International Journal of Energy Research*, Vol. 32, pp. 877–895.

Kamoji MA, Kedare SB, and Prabhu SV, (2009), Performance tests on helical Savonius rotors, Renewable Energy, Vol. 34, pp. 521–529.

Kamoji MA, Kedare SB, and Prabhu SV, (2009), Experimental investigations on single stage modified Savonius rotor, *Applied Energy*, Vol. 86, pp. 1064–1073.

Khan MJ, Bhuyan G, Iqbal MT, and Quaicoe JE, (2009), Hydrokinetic energy conversion systems and assessment of horizontal and vertical axis turbines for river and tidal applications: A technology status review, *Applied Energy*, Vol. 86, pp. 1823–1835.

Khan MJ, Iqbal MT, and Quaicoe JE, (2008), River current energy conversion systems: Progress, prospects and challenges, *Renewable and Sustainable Energy Reviews*, Vol. 12, pp. 2177–2193.

Khan, MNI , Iqbal MT, Hinchey M, and Masek V, (2009), Performance of Savonius rotor as a water current turbine, *Journal of Ocean Technology*, Vol. 4, No. 2, pp. 71–83.

Kim G, Lee ME, Lee KS, Park JS, Jeong WM, Kang SK, Soh JG, and Kim H, (2012), An overview of ocean renewable energy resources in Korea, *Renewable and Sustainable Energy Reviews*, Vol. 16, pp. 2278–2288.

Kirke BK, (2011), Tests on ducted and bare helical and straight blade Darrieus hydrokinetic turbines, *Renewable Energy*, Vol. 36, pp. 3013–3022.

Kline SJ, and McClintock FA, (1953), Describing uncertainties in single-sample experiments. Mechanical Engineering, Vol. 75, pp. 3–8.

Kota S, Bayne, SB, and Nimmagadda S, (2015), Offshore wind energy: A comparative analysis of UK, USA and India, *Renewable and Sustainable Energy Reviews*, Vol. 41, pp. 685–694.

Kotb, MA, and Aldoss TK, (1991), Flowfield around a partially-blocked Savonius rotor, *Applied Energy*, Vol. 38, No. 2, pp. 117–132

Kumar A, and Saini RP, (2016), Performance parameters of Savonius type hydrokinetic turbine – A Review, *Renewable and Sustainable Energy Reviews*, Vol. 64, pp. 289–310.

Kumar D, and Sarkar S, (2016), A review on the technology, performance, design optimization, reliability, techno-economics and environmental impacts of hydrokinetic energy conversion systems, *Renewable and Sustainable Energy Reviews*, Vol. 58, pp. 796–813.

Kumar A, and Saini RP, (2017), Performance analysis of a Savonius hydrokinetic turbine having twisted blades, *Renewable Energy*, Vol. 108, pp. 502–522.

Lago LI, Ponta FL, and Chen L, (2010), Advances and trends in hydrokinetic turbine systems, *Energy for Sustainable Development*, Vol. 14, pp. 287–296.

Lanzafame R, Mauro S, Messina M, (2014), 2D CFD modeling of H-Darrieus wind turbines using a transition turbulence model, *Energy Procedia*, Vol. 45, pp. 131–140.

Laws ND, and Epps BP, (2016), A review on the technology, performance, design optimization, reliability, techno-economics and environmental impacts of hydrokinetic energy conversion systems, *Renewable and Sustainable Energy Reviews*, Vol. 57, pp. 1245–1259.

Le TQ, Lee KS, Park JS, Ko JH, (2014), Flow-driven rotor simulation of vertical axis tidal turbines: a comparison of helical and straight blades, *International Journal of Naval Architecture and Ocean Engineering*, Vol. 6, pp. 257–268.

Marsh P, Ranmuthugala D, Penesis I, and Thomas G, (2015), Numerical investigation of the influence of blade helicity on the performance characteristics of vertical axis tidal turbines, *Renewable Energy*, Vol. 81, pp. 926–935.

Marsh P, Ranmuthugala D, Penesis I, and Thomas G, (2016), Numerical simulation of the loading characteristics of straight and helical-bladed vertical axis tidal turbines, *Renewable Energy*, Vol. 94, pp. 418–428.

Menter FR, (1994), Two-equation eddy-viscosity turbulence models for engineering Applications, *AIAA Journal*, Vol. 32, No. 8, pp. 1598–1605.

Moffat RJ, (1988), Describing the uncertainties in experimental results, *Experimental Thermal and Fluid Science*, Vol. 1, No. 1, pp. 3–17.

Mahmoud NH, El-Haroun AA, Wahba E, and Nasef MH, (2012), An experimental study on improvement of Savonius rotor performance, *Alexandria Engineering Journal*, Vol. 51, No.1, pp. 19–25.

Mohamed MH, Janiga G, Pap E, and Thevenin D, (2010), Optimization of Savonius turbines using an obstacle shielding the returning blade, *Renewable Energy*, Vol. 35, No. 11, pp. 2618–2626.

Mohamed MH, Janiga G, Pap E, and Thevenin D, (2011), Optimal blade shape of a modified Savonius turbine using an obstacle shielding the returning blade, *Energy Conversion and Management*, Vol. 52, No. 1, pp. 236–42.

Nasef M, El-Askary W, AbdEL-Hamid A, and Gad H, (2013), Evaluation of Savonius rotor performance: static and dynamic studies, *Journal of Wind Engineering and Industrial Aerodynamics*, Vol. 123, pp. 1–11.

Nguyen CC, Le THH, and Tran PH, (2015), A numerical study of thickness effect of the symmetric NACA 4-digit airfoils on self-starting capability of a 1kW H-type vertical axis wind turbine, *International Journal of Mechanical Engineering and Applications*, Vol. 3, pp. 7-16.

Niblick AL, (2012), Experimental and analytical study of helical cross-flow turbines for a tidal micropower generation system, *Master's thesis*, University of Washington.

Ogawa T, (1984), Theoretical study on the flow about Savonius rotor, *ASME Transactions: Journal of Fluids Engineering*, Vol. 106, No. 1, pp. 85–91.

Ogawa T, and Yoshida H, (1986), The effects of a deflecting plate and rotor end plates on performance of Savonius-type wind turbine, *Bulletin of JSME*, Vol. 29, No. 253, pp. 2115–2121.

Olyaie E, Banejad H, Chau KW, and Melesse AM, (2015), A comparison of various artificial intelligence approaches performance for estimating suspended sediment load of river systems: a case study in United States, *Environmental Monitoring and Assessment*, Vol. 187, No. 4, pp.1–22.

Owen A, and Bryden IG, (2007), Energy extraction implications of structurally significant velocity variation in tidal currents, *Oceans*, pp. 1–5.

Paraschivoiu I, (2002), Wind turbine design: with emphasis on Darrieus concept, presses inter Polytechnique, Canada.

Patel V, Bhat G, Eldho TI, and Prabhu SV, (2017), Influence of overlap ratio and aspect ratio on the performance of Savonius hydrokinetic turbine, *International Journal of Energy Research*, Vol. 41, pp. 829–844.

Plourde BD, Abraham JP, Mowry GS, and Minkowycz WJ, (2012), Simulations of three-dimensional vertical-axis turbines for communications applications, *Wind Engineering*, Vol. 36, pp. 443–454.

Pongduang S, Kayankannavee C, and Tiaple Y, (2015), Experimental investigation of helical tidal turbine Characteristics with different twists. *International Conference on Alternative Energy in Developing Countries and Emerging Economies*, *Energy Procedia*, Vol. 79, pp. 409–414.

Pope K, Dincer I, and Naterer GF, (2010), Energy and exergy efficiency comparison of horizontal and vertical axis wind turbines, *Renewable Energy*, Vol. 35, No. 9, pp. 2102–2113.

Radkey RL, Hibbs BD, (1981), Definition of Cost Effective River Turbine Designs, Tech. Rep. AV-FR-81/595 (DE82010972), Report for US Department of Energy, *Aerovironment Inc.*, Pasadena, California.

Rourke FO, Boyle F, and Reynolds A, (2010), Marine current energy devices: Current status and possible future applications in Ireland, *Renewable and Sustainable Energy Reviews*, Vol. 14, pp. 1026–1036.

Roy S, and Ducoin A, (2016), Unsteady analysis on the instantaneous forces and moment arms acting on a novel Savonius-style wind turbine, *Energy Conversion and Managemen*t, Vol. 121, pp. 281–296

. **Roy S, and Saha UK**, (2013), Review of experimental investigations into the design, performance and optimization of the Savonius rotor, *IMechE Part A: Journal of Power and Energy*, Vol. 227, No. 4, 528–542.

Roy S, and Saha UK, (2013), Review on the numerical investigations into the design and development of Savonius wind rotors, *Renewable and Sustainable Energy Reviews*, Vol. 24, pp. 73–83.

Roy S, and Saha UK, (2014), An adapted blockage factor correlation approach in wind tunnel experiments of a Savonius-style wind turbine, *Energy Conversion and Management*, Vol. 86, pp. 418–427.

Sanusi A, Soeparman S, Wahyudi S, and Yuliati L, (2016), Experimental study of combined blade Savonius wind turbine, *International Journal of Renewable Energy Research*, Vol. 6, No. 2, pp. 614–619.

Sarma NK, Biswas A, and Misra RD, (2014), Experimental and computational evaluation of Savonius hydrokinetic turbine for low velocity condition with comparison to Savonius wind turbine at the same input power, *Energy Conversion and Management*, Vol. 83, pp. 88–98.

Satir M, Murphy F, and McDonnell K, (2018), Feasibility study of an offshore wind farm in the Aegean Sea, Turkey, *Renewable and Sustainable Energy Reviews*, Vol. 81, pp. 2552–2562.

Savonius SJ, 1931, The S-rotor and its applications, *Mechanical Engineering*, Vol. 53, No. (5), 333–338.

Scheurich F, Fletcher TM, and Brown RE, (2010), The influence of blade curvature and helical blade twist on the performance of a vertical-axis wind turbine, *48th AIAA Aerospace Sciences Meeting Including the New Horizons Forum and Aerospace Exposition*, 4–7 January, Orlando, Florida, pp. 1–16.

Shankar PN, (1979), Development of vertical-axis wind turbines, *Proc. Indian Acad Sci*., C2, pp. 49–66.

Sharma NK, Biswas A and Misra RD, (2014), Experimental and computational evaluation of savonius hydrokinetic turbine for low velocity condition with comparison to Savonius wind turbine at the same input power, *Energy Conversion and management*, Vol. 83, pp. 88–98.

Sheldahl RE, Feltz LV, Blackwell BF, (1978), Wind tunnel performance data for two and three-bucket Savonius rotors, *AIAA Journal of Energy*, Vol. 2, No. 3, pp. 160–164.

Shiono M, Suzuki K, and Kiho S, (2002), Output characteristics of Darrieus water turbine with helical blades for tidal current generations, *Proceedings of the Twelfth International Offshore and Polar Engineering Conference*, May 26–31, Kitakyushu, Japan, pp. 859–864.

Singh RK, Ahmed MR, (2013), Blade design and performance testing of a small wind turbine rotor for low wind speed applications, *Renewable Energy*, Vol. 50, pp. 812 – 819.

Sivasegaram S, (1978), Secondary parameters affecting the performance of resistance-type vertical-axis wind rotors, *Wind Engineering*, Vol. 2, pp. 49–58.

Sornes K, (2010), Small scale water current turbines for river applications, *Zero Emission Research Organization Report*, Oslo.

Thropton Energy, (2010), http://www.throptonenergy.co.uk/.

Tian W, Song B, Van Zwieten JH, Pyakurel P, (2015), Computational fluid dynamics prediction of a modified Savonius wind turbine with novel blade shapes, *Energies*, Vol. 8, No. 8, pp. 7915–7929.

Tjiu W, Marnoto T, Mat S, Ruslan MH, Sopian K, (2015), Darrieus vertical axis wind turbine for power generation I: assessment of Darrieus VAWT configurations, *Renewable Energy*, Vol. 75, pp. 60–71

Tsai J, and Chen F, (2014), The conceptual design of a tidal power plant in Taiwan, *Journal of Marine Science and Engineering*, Vol. 2, pp. 506–533.

Twidell J, and Weir AD, (2006), *Renewable Energy Resources* (2nd edition), London: *Taylor & Francis.*

VanZwieten J, McAnally W, Ahmad J, Davis T, Martin J, Bevelhimer M, Cribbs A, Lippert R, Hudon T, and Trudeau M, (2015), In-Stream hydrokinetic power: Review and appraisal, *ASCE Journal Energy Engineering*, Vol. 141, No. 3, pp. 1–16.

Vermaak HJ, Kusakana K, and Koko SP, (2003). The challenge of rural electrification. *Energy for Sustainable Development*, Vol. 7, No. 1, pp. 69–76.

Wang WC, Xu DM, Chau KW and Lei GJ, (2014), Assessment of river water quality based on theory of variable fuzzy sets and fuzzy binary comparison method, *Water Resources Management*, Vol. 28, No. 12, pp. 4183–4200.

Wenehenubun F, Saputra A, and Sutanto H, (2015), An experimental study on the performance of Savonius wind turbines related with the number of blades, *Energy Procedia*, Vol. 68, pp. 297–304.

Whiting J, (2016), Uldolmok tidal power station, https://tethys.pnnl.gov/annex-iv-sites/uldolmok-tidal-power-station.

Wilson RE, Lissaman PBS, Walker SN, (1976), Aerodynamic performance of wind turbines, ERDA/NSF/04014-7611, pp. 111–164.

Winchester JD, and Quayle SD, (2009), Torque ripple and variable blade force: A comparison of Darrieus and Gorlov-type turbines for tidal stream energy conversion. *Proceedings of the 8th European Wave and Tidal Energy Conference*, Sweden, pp. 668–676.

Wong KH, Chong WT, Sukiman, NL, Poh, SC, Shiah YC, and Wang CT, (2017), Performance enhancements on vertical axis wind turbines using flow augmentation systems: A review, *Renewable and Sustainable Energy Reviews*, Vol. 73, pp. 904–921.

Yaakob O, Ahmed YM, Ismail MA, (2012), Validation study for Savonius vertical axis marine current turbine using CFD simulation, *6th Asia-Pacific workshop on marine hydrodynamics (APHydro2012)*, September 3–4, Malaysia.

Yang B, and Lawn C, (2011), Fluid dynamic performance of a vertical axis turbine for tidal currents, *Renewable Energy*, Vol. 36, pp. 3355–3366.

Yuce MI, and Muratoglu A, (2015), "Hydrokinetic energy conversion systems: A technology status review, *Renewable and Sustainable Energy Reviews*, Vol. 43, pp. 72–82.

Vance W, (1973), Vertical-axis wind rotors–status and potential, *Proceedings of the conference on wind energy conversion systems*, pp. 96–102.

Van Dusen ES, and Kirchhoff RH, (1978), A two dimensional vortex sheet model of a Savonius rotor, Fluid engineering in advanced energy systems, *Proceedings of the ASME winter annual meeting*, , December 10–15, San Francisco, California.

Zhao Z, Zheng Y, Xu X, Liu W, and Hu G, (2009), Research on the improvement of the performance of Savonius rotor based on numerical study, *Proceedings of the IEEE International Conference of Sustainable Power Generation and Supply*, April 6–7, Nanjing, China.

Appendix – A

Measurement Uncertainty Analysis

The uncertainty (also called, error) in measurement of various quantities and propagation of these errors are discussed in this section. Errors may occur in any experiment mainly due to instrument's inaccuracy, inappropriate calibration and human error. Although, the human errors can be reduced up to certain level through repeated experiments, the measuring instruments often have errors regardless of the calibration performed by the manufacturer. The experimental turbine setup is an assembly of various apparatus with corresponding uncertainties or relative errors. The uncertainty analysis for the turbine performance is assessed by using the prescribed methods (Kline and McClintock 1953; Moffat 1988; Holman 2007). The method is based on a careful specification of the uncertainties in the various primary experimental measurements. These are systematic errors which are dependent on the resolution of the measuring device. Consider an experimental result, M, is a given function of the independent variables $x_1, x_2, x_3, x_4 \ldots \ldots x_n$.

$$M = M(x_1, x_2, x_3, x_4 \ldots \ldots x_n) \tag{A1}$$

Let, M be the uncertainty in the result and $\Delta M_1, \Delta M_2, \Delta M_3 \ldots\ldots \Delta M_n$ be the uncertainties in the independent variables. If the uncertainties in the independent variables are all given with the same odds, then the uncertainty in the result having these odds is given as,

$$\Delta M = \left[\left(\frac{\partial M}{\partial x_1} \Delta M_1 \right)^2 + \left(\frac{\partial M}{\partial x_2} \Delta M_2 \right)^2 + \ldots\ldots + \left(\frac{\partial M}{\partial x_n} \Delta M_n \right)^2 \right] \tag{A2}$$

The uncertainties of each independent parameter of SHTs, HHTs and SWTs along with the overall relative measurement uncertainty are discussed in the following sections. Some measurement errors are taken from the manual from the equipment and for others it is estimation.

The uncertainties of tip-speed ratio (TSR), torque coefficient (C_Q) and power coefficient (C_P) are evaluated with the help of following Eqns:

$$\frac{\partial(TSR)}{TSR} = \sqrt{\left(\frac{\partial N}{N}\right)^2 + \left(\frac{\partial V}{V}\right)^2} \quad \text{(A3)}$$

$$\frac{\partial(C_Q)}{C_Q} = \sqrt{\left(2\frac{\partial V}{V}\right)^2 + \left(\frac{\partial T}{T}\right)^2} \quad \text{(A4)}$$

$$\frac{\partial(C_P)}{C_P} = \sqrt{\left(\frac{\partial(TSR)}{TSR}\right)^2 + \left(2\frac{\partial V}{V}\right)^2 + \left(\frac{\partial T}{T}\right)^2} \quad \text{(A5)}$$

Following are the details of uncertainties of different components of the experimental set-ups and estimated uncertainties of performance parameters:

Experiments with SHT:

The uncertainties (relative error) associated with the independent parameters of the turbine are as follows: contact-type tachometer (±0.15%), digital spring balance (±0.2%) and velocity meter (±1.5%). Considering these values, the overall measurement of *TSR* is expected to be ±1.51% accurate and the estimated torque coefficient, power coefficient are expected to have accuracy within ±3.01% and ±3.36% respectively.

Experiments with HHT:

For the initial set of experiments for investigation of effect of solidity ratio, the instruments used contain uncertainties as follows: contact-type tachometer (±0.15%), digital spring balances (±0.2%), propeller-type current meter (±1.5%). Thus, the overall uncertainties associated with tip-speed ratio, torque coefficient and power coefficient measurement are obtained to be ±1.51% and ±3.01% and ±3.36%, respectively.

Similarly in the experiments for effect of multi-stepping, the uncertainties associated with the instruments are as follows: non-contact type tachometer (accuracy: ±0.15%), spring balance (±3.6%), and velocity meter (±1.5%). Therefore, the estimated uncertainties with tip-speed ratio, torque coefficient and power coefficient are calculated to be around ±1.51% and ±4.68, ±4.92%, respectively.

Experiments with SWT:

In the experiments of SWT, following are the uncertainties of the instruments: contact-type tachometer (±0.15%), digital spring balances (±0.2%), manometer (±0.3%). Thus, uncertainties associated with tip-speed ratio, torque coefficient and power coefficient estimations are found to be ±0.61, ±0.63 and ±0.88, respectively.

Appendix – B

Turbulence Model

For a realistic modeling of the flow field around the turbine, it is essential to account for turbulence. The turbulent flows are characterized by fluctuating velocity fields and these fluctuations combine the transported quantities (momentum, energy and species concentrations) and make the transported quantities to fluctuate as well. These kind fluctuations can be of small scale and high frequency and it is computationally expensive to simulate directly in practical engineering calculations. As a substitute, the instantaneous (exact) governing equations can be time averaged, ensemble-averaged, or otherwise manipulated in order to eliminate the resolution of small scale, resulting in a modified set of equations that are computationally less expensive to solve. However, the modified set of equations contains few additional unknown variables, and thus turbulence models are needed to determine these variables in terms of known quantities (ANSYS Inc. 2009). In the present study, the shear-stress transport (SST) k-ω model turbulence model is applied to solve the flow governing equations.

The SST k-ω model was developed by Menter (1994) and it combines the advantages of k-ω model and k-ϵ model while capturing the flow field in the near wall region and far field region respectively. The SST k-ω model is similar to standard k-ω model, however it includes the following features:

- The standard k-ω model and transformed k-ϵ model are both multiplied by a blending function and thereafter both are added together.
- The blending function is designed in such a way that it activates the standard k-ω model in the near wall region, and zero away from the surface, it activates the transformed k-ϵ model.
- The SST k-ω model incorporates a damped cross diffusion derivative term in the ω equation.
- The turbulent viscosity term is modified to account for the transport of the turbulent shear stress.
- The modeling constants are also different.

Due to these added refinements, the SST k-ω model is more accurate and reliable for a wider class of flows (e.g., adverse pressure gradients, flow over airfoils, rotating flows etc.) as compared to the standard k-ω model.

Transport equations for the standard *k-ω* model:

In *SST k-ω* model, the turbulence kinetic energy (*k*), and the specific dissipation rate (*ω*) are obtained from the following transport equations:

$$\rho(\frac{\partial(\rho k)}{\partial t} + \frac{\partial(\rho k u_i)}{\partial x_i} = \frac{\partial}{\partial x_j}\left(\Gamma_k \frac{\partial k}{\partial x_j}\right) + \tilde{G}_k - Y_k + S_k \quad \text{(B1)}$$

and

$$\rho(\frac{\partial(\rho \omega)}{\partial t} + \frac{\partial(\rho \omega u_i)}{\partial x_i} = \frac{\partial}{\partial x_j}\left(\Gamma_\omega \frac{\partial \omega}{\partial x_j}\right) + G_\omega - Y_\omega + D_\omega + S_\omega \quad \text{(B2)}$$

where, G_k represents the generation of turbulence kinetic energy due to mean velocity gradients, G_ω denotes the generation of ω, Γ_k and Γ_ω represent the effective diffusivity of k and ω, respectively, Y_k and Y_ω signifies the dissipation of k and ω, S_k and S_ω represent the user defined functions for k and ω, respectively, D_w indicates the cross-diffusion term.

The equations for Γ_k and Γ_ω are estimated using Eqn. B3 and Eqn. B4.

$$\Gamma_k = \mu + \frac{\mu_t}{\sigma_k} \quad \text{(B3)}$$

$$\Gamma_\omega = \mu + \frac{\mu_t}{\sigma_\omega} \quad \text{(B4)}$$

where, σ_k and σ_ω are the turbulent Prandtl numbers for k and ω, respectively.

However, the turbulent viscosity, μ_t, the turbulent Prandtl numbers, σ_k and σ_ω are computed as follows:

$$\mu_t = \frac{\rho k}{\omega} \frac{1}{\max\left[\frac{1}{\alpha^*}, \frac{SF_2}{\alpha_1 \omega}\right]} \quad \text{(B5)}$$

where, S is the strain rate magnitude.

$$\alpha^* = \alpha_\infty^*\left(\frac{\alpha_0^* + \mathrm{Re}_t / R_k}{1 + \mathrm{Re}_t / R_k}\right) \quad \text{(B6)}$$

where, $\mathrm{Re}_t = \frac{\rho k}{\mu \omega}$, $R_k = 6$, $\alpha_0^* = \frac{\beta_i}{3} = \frac{0.072}{3}$

$$\sigma_k = \frac{1}{(F_1 / \sigma_{k,1}) + ((1 - F_1) / \sigma_{k,2})} \quad \text{(B7)}$$

$$\sigma_{\omega} = \frac{1}{(F_1 / \sigma_{\omega,1}) + ((1-F_1) / \sigma_{\omega,2})} \tag{B8}$$

The blending functions, F_1 and F_2 are given by:

$$F_1 = \tanh(\phi_1^4) \tag{B9}$$

$$\phi_1 = \min\left[\max\left(\frac{\sqrt{k}}{0.09\omega y}, \frac{500\mu}{\rho y^2 \omega}\right), \frac{4\rho k}{\sigma_{w,2} D_{\omega}^{+} y^2}\right] \tag{B10}$$

$$D_{\omega}^{+} = \max\left[2\rho \frac{1}{\sigma_{\omega,2}} \frac{1}{\omega} \frac{\partial k}{\partial x_j} \frac{\partial \omega}{\partial x_j}, 10^{-10}\right] \tag{B11}$$

$$F_2 = \tanh(\phi_2^4) \tag{B12}$$

$$\phi_2 = \max\left[2\frac{\sqrt{k}}{0.09\omega y}, \frac{500\mu}{\rho y^2 \omega}\right] \tag{B13}$$

where, y is the distance to the next surface.

σ_1= 0.31, $\sigma_{k,1}$ = 1.176, $\sigma_{k,2}$ = 1, $\sigma_{\omega,1}$ = 2, $\sigma_{\omega,2}$ = 1.168.

$$Y_k = \rho \beta_i \omega^2 \tag{B14}$$

The modified β_i used in this model is given by:

$$\beta_i = F_1 \beta_{i,1} + (1-F_1)\beta_{i,2} \tag{B15}$$

where, $\beta_{i,1}$ = 0.075, $\beta_{i,2}$ = 0.0828

The cross-diffusion term, D_{ω} is given by:

$$D_{\omega} = 2(1-F_1)\rho\sigma_{\omega,2} \frac{1}{\omega} \frac{\partial k}{\partial x_j} \frac{\partial \omega}{\partial x_j} \tag{B16}$$

List of Publications

International Journals

1. **Talukdar PK**, Sardar A. Kulkarni V, and Saha UK, (2018), Parametric analysis of model Savonius hydrokinetic turbines through experimental and computational investigations, ***Energy Conversion and Management***, Vol. 158, 36–49.

2. **Talukdar PK**, Kulkarni V, and Saha UK, (2018), Field testing of model hydrokinetic helical-bladed turbine for small-scale power generation, ***Renewable Energy***, Vol. 127, 158–167.

3. **Talukdar PK**, Kulkarni V, and Saha UK, (2018), Performance estimation of Savonius wind and Savonius hydrokinetic turbines under identical power input, ***Journal of Renewable and Sustainable Energy***, Vol. 10, 1–15.

International Conferences

4. **Talukdar PK**, Kulkarni V, and Saha UK, (2018), Performance characteristics of vertical-axis off-shore Savonius wind and Savonius hydrokinetic turbines, ***ASME 37th International Conference on Ocean, Offshore and Arctic Engineering***, Paper No. OMAE2018–78497, June 17–22, Madrid, Spain.

5. **Talukdar PK**, Kulkarni V, Das AK., Dwivedy SK, Kakoty SK, Mahanta P and Saha UK, (2017), In-situ experiments to estimate the performance characteristics of a double-step helical-bladed hydrokinetic turbine, ***ASME Gas Turbine India Conference***, Paper No. GTINDIA 2017–4572, December 07–08, Bangalore, India.

6. **Talukdar PK**, Kulkarni V, Dehingia D, and Saha UK, (2017), Evaluation of a model helical–bladed hydrokinetic turbine characteristics from in-situ experiments, ***ASME 11th International Conference on Energy Sustainability***, Paper No. ES2017–3490, June 26–30, Charlotte, NC, USA.

7. **Talukdar PK**, Medhi D, Kulkarni V, and Saha UK, (2016), Parametric analysis of a hydrokinetic helical turbine through numerical simulation, ***Asian Congress on Gas Turbines***, Paper No. ACGT 2016–95, 14–16 November, Indian Institute of Technology Bombay, Mumbai, India.

8. **Talukdar PK**, Kumar S, Kulkarni V, Das AK, and Saha UK, (2015), Onsite testing of a zero head vertical–axis helical water turbine for power generation, ***ASME Gas Turbine India Conference***, Paper No. GTINDIA 2015–1230, December 02–03, Hyderabad, India.